Imagerie et analyses chimiques à haute résolution spatiale, à basse tension d'accélération des électrons, avec un FE-SEM de pointe.

Pr. Raynald Gauvin, Ph.D.,
Nicolas Brodusch, Technician,
Hendrix Demers, Ph.D.,
Université McGill, Montréal, Canada.

MC X-Ray: Nouveau Programme Monte Carlo memrg.com

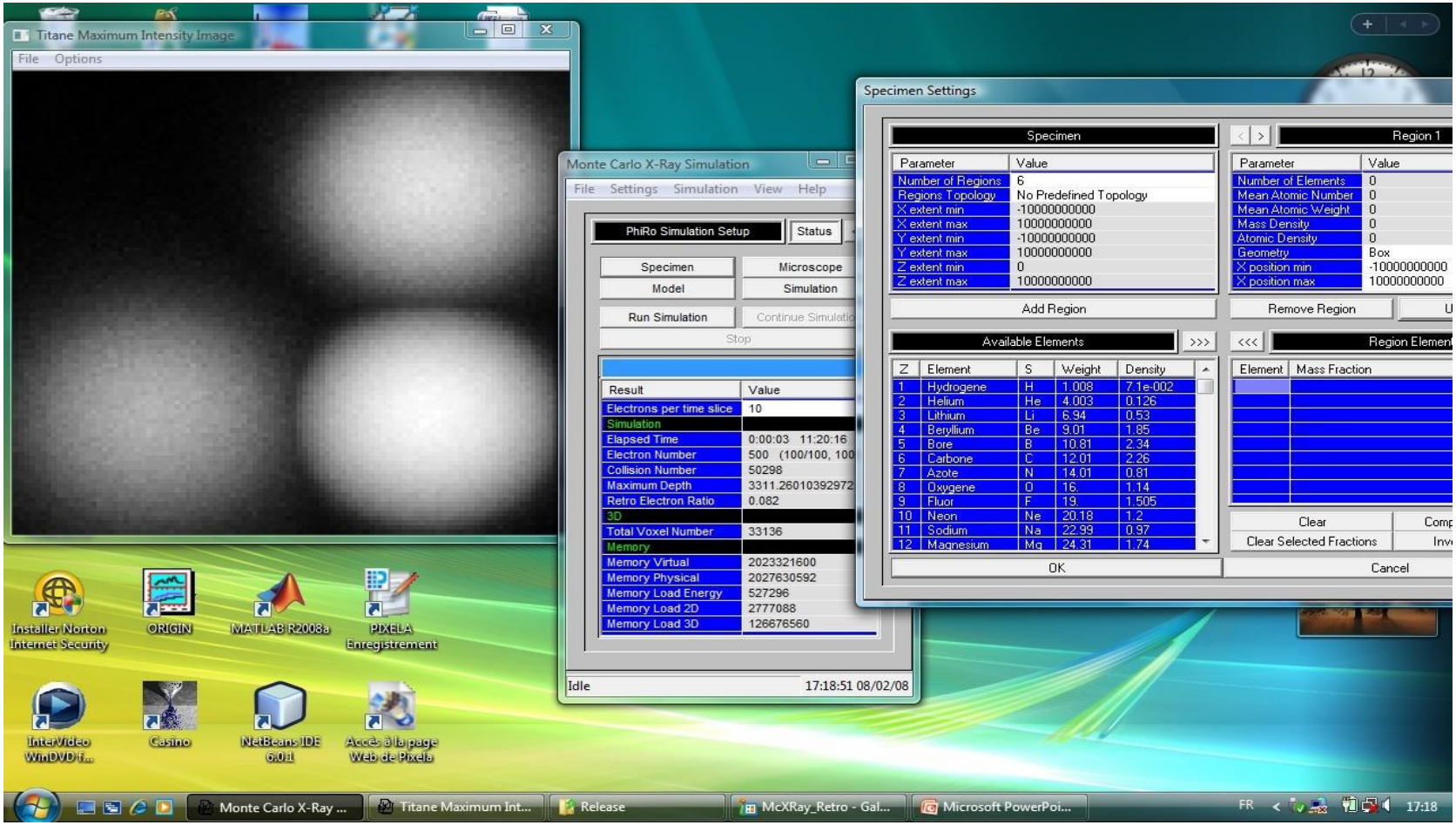

R. Gauvin and *P. Michaud* (2009), "MC X-Ray, a New Monte Carlo Program for Quantitative X-Ray Microanalysis of Real Materials", Microscopy and Microanalysis, 15 (Supp.2), p. 488-489.

Results – Map – W on C

1 µm W Sphere on C, 20 keV, 40° TOA

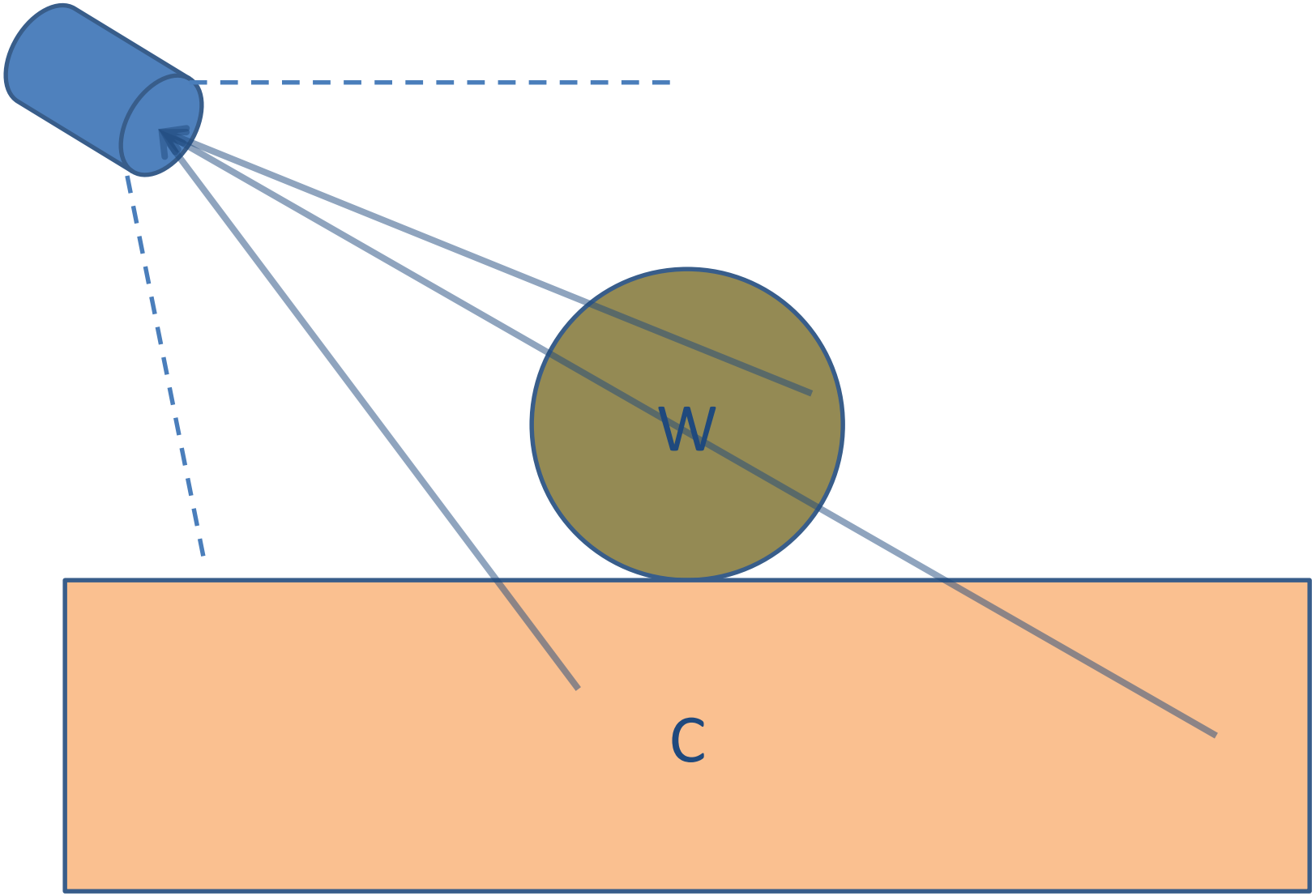

Results – Map – W on C

1 µm W Sphere on C, 20 keV, 40° TOA

C Kα1	W Mα
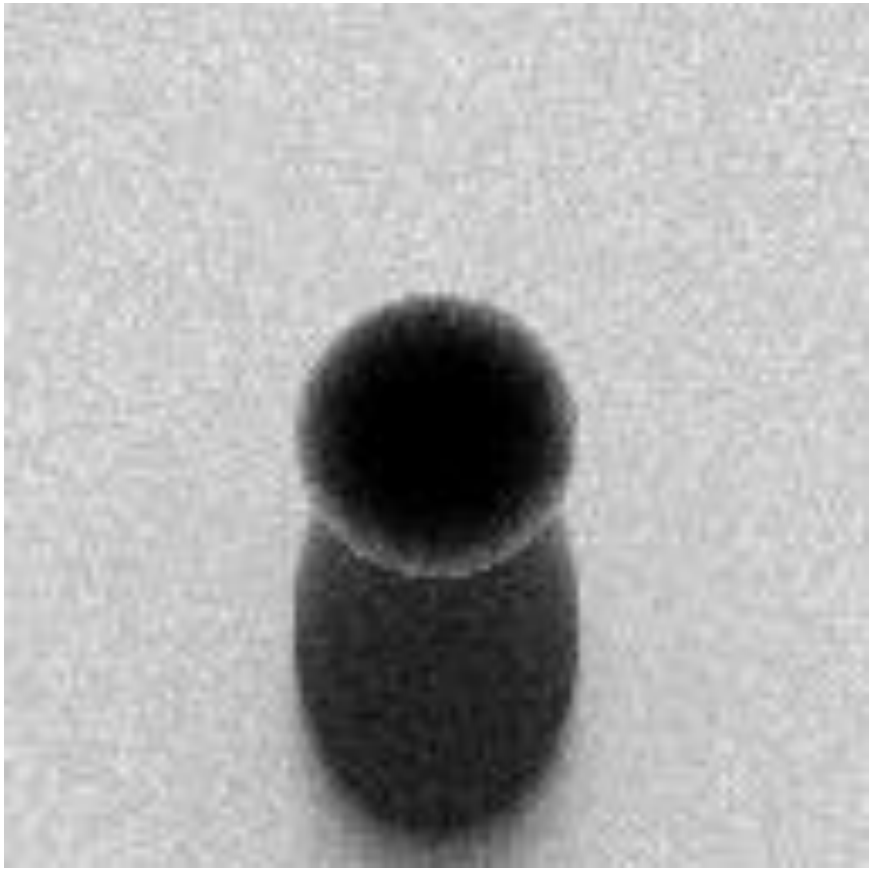	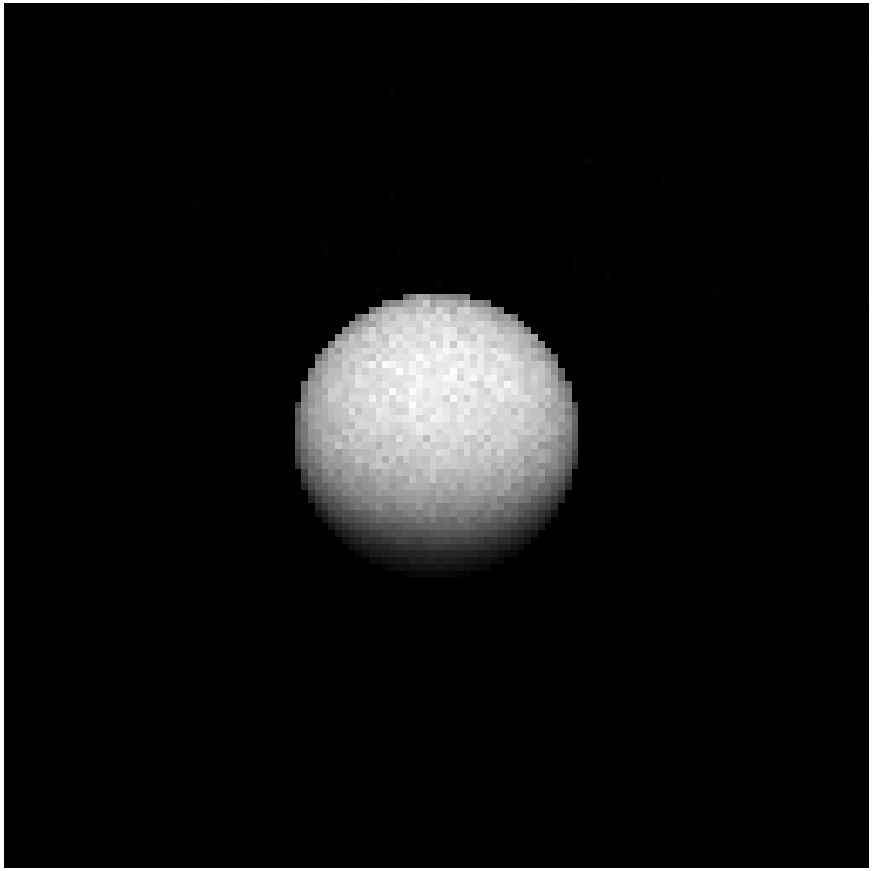

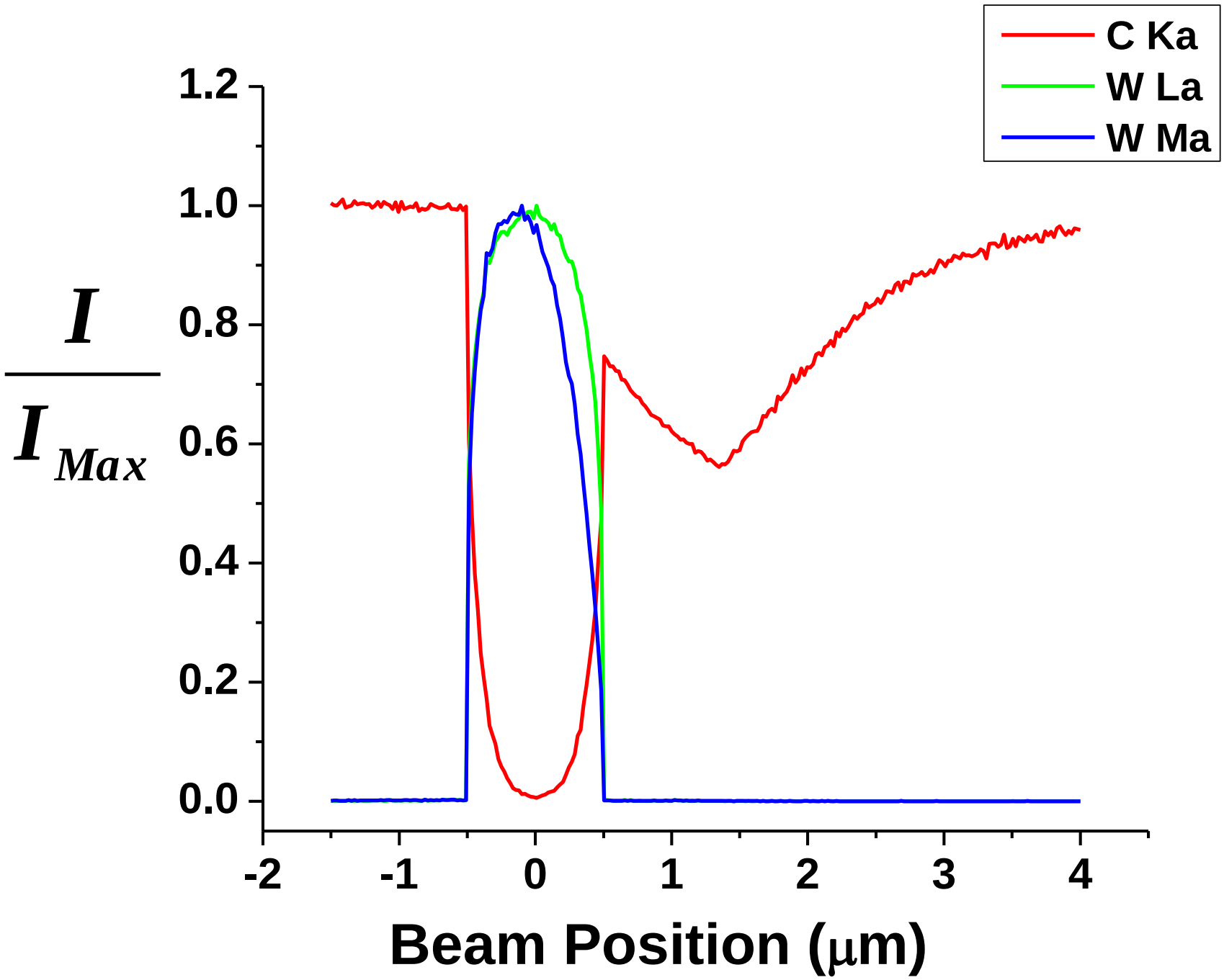
C Ka
W La
W Ma
1.2
1.0
0.8
0.6
0.4
0.2
0.0
-2
-1
0
1
2
3
4
I / I Max
Beam Position (μm)

C_{Al} = 0.0005, Al - Fe, 20 keV

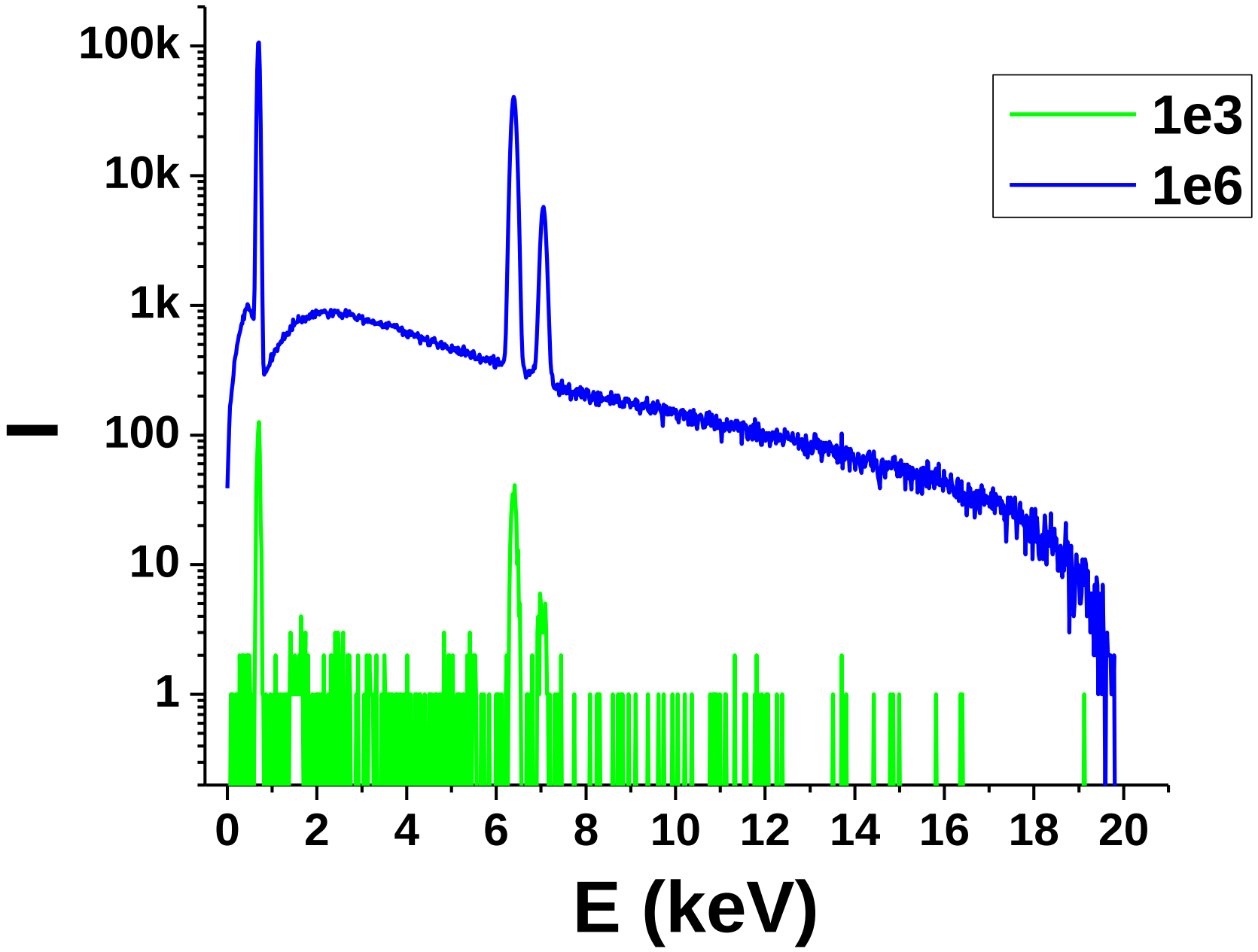

C_{Al} = 0.0005, Al - Fe, 20 keV

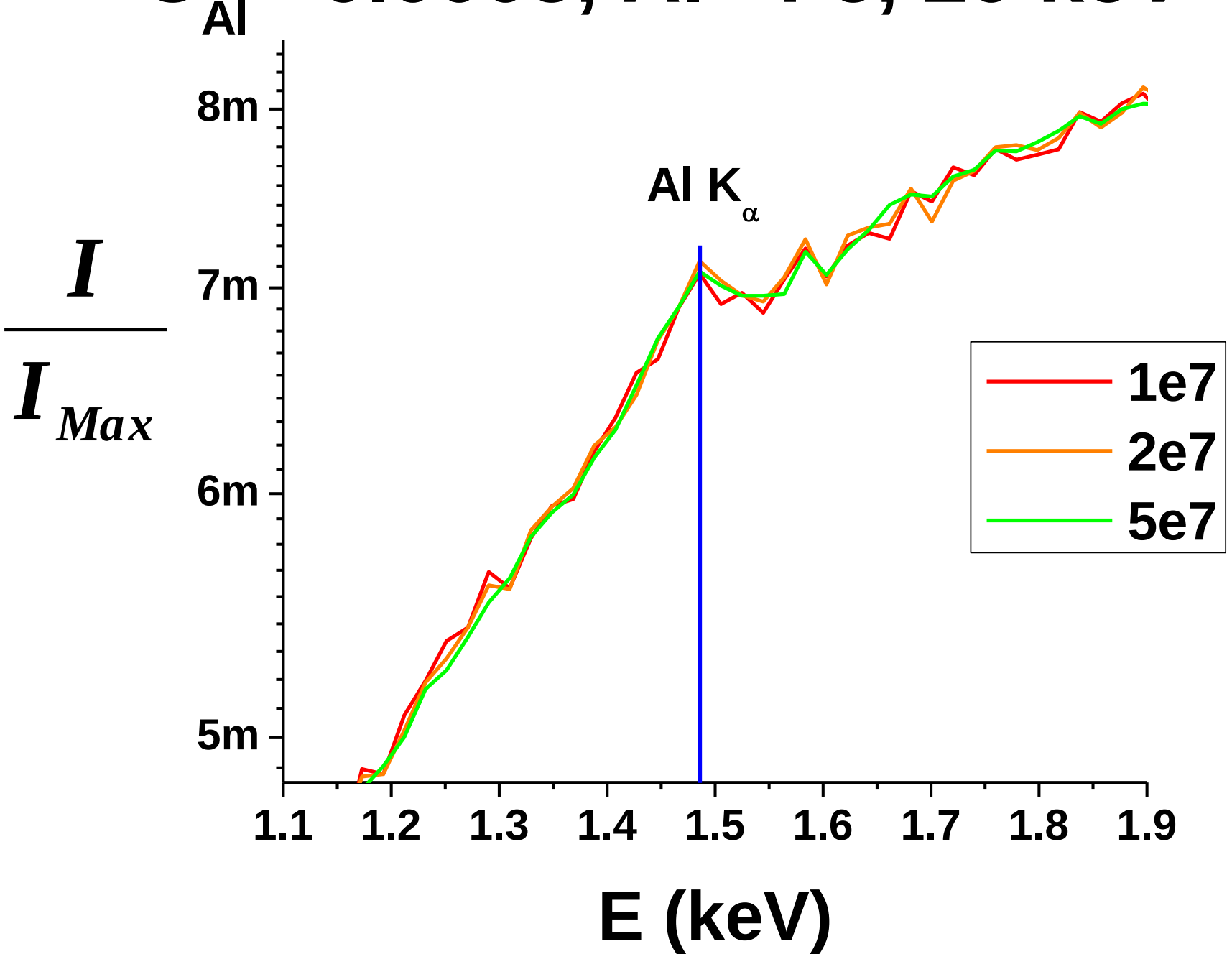

$$\frac{I}{I_{Max}}$$

Basse Tension MEB

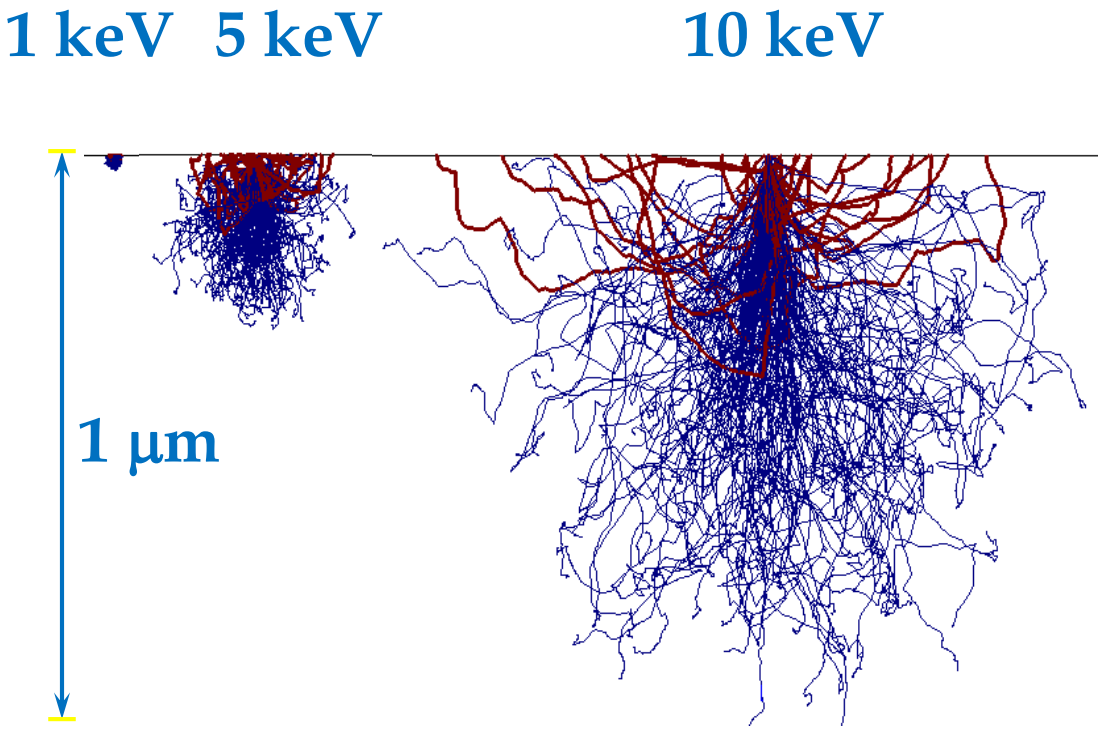

- Petit volume d'interaction
- Meilleure résolution spatiale
- Energie minimale dépends des raies disponibles.

Monte Carlo Simulations
10 nm MnS Inclusion in Fe

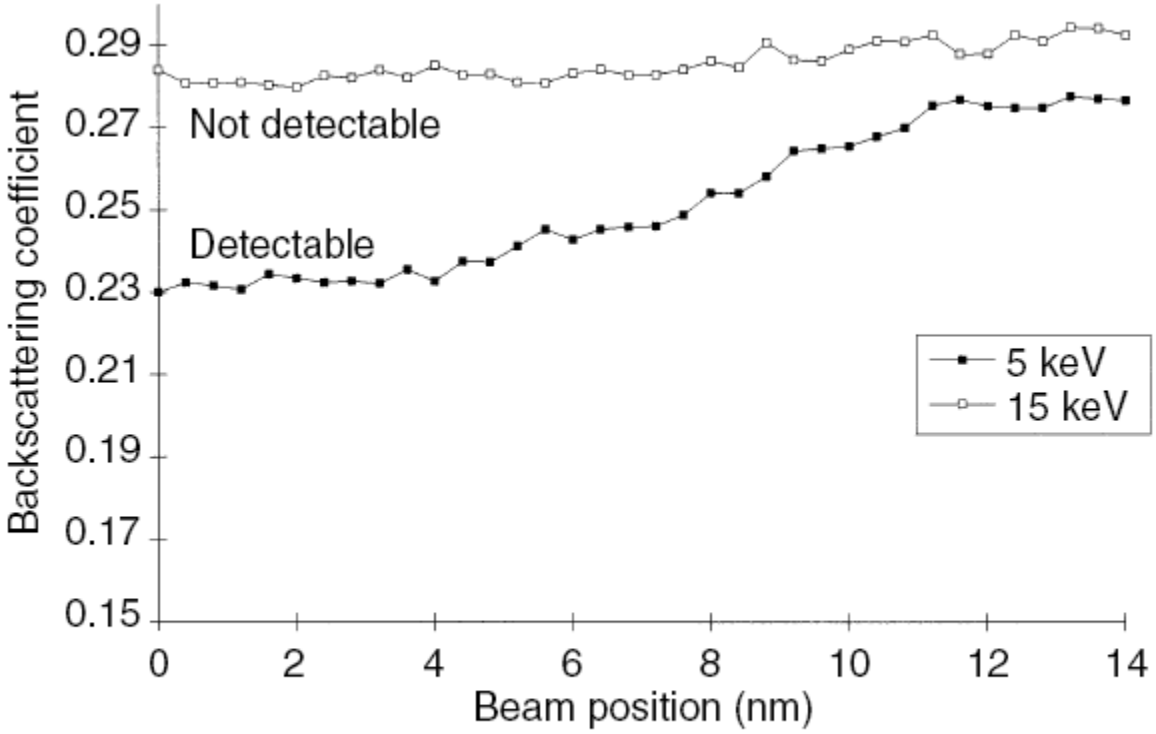

FIG. 24 Simulated profile for a 10 nm radius hemispherical inclusion of the MnS/Fe system at $E_o = 5$ and 15 keV.

R. Gauvin, P. Hovington, D.Drouin (1995) SCANNING, Vol. 17, 202–219.

Hitachi S-4500 (1996)

Nb(CN) Precipitates in Steel
S-4500

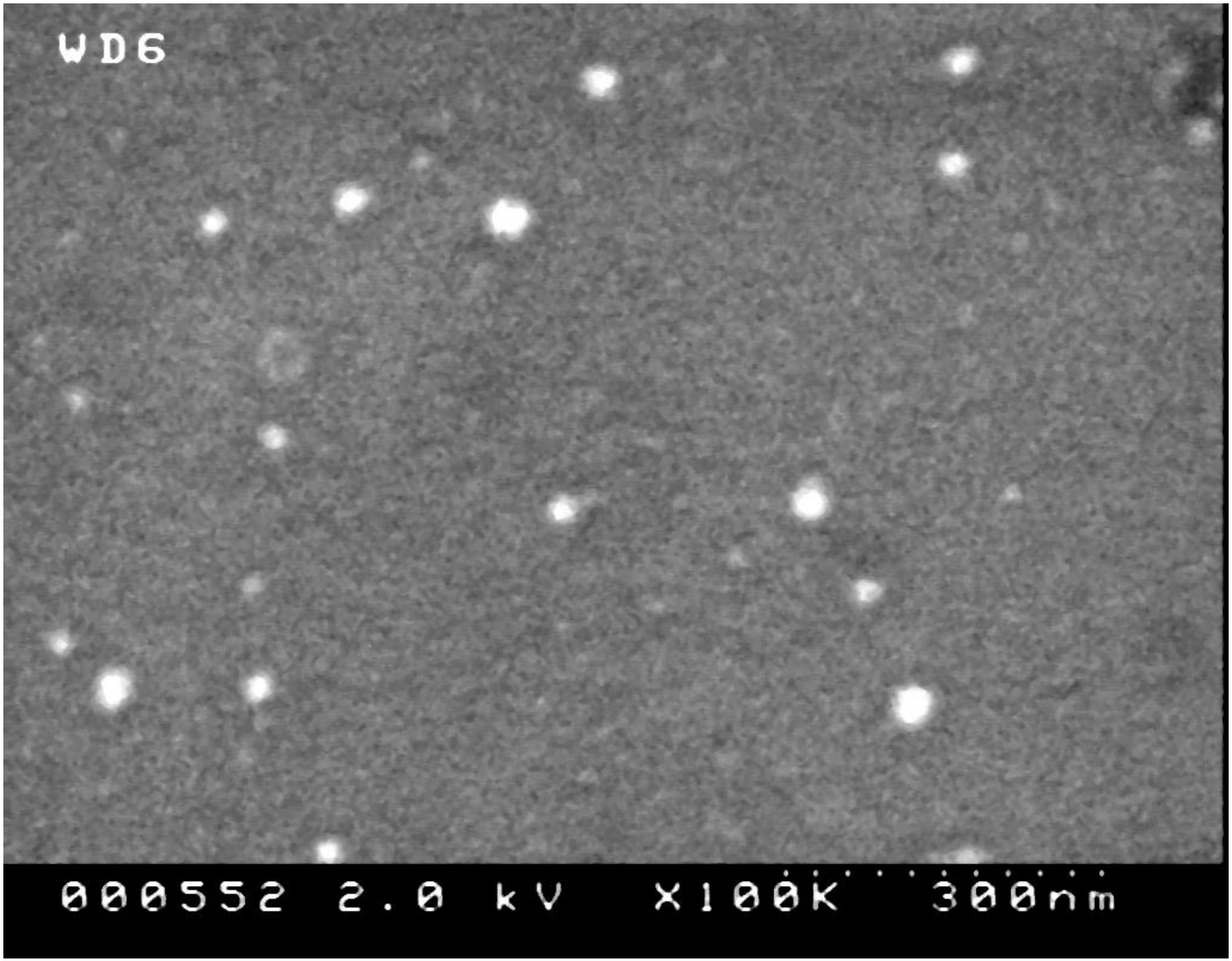

Etched Nb(CN) precipitates in Steel

70 nm, 5 keV

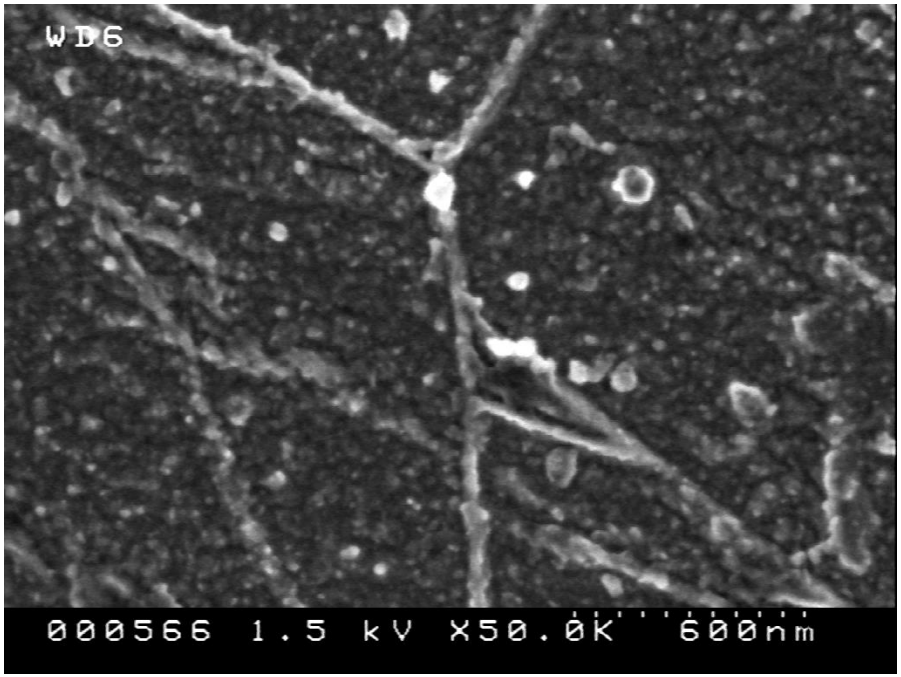

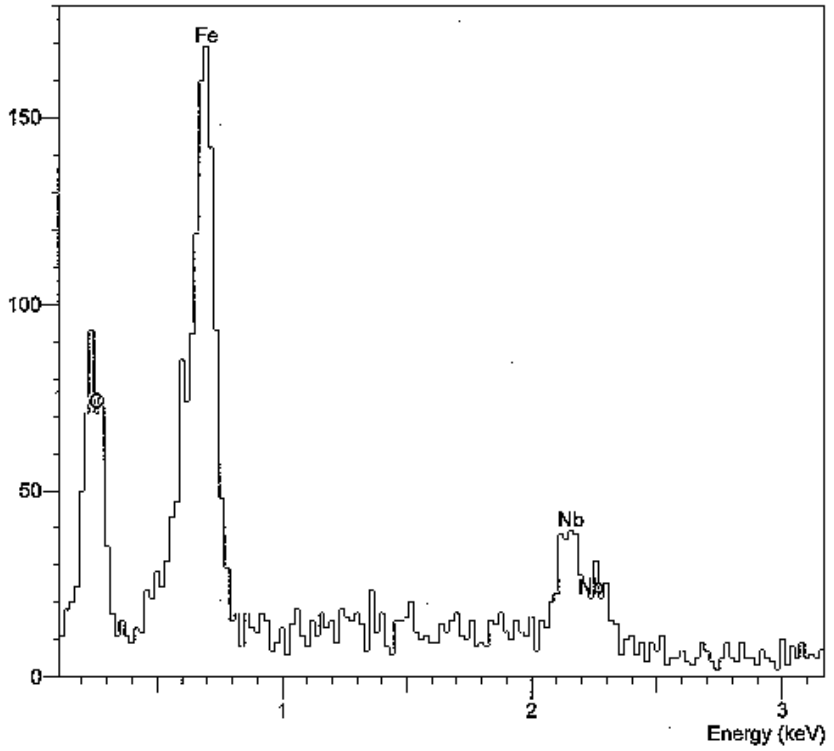

R. Gauvin and S. Yue (1997), "The observation of NbC precipitates in steel in the nanometer range using a field emission gun scanning electron microscope", Microscopy & Microanalysis, Vol. 3, Supp. 2, pp. 1243-1244.

HITACHI FE-SEM S-4700 (2001)

2.1 nm resolution at 1 kV

1.5 nm resolution at 15 kV

Cu on MWCN, 100 KX, 3 keV

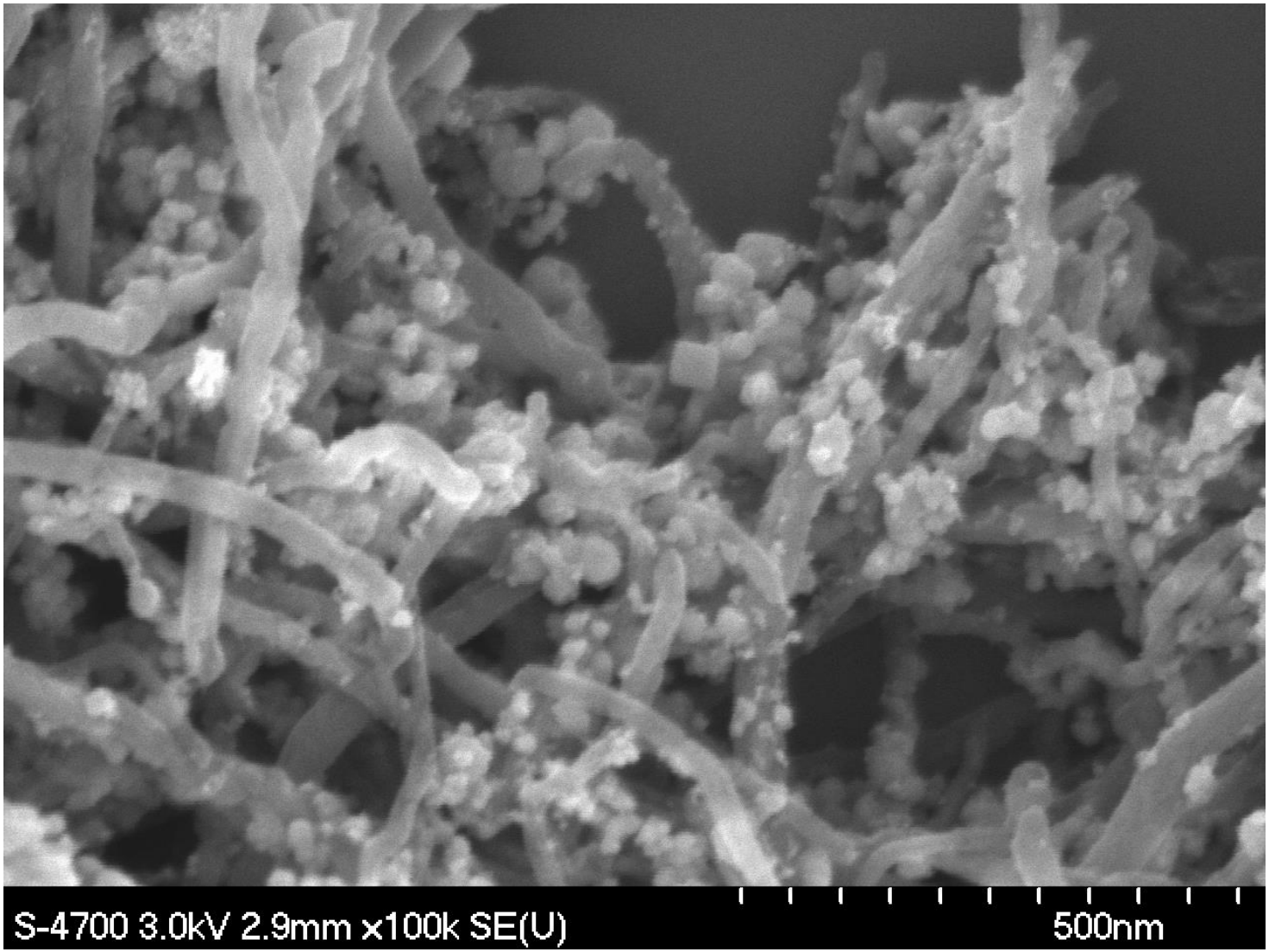

Low Voltage X-Ray Microanalysis
3 keV, INCA System

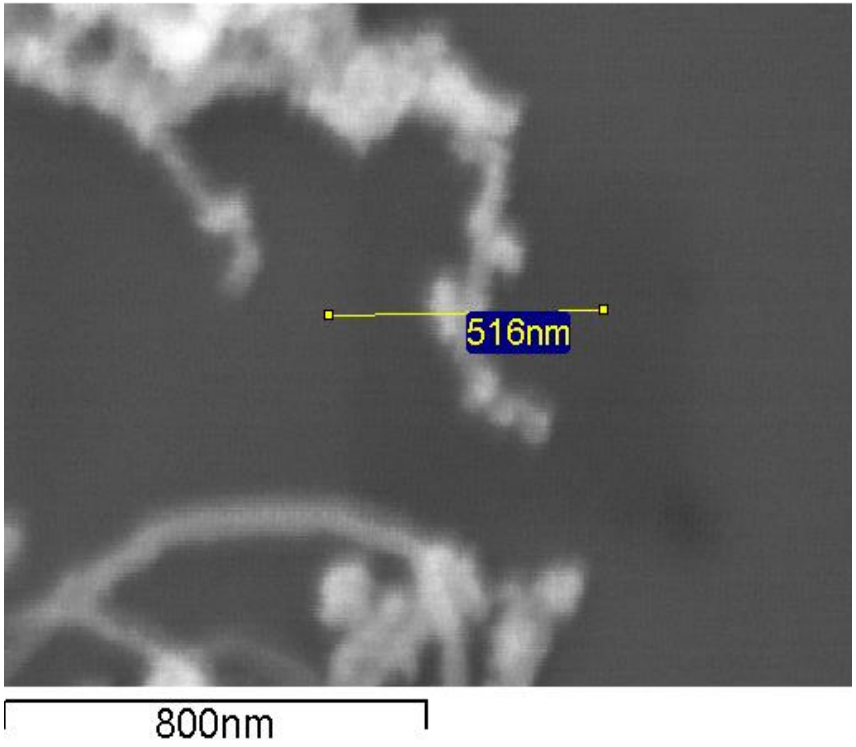

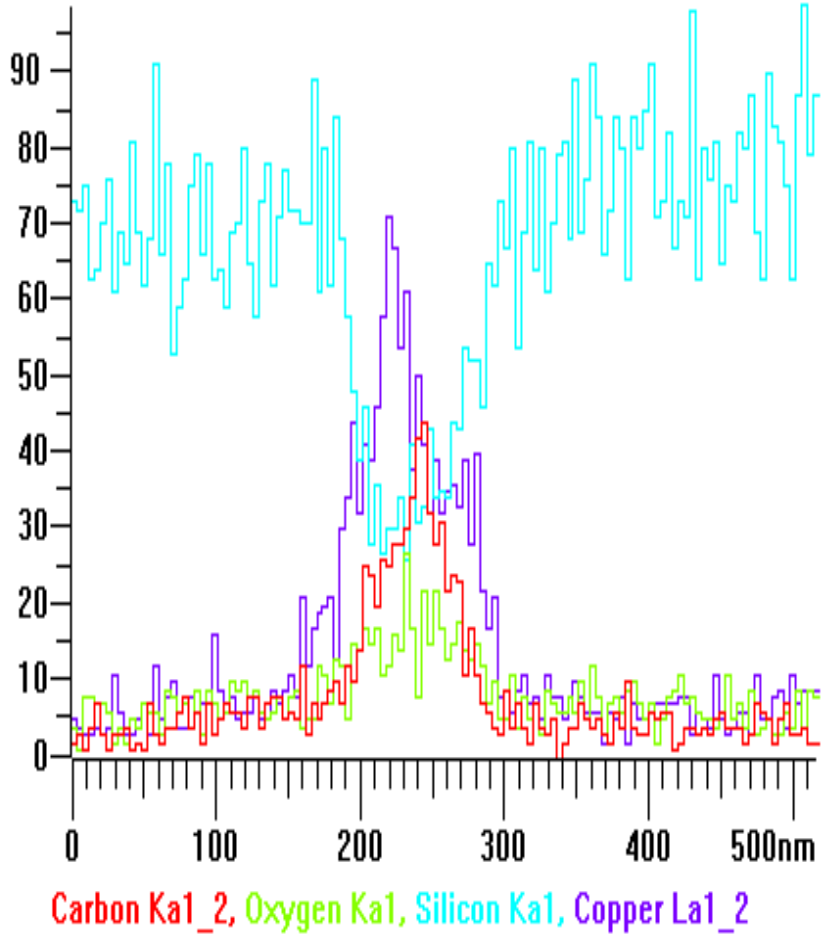

Hitachi Cold FE SU-8000 (2010)

0.5 nm resolution at 30 keV

2 nm resolution at 0.2 keV

HITACHI SU-8000

New

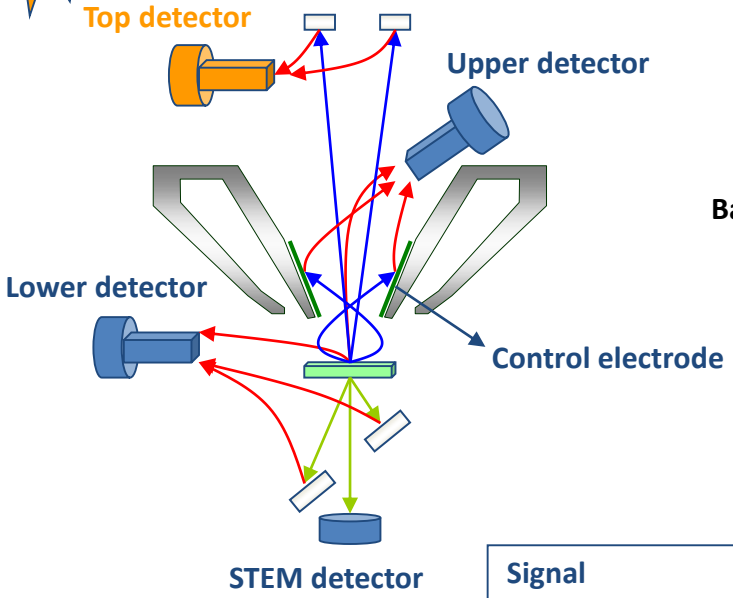

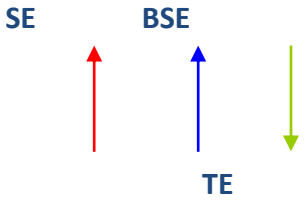

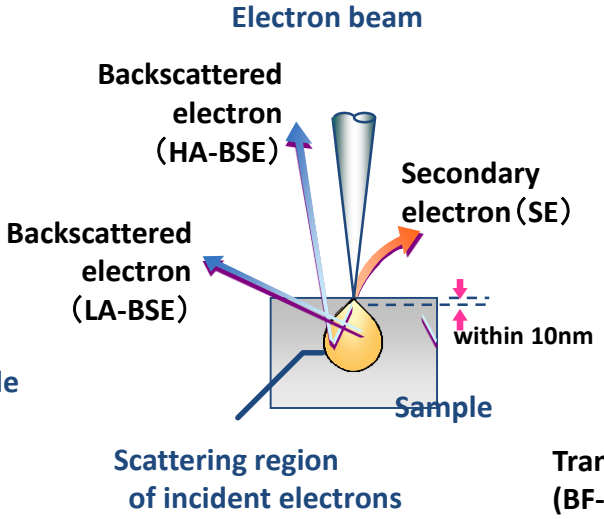

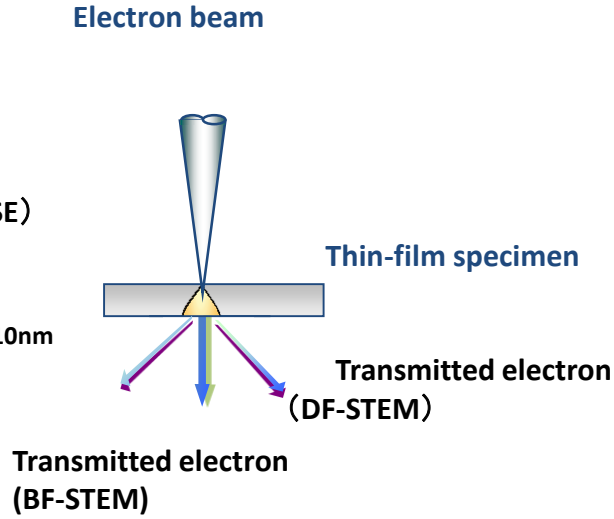

Signal	Abbrev.	Detector	Included information
Backscattered electron	HA-BSE	Top	Compositional + Crystal
Backscattered electron	LA-BSE	Upper	Compositional + Crystal +Topographical (with Charge reduction)
Secondary electron	SE	Upper	surface (incl. Voltage contrast)
Secondary electron	Lower	Lower	Topographical
Transmitted electron	BF-STEM	STEM	Internal + Crystallographic
Transmitted electron	DF-STEM	Lower	Internal + Compositional

Al_2O_3 Spheres

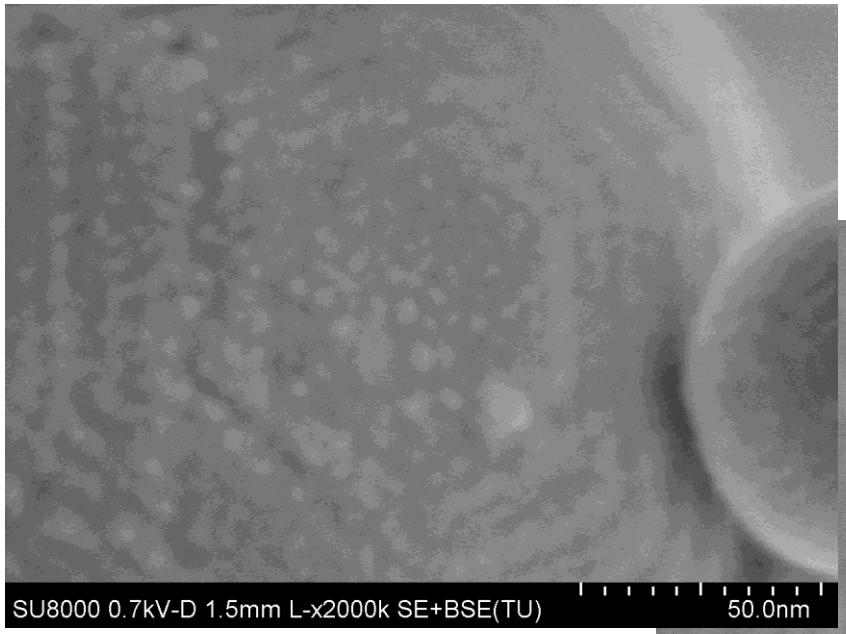

SE+BSE(TU)
FOV: 173 nm
SNR: 3.5
Resolution: 1.9 nm

SE(T)F100
FOV: 253 nm
SNR: 2.9
Resolution: 2.5 nm

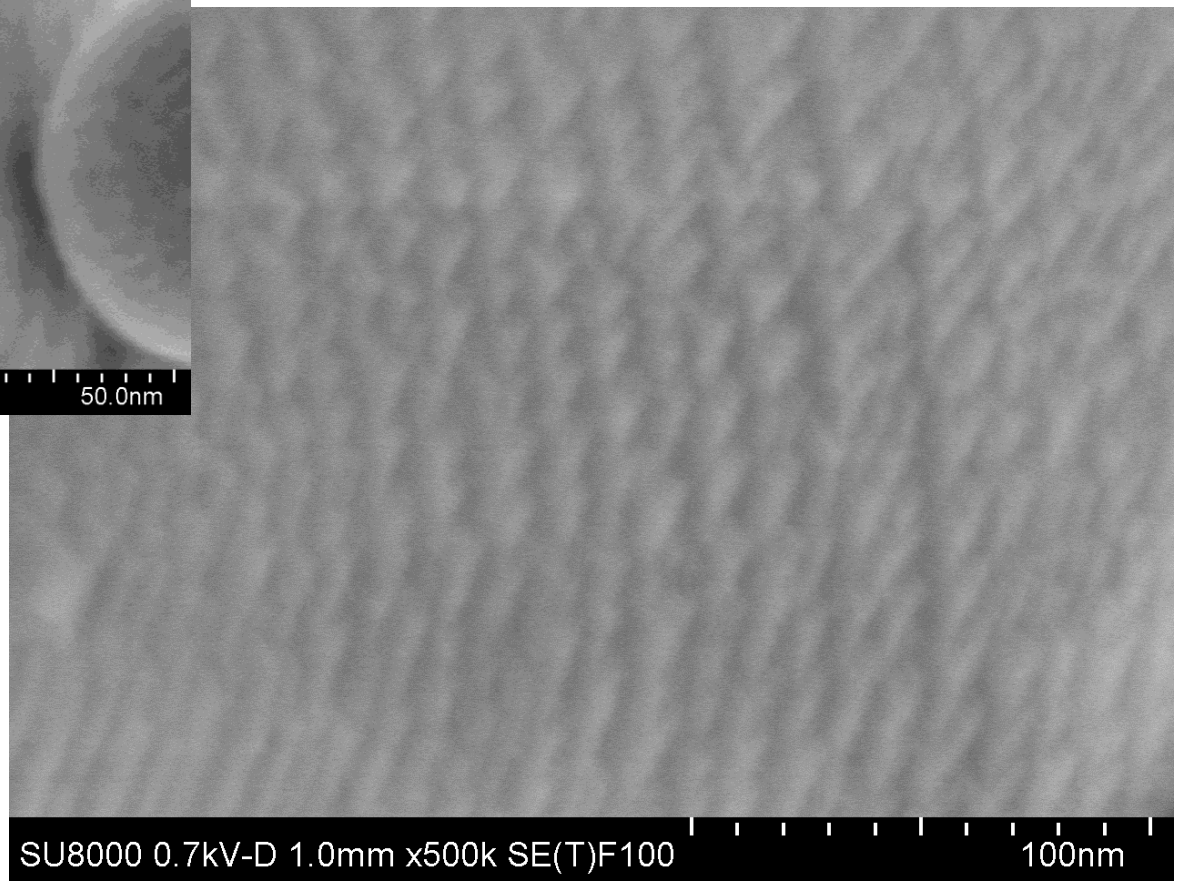

NordlysS EDSD System

EBSD Feuilles de Li

N. Brodusch, K. Zaghib and R. Gauvin (2014), “Electron Backscatter Diffraction Applied to Lithium Sheets Prepared by Broad Ion Beam Milling”, Microscopy Research and Technique, in press.

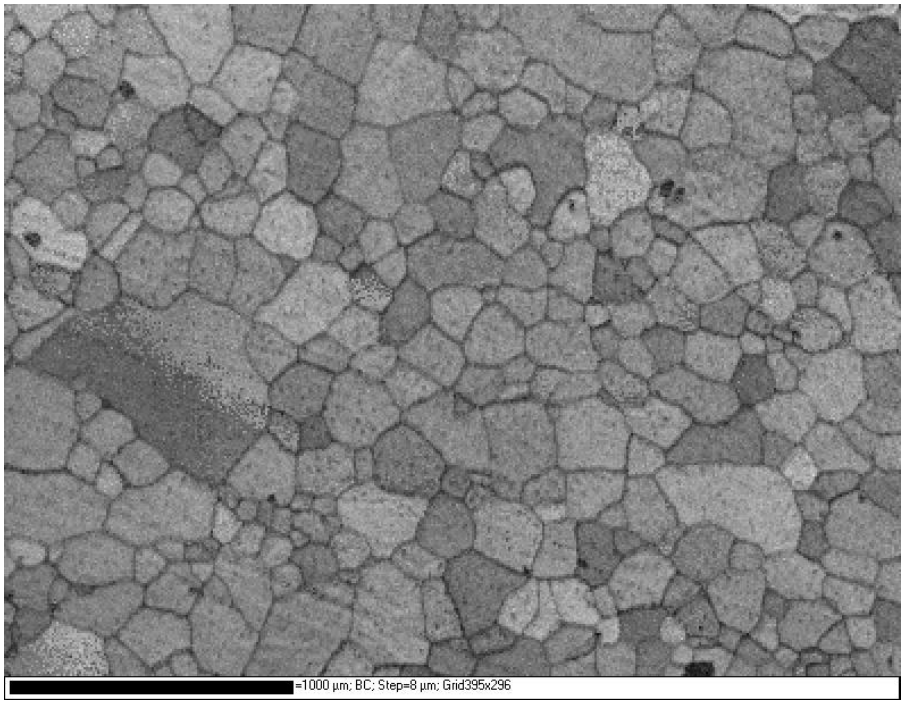

Band contrast map

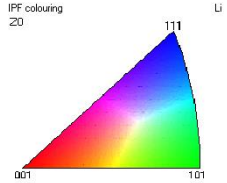

Inverse pole figure map

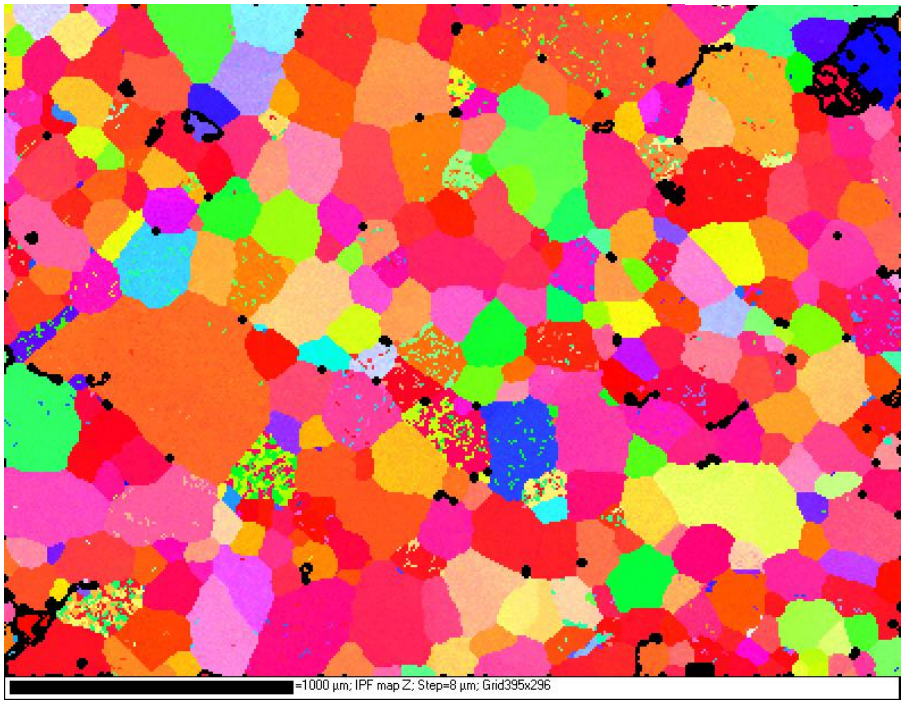

Channelling

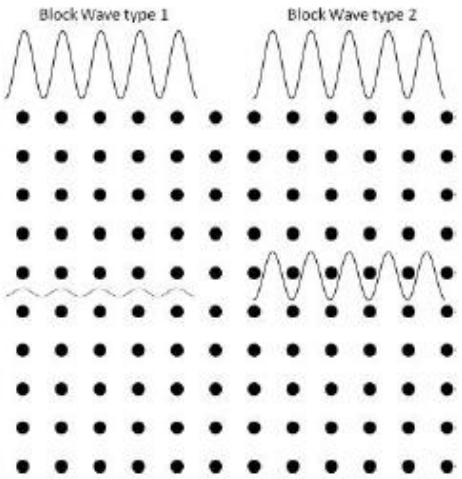

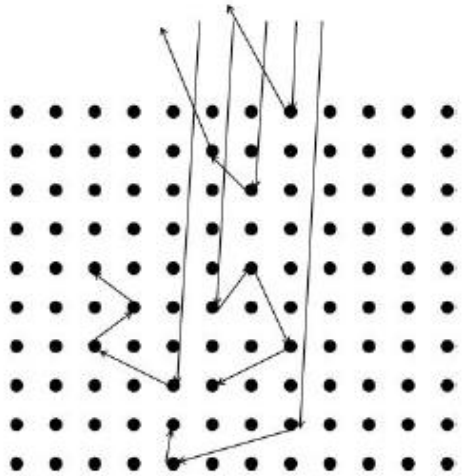

Low retrodiffusion yield

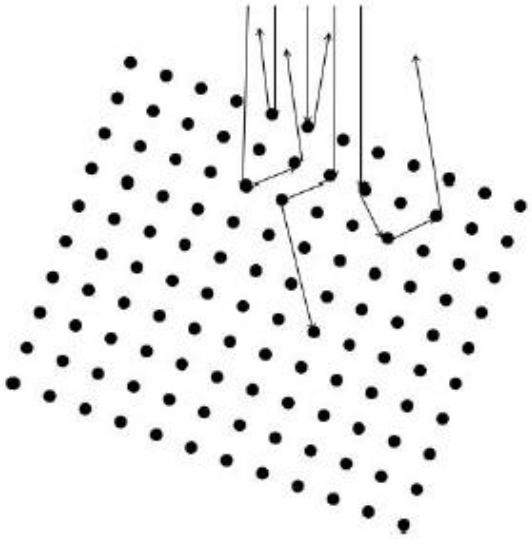

High retrodiffusion yield

Channeling contrast 1 kV (Zr Alloy)

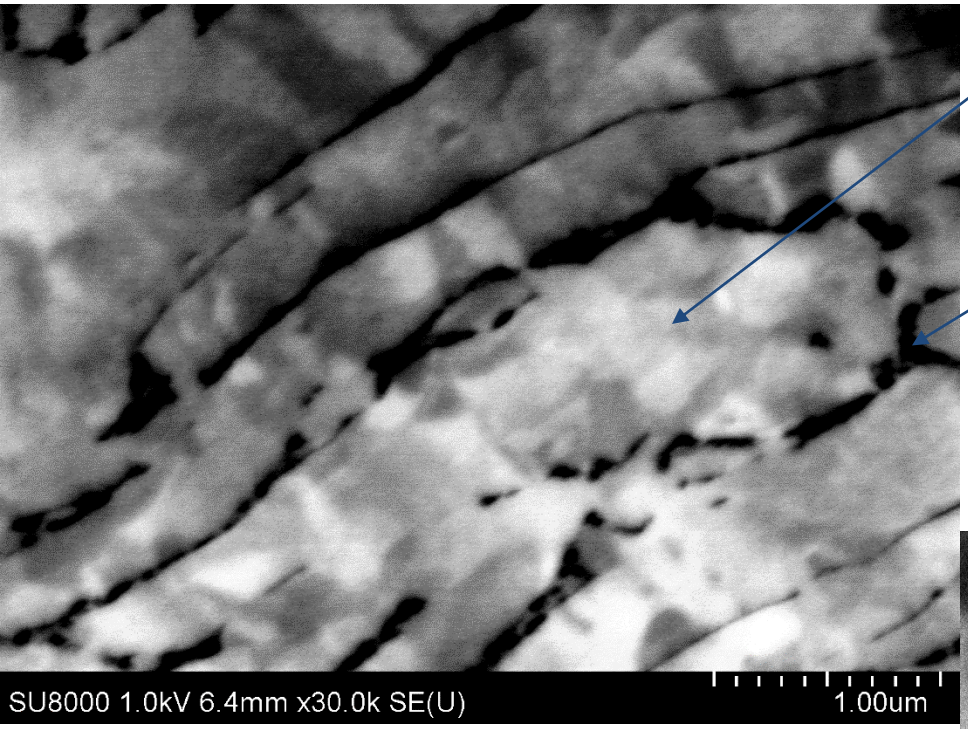

α phase

β phase

BackScattered Electrons (PD-BSE detector)

Secondary Electrons (Upper detector)

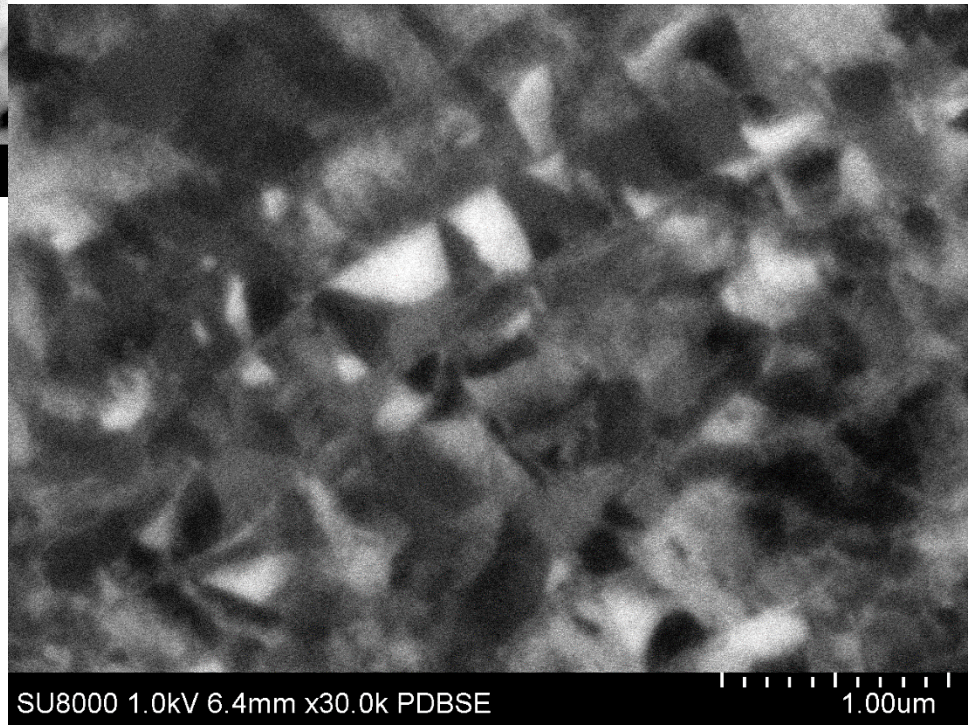

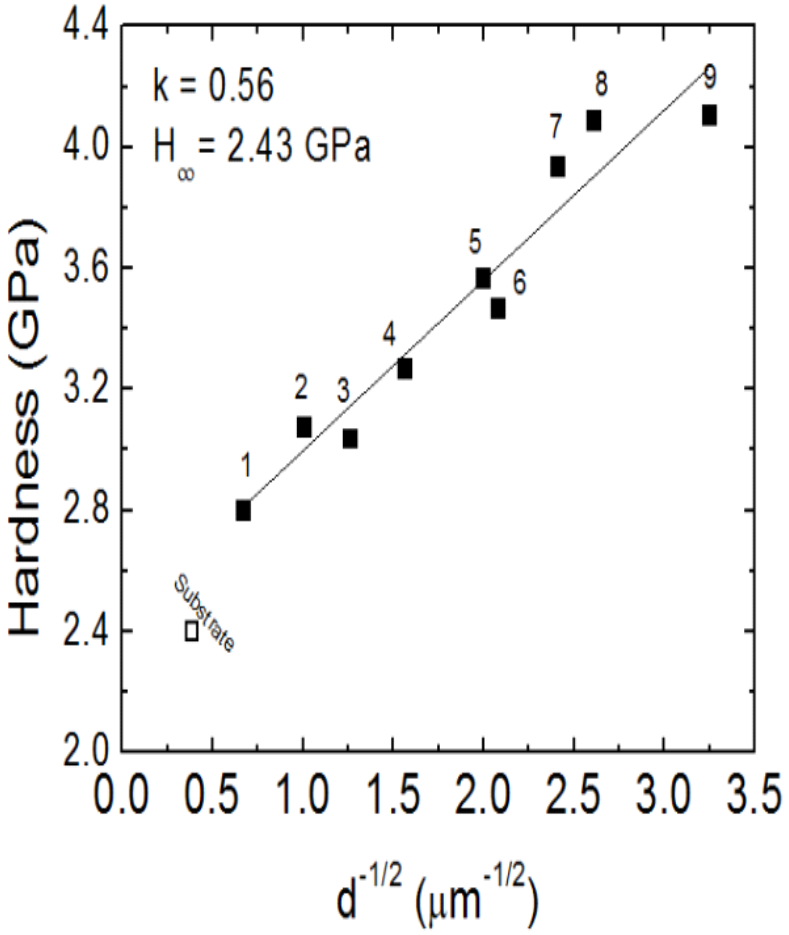

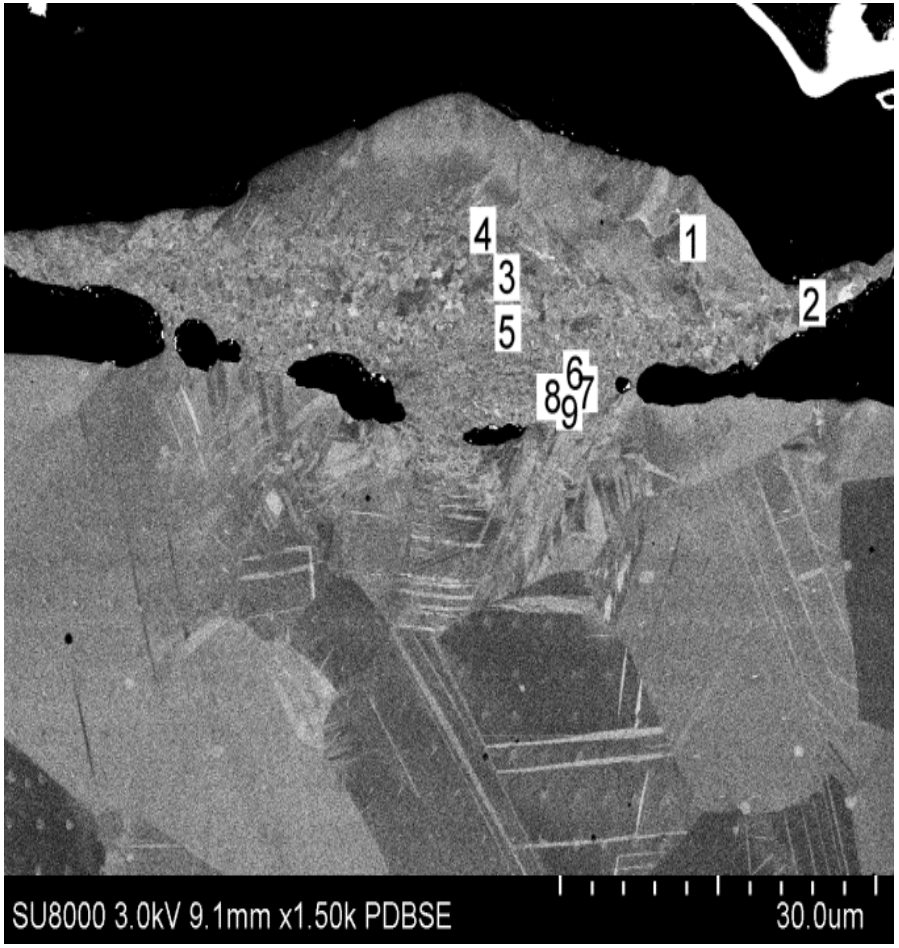

Dina Goldbaum, Richard R. Chromik, Nicolas Brodusch and Raynald Gauvin (2014), Microscopy and Microanalysis, in press.

X-Max

400000 cps @ 80 mm2

In practice

Detector area	20mm²	50mm²	80mm²
Resolution (eV):			
MnK_{α} resolution	129	129	129
Operating angle	0° to 45°		
Temperature range	10°C to 30°C		
Altitude	Sea level to 1,500m		

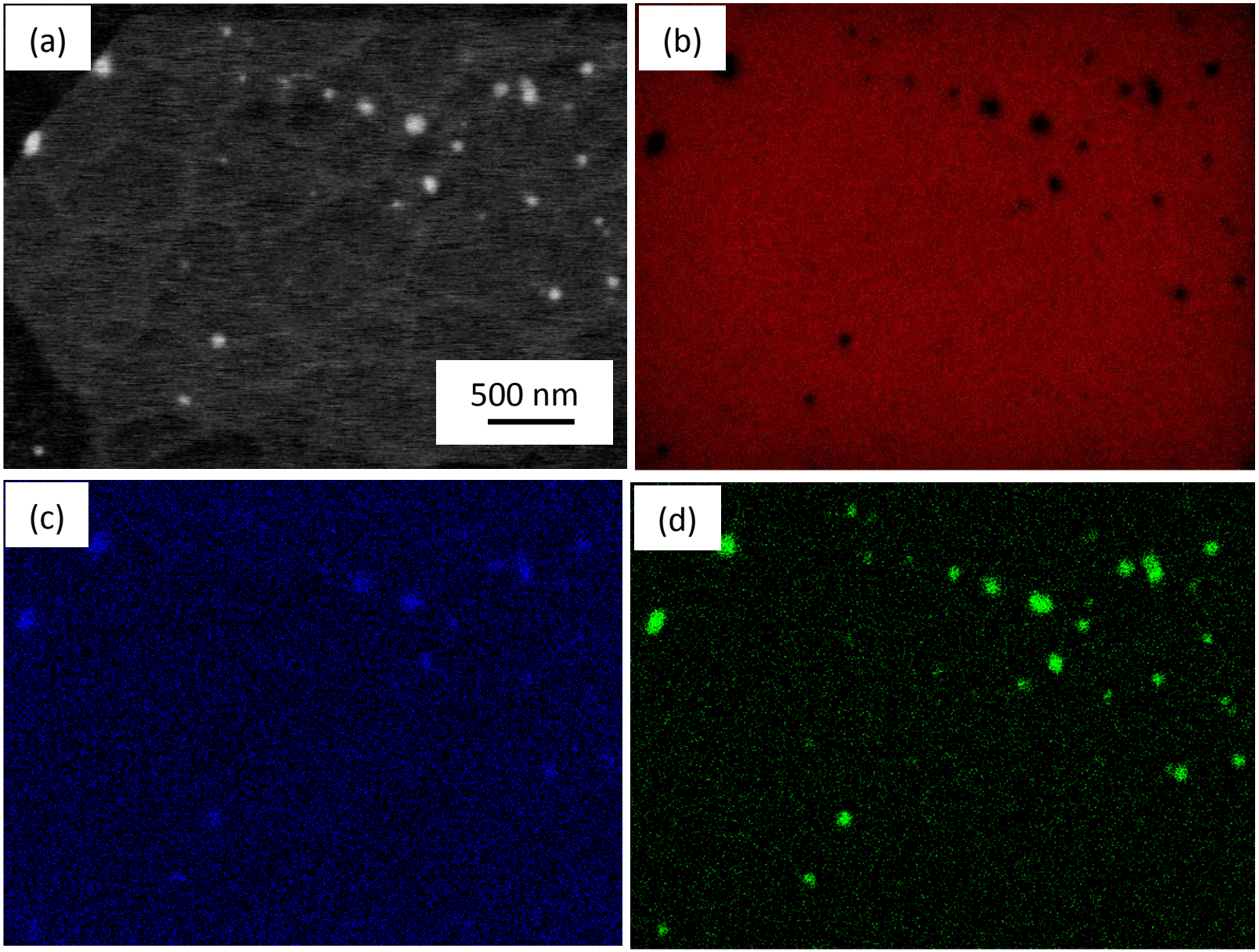

Figure 7. (a) SEM-BSE image, (b) Mg, (c) Al and (Ca) X-ray maps

Al_3Zr Precipitate, 3 kV, Al 2099

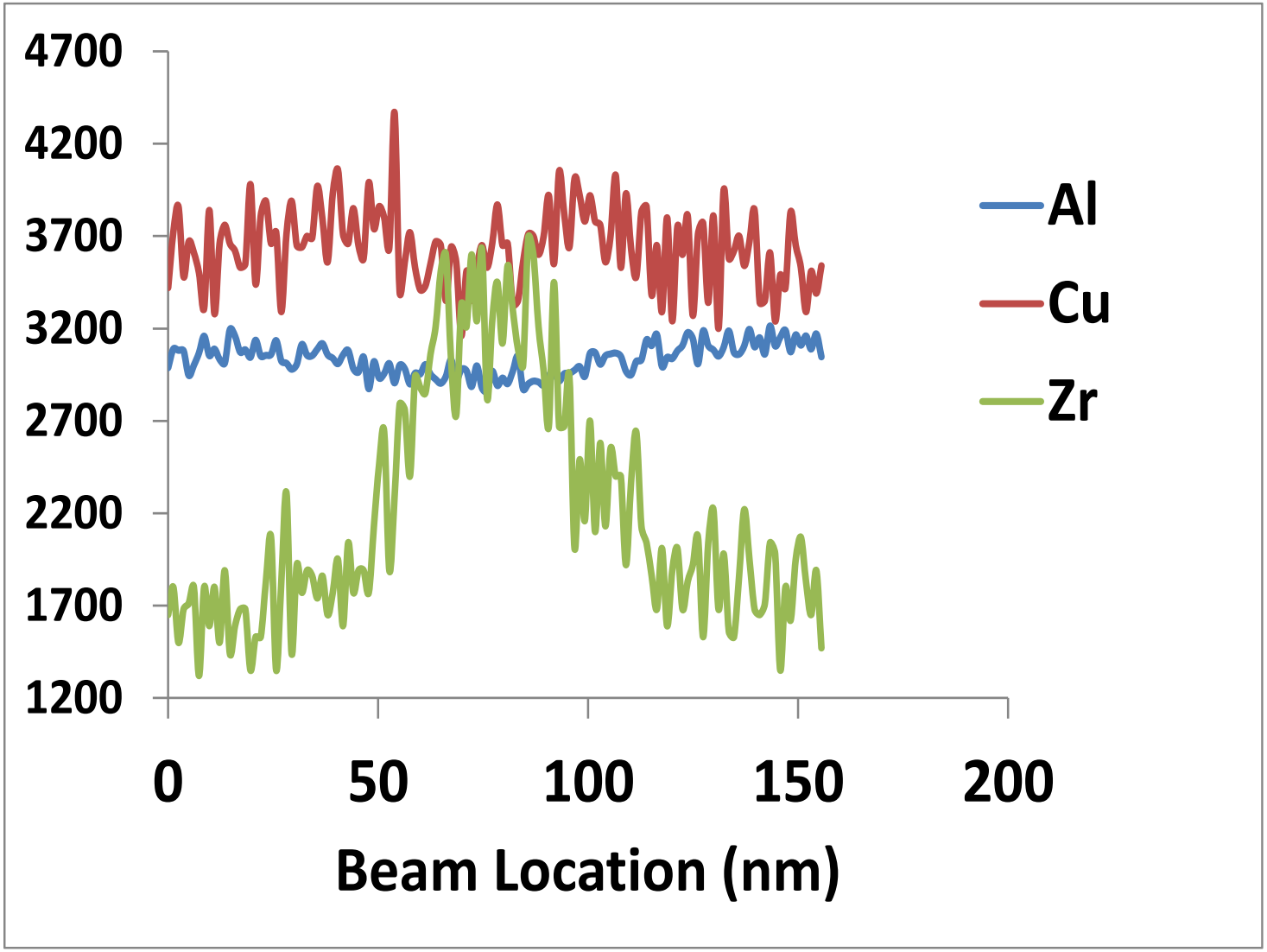

SU-8000 Cold Field Emission SEM

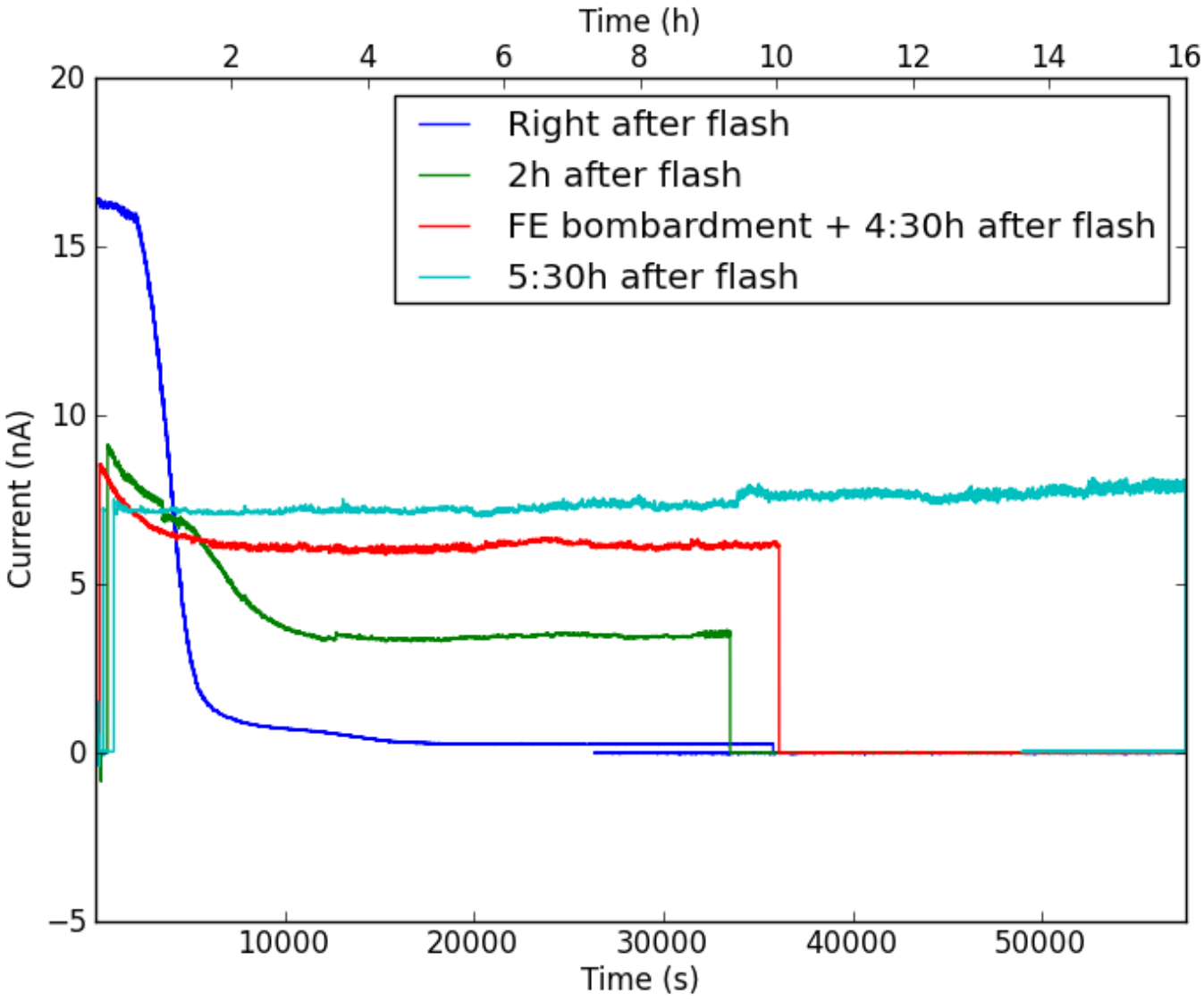

Quantitative Analysis in the SEM

$$\frac{C_i}{C_{(i)}} = [ZAF]_i \frac{I_i}{I_{(i)}} = [ZAF]_i k_i$$

$$\frac{C_i}{C_{(i)}} = \frac{\left[\int_0^\infty \varphi(\rho z) e^{-\chi \rho z} d\rho z\right]_{(i)}}{\left[\int_0^\infty \varphi(\rho z) e^{-\chi \rho z} d\rho z\right]_i} k_i$$

Same Fluorescence correction in both methods, if necessary.

Both $\varphi(\rho z)$ curves normalized for the same thin foil

X-Ray Microanalysis
Cliff and Lorimer Method

$$\frac{C_A}{C_B} = K_{AB} \frac{I_A}{I_B}$$

No X-Ray Absorption and Fluorescence

G. Cliff & G. W. Lorimer (1975), Journal of Microscopy, Vol. 103, pp. 203 – 207.

Quantitative X-Ray Microanalysis
The f Ratio Method

$$f_A = \frac{I_A}{I_A + I_B}$$

P. Horny, E. Lifshin, H. Campbell and R. Gauvin (2010), “Development of a New Quantitative X-Ray Microanalysis Method for Electron Microscopy”, Microscopy & Microanalysis, Vol. 16, No. 6, pp. 821-830.

Generalization of the Method

$$f_i = \frac{I_i}{\sum_{j=1}^{n} I_j}$$

$$f_i = \frac{1}{\sum_{j=1}^{n} F_{ji} \frac{c_j}{c_i}}$$

$$F_{ji} = K_{ij} \frac{\gamma_j}{\gamma_i} \frac{(1 + \delta_c + \delta_{BF})_j}{(1 + \delta_c + \delta_{BF})_i}$$

$$K_{ij} = \Lambda_{\mathrm{ij}} \frac{Q_j \omega_j \alpha_j (1 + T_j) \varepsilon_j A_i}{Q_i \omega_i \alpha_i (1 + T_i) \varepsilon_i A_j}$$

$$\gamma_i = \int_0^{t \; or \; \infty} \varphi(\rho z) \, e^{-\left(\sum_{j=1}^{n} c_j \frac{\mu}{\rho}\right]_j^i \right) cosec\psi \rho z} \, d\rho z$$

$$In \; TEM, \varphi(\rho z) \cong 1$$

Computation with adjusted factor

$$f_A = \frac{(I_A)^S}{(I_A)^S + \Lambda_{A-B}(I_B)^S}$$

Computation of calibration factor

$$f_A = \frac{I_A}{I_A + I_B}$$

$$\Lambda_{A-B} = \left(\frac{1 - f_A}{f_A}\right)^M \left(\frac{f_A}{1 - f_A}\right)^S$$

R. Gauvin (2012), "What remains to be done to allow Quantitative X-Ray Microanalysis to become a Characterization Technique used with every EDS Spectra Acquired?", **Invited Paper**, Microscopy & Microanalysis, 18, 5, pp. 915 - 940.

f Ratio Method

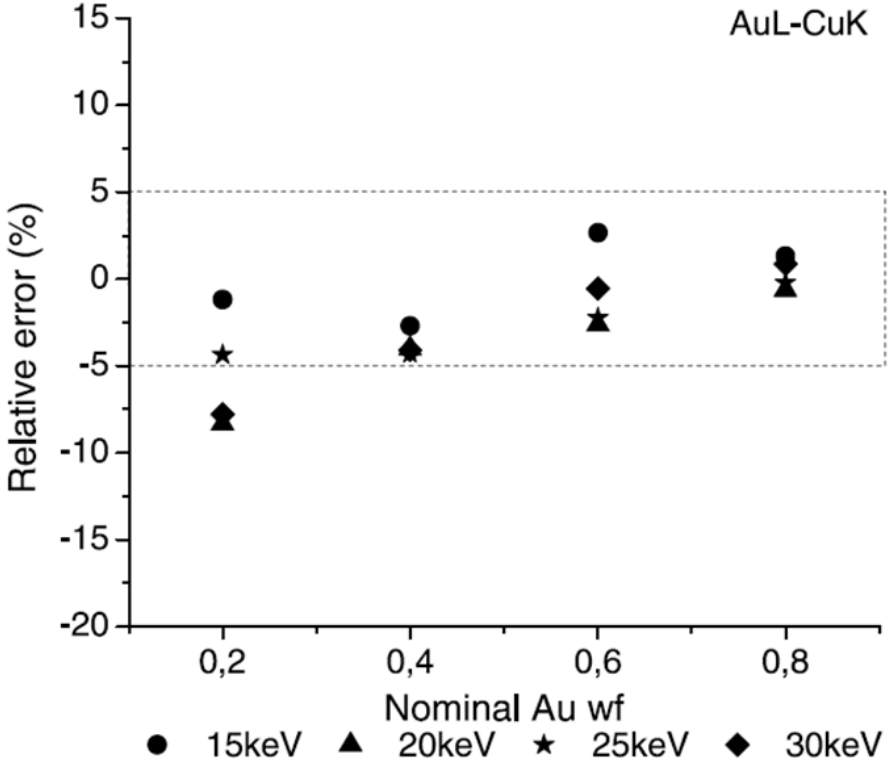

Standardless

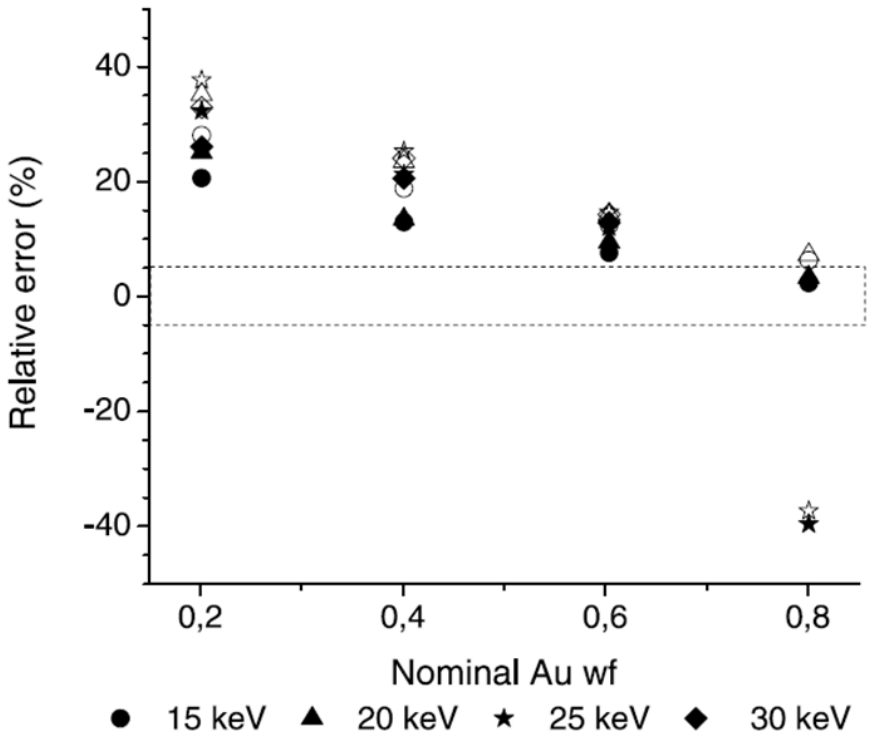

Mg – Al Diffusion Couple

Mg **γ – $Al_{12}Mg_{17}$** **β – Al_3Mg_2** **Fe in Al** **Al**

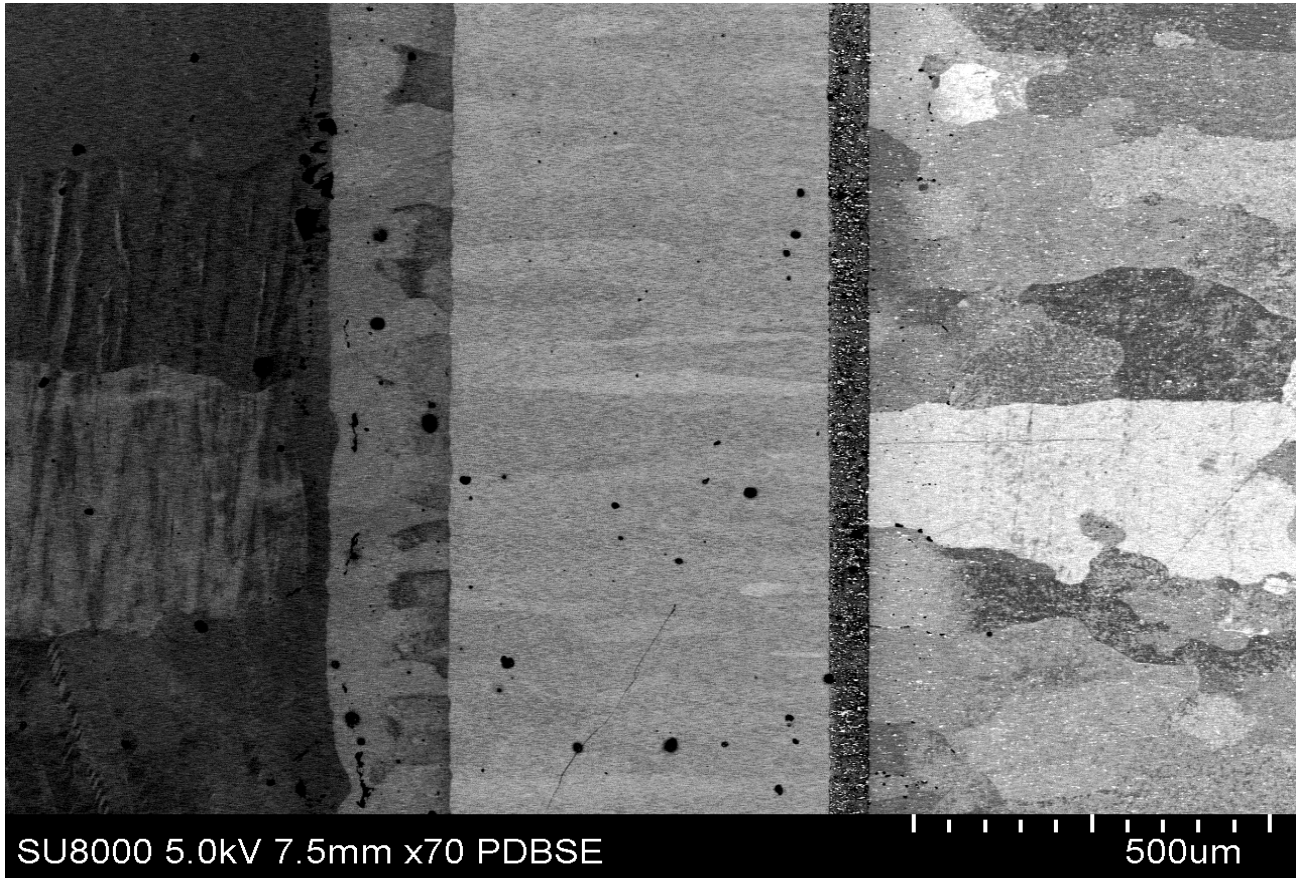

R. Gauvin, N. Brodusch, P. Michaud (2012). "Determination of Diffusion Coefficients with Quantitative X-Ray Microanalysis at High - Spacial Resolution". Defect and Diffusion Forum. Vol - 323-325, pp. 61-67.

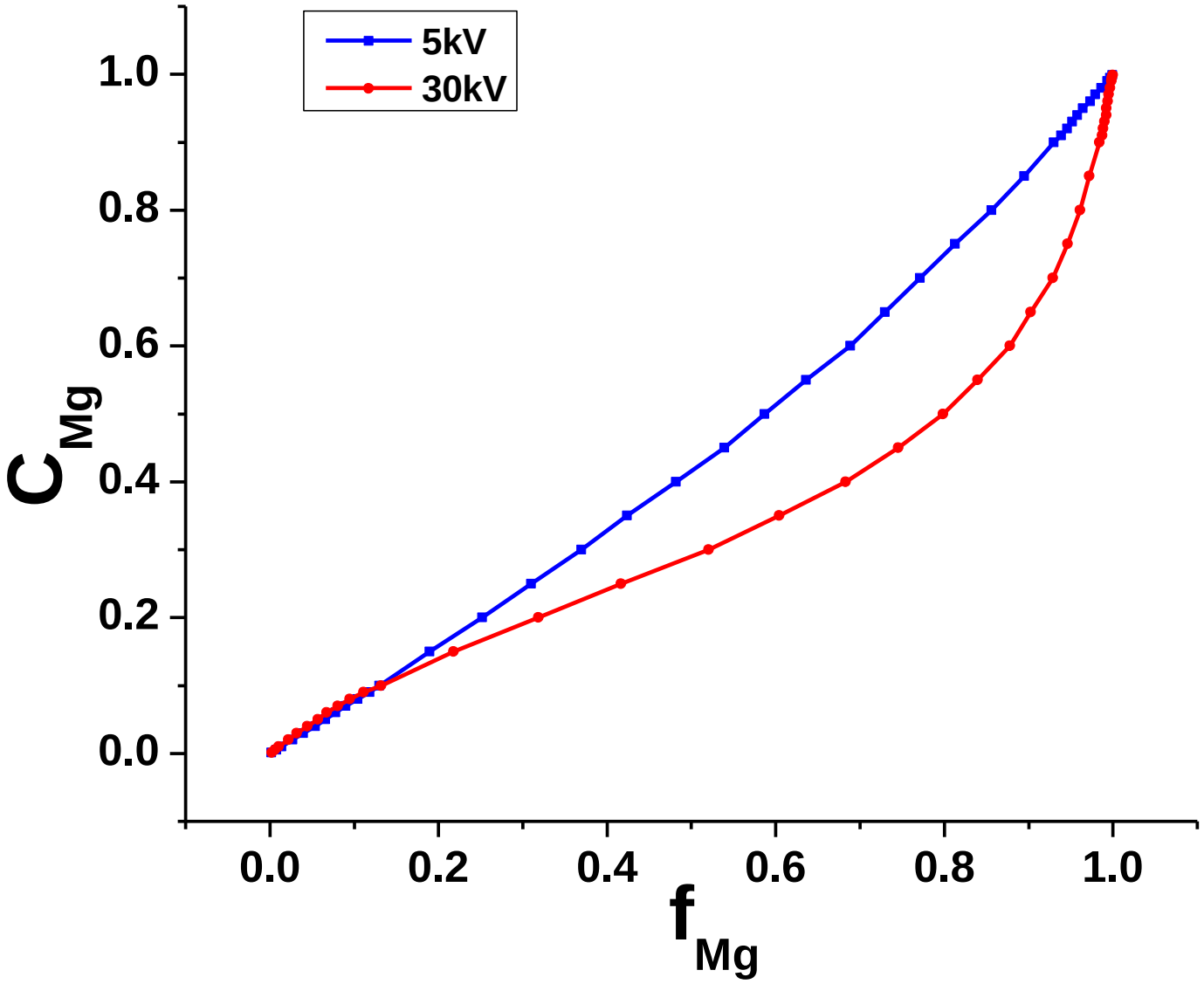
5kV
30kV
1.0
0.8
0.6
0.4
0.2
0.0
C Mg
0.0
0.2
0.4
0.6
0.8
1.0
f Mg

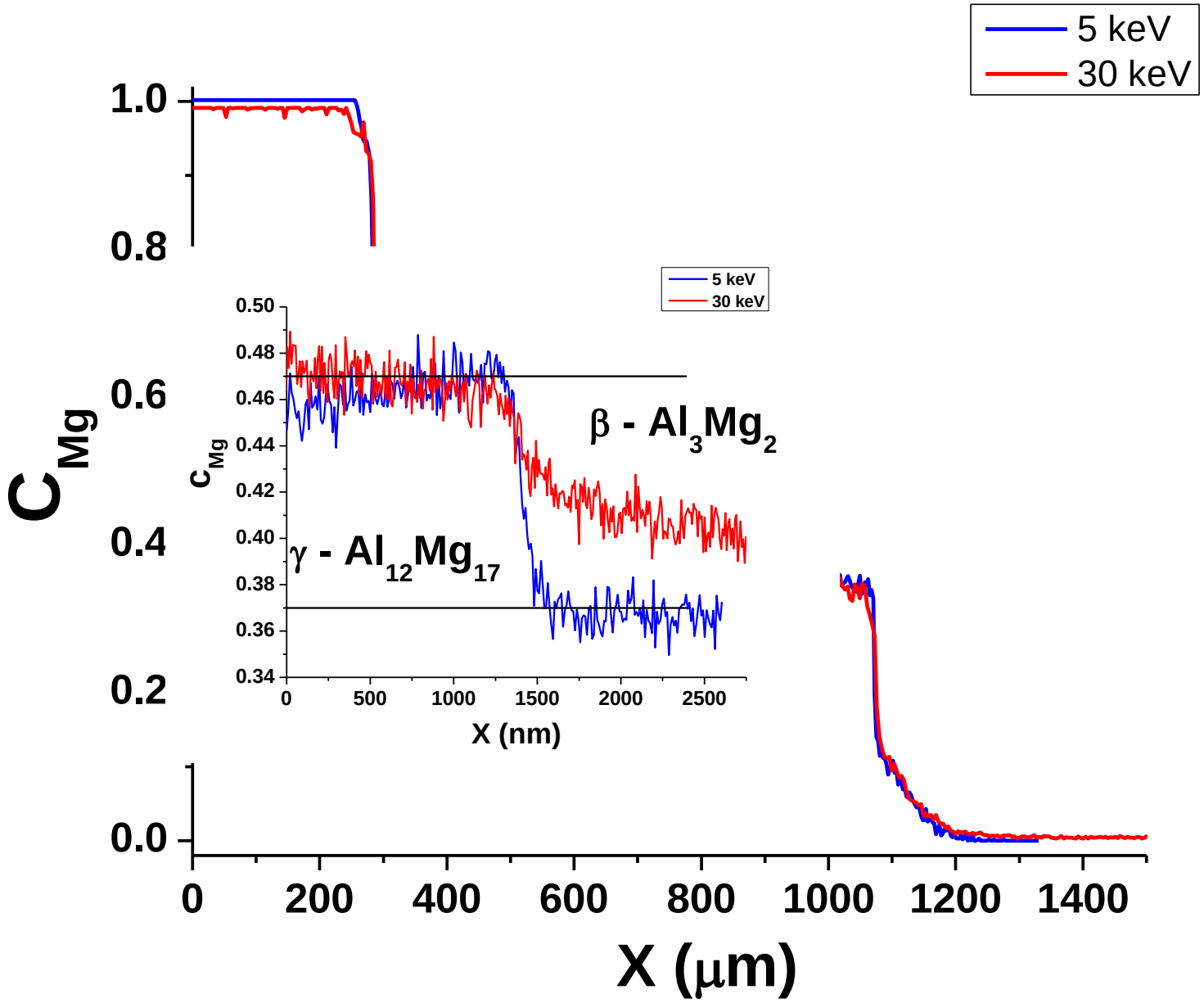
5 keV
30 keV
1.0
0.8
0.6
0.4
0.2
0.0
C_Mg
0
200
400
600
800
1000
1200
1400
X (μm)
5 keV
30 keV
0.50
0.48
0.46
0.44
0.42
0.40
0.38
0.36
0.34
c_Mg
β - Al3Mg2
γ - Al12Mg17
0
500
1000
1500
2000
2500
X (nm)

Grain Boundary Diffusion

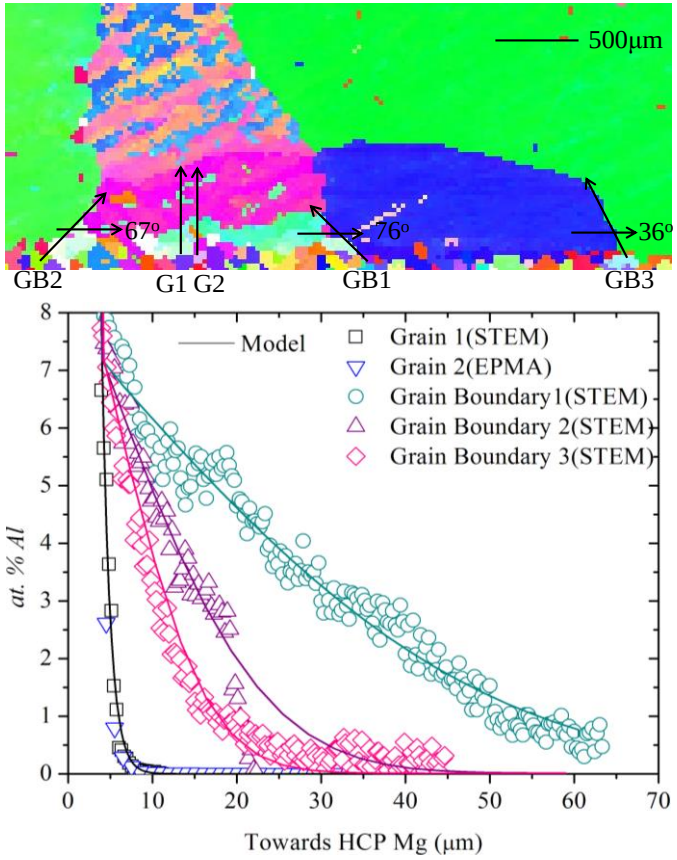

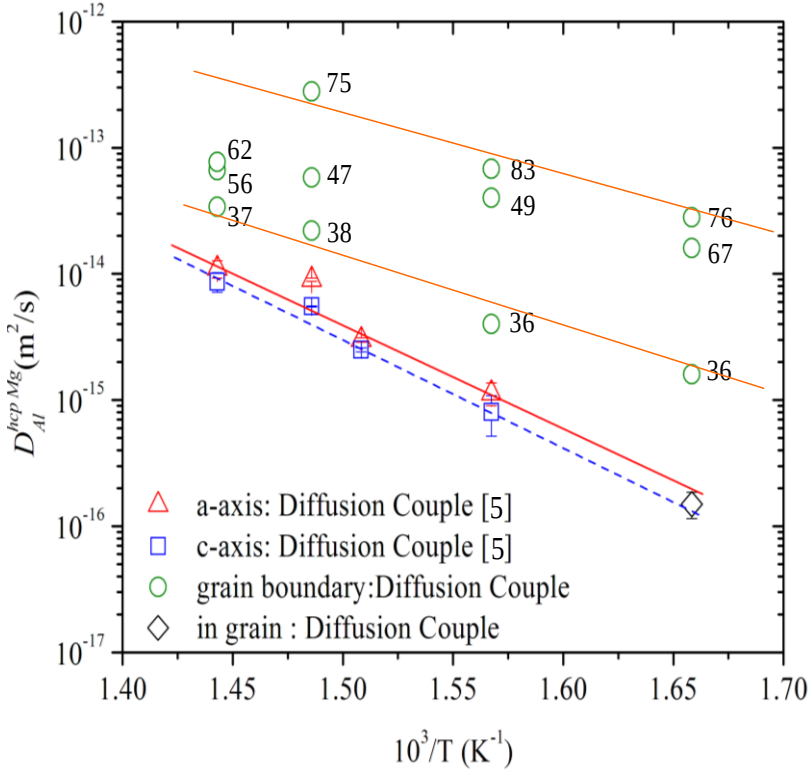

S. K. Das, N. Brodusch, R. Gauvin and I.-H. Jung (2014), "Grain boundary diffusion of Al in Mg", Scripta Materialia, 80, pp. 41-44.

STEM, Al, 30 kV, 80 nm

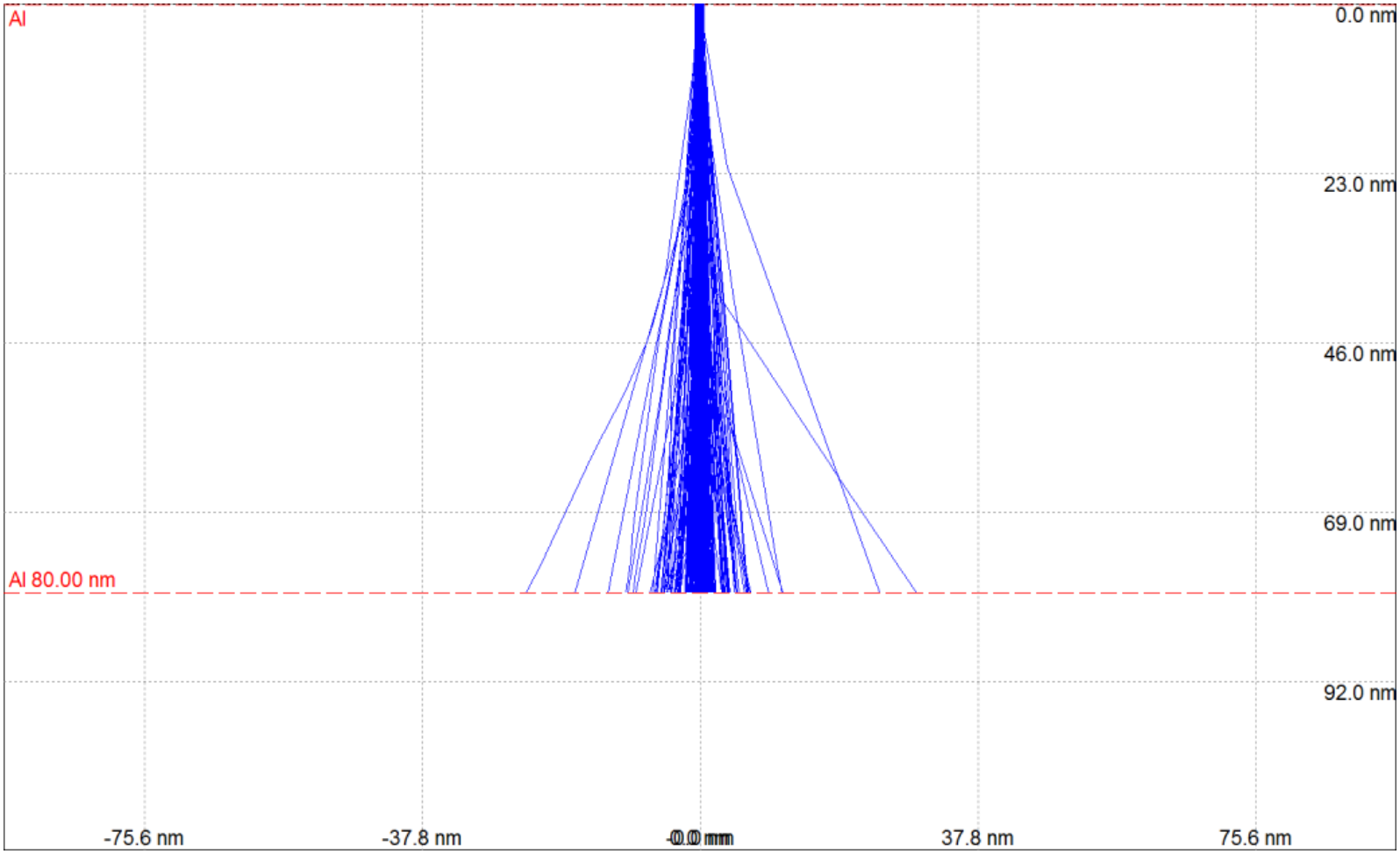

80 nm Thin Film

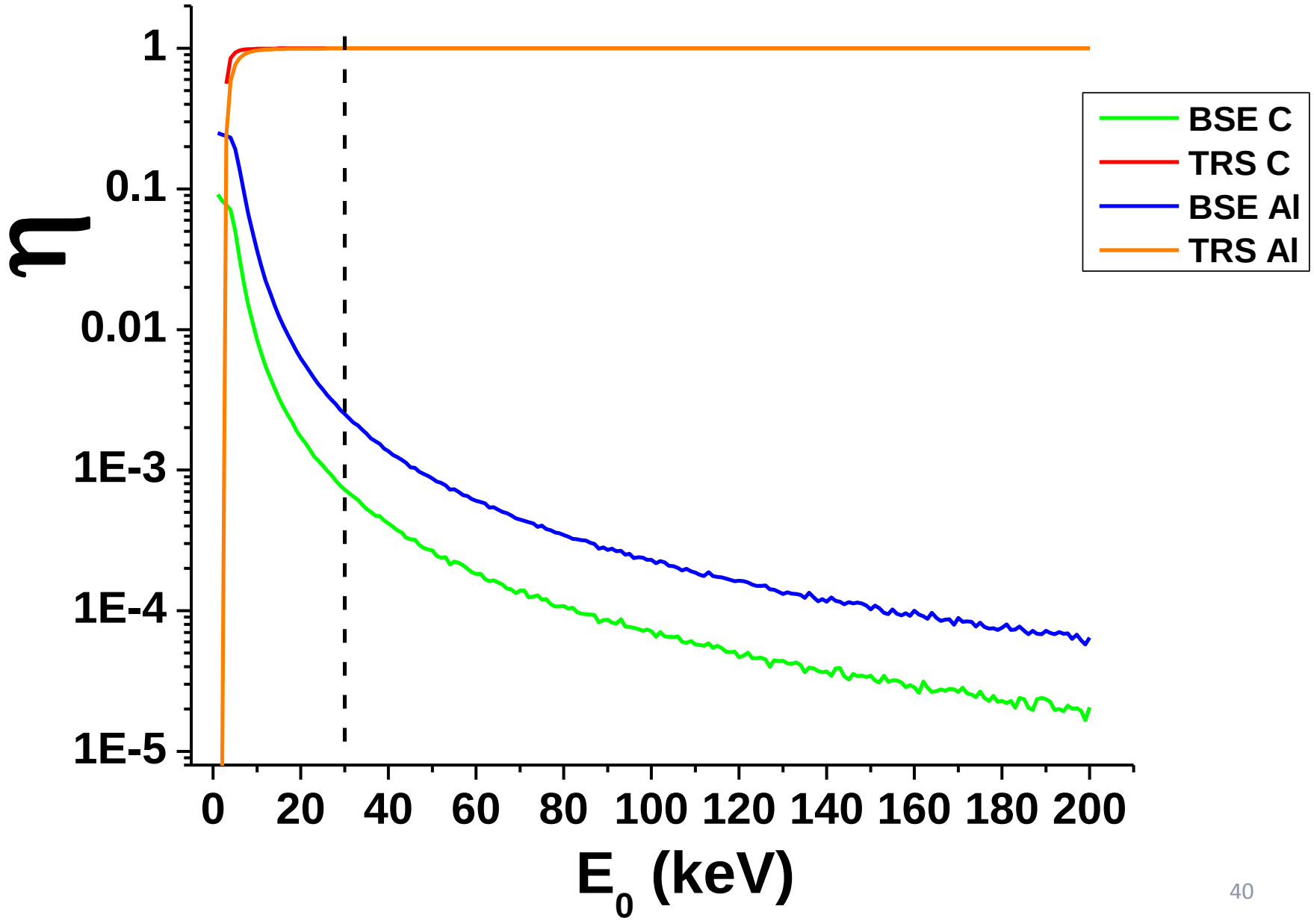

Alloy 2099 T83

HD – 2700 200 kV

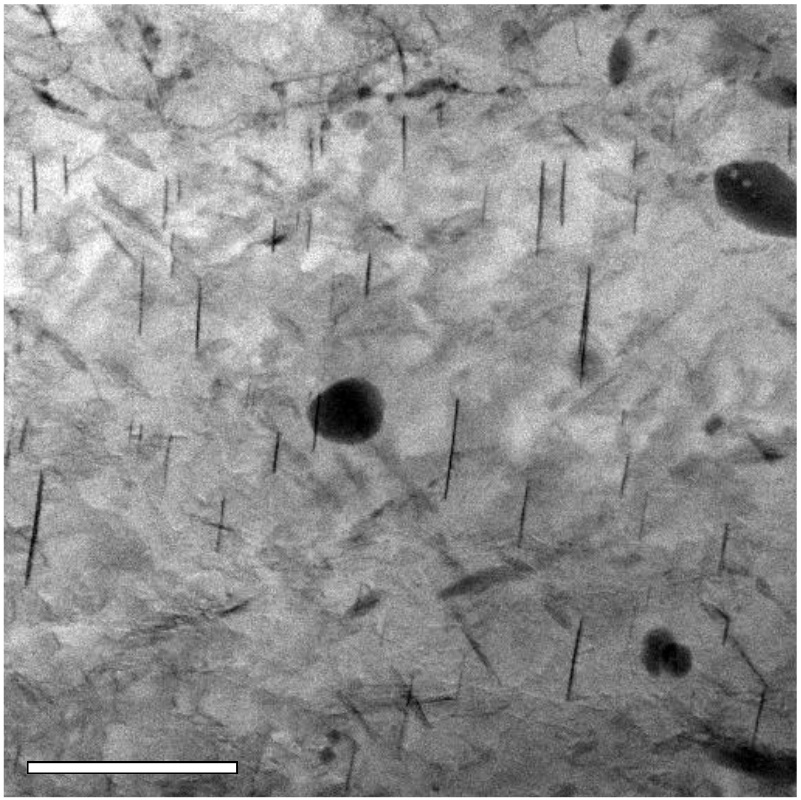

SU-8000 30 kV

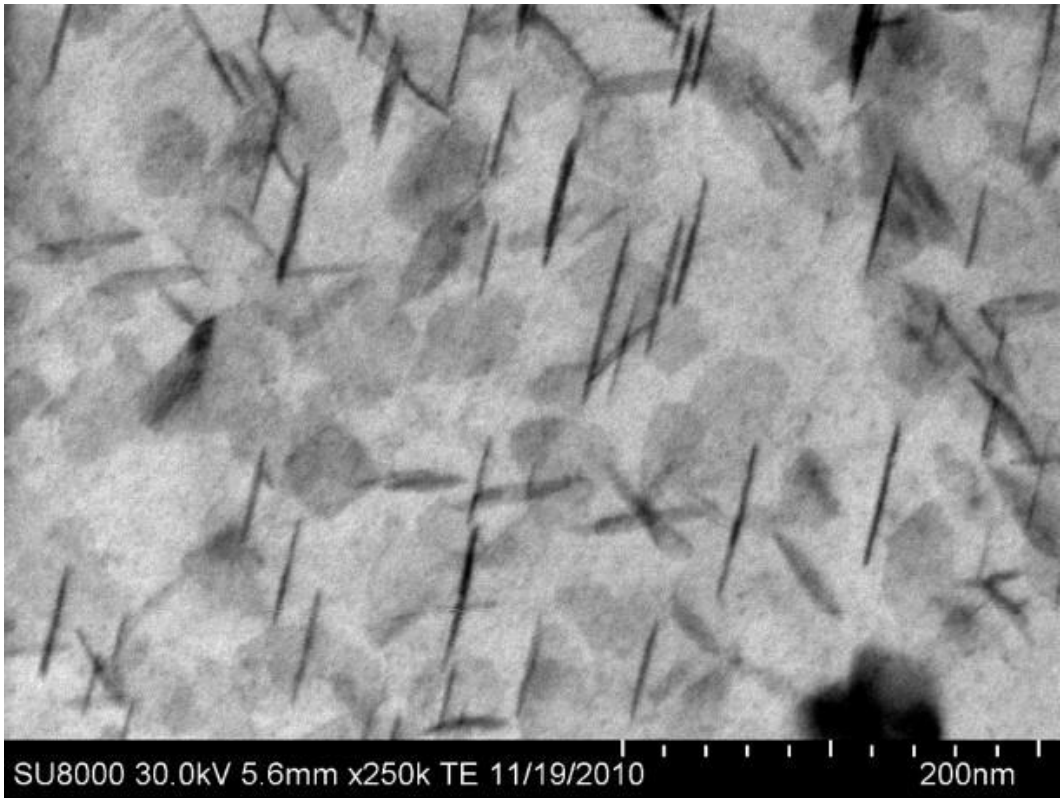

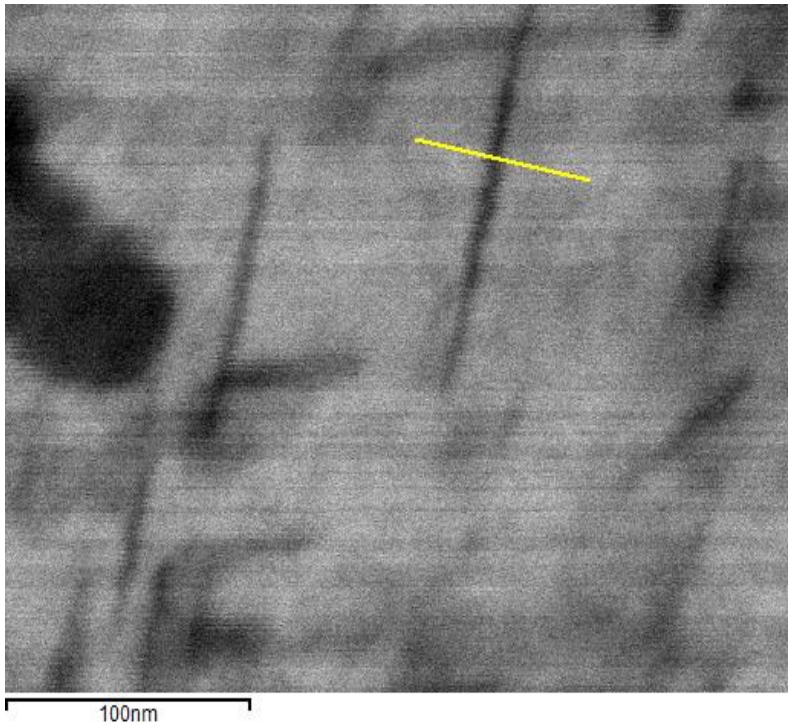

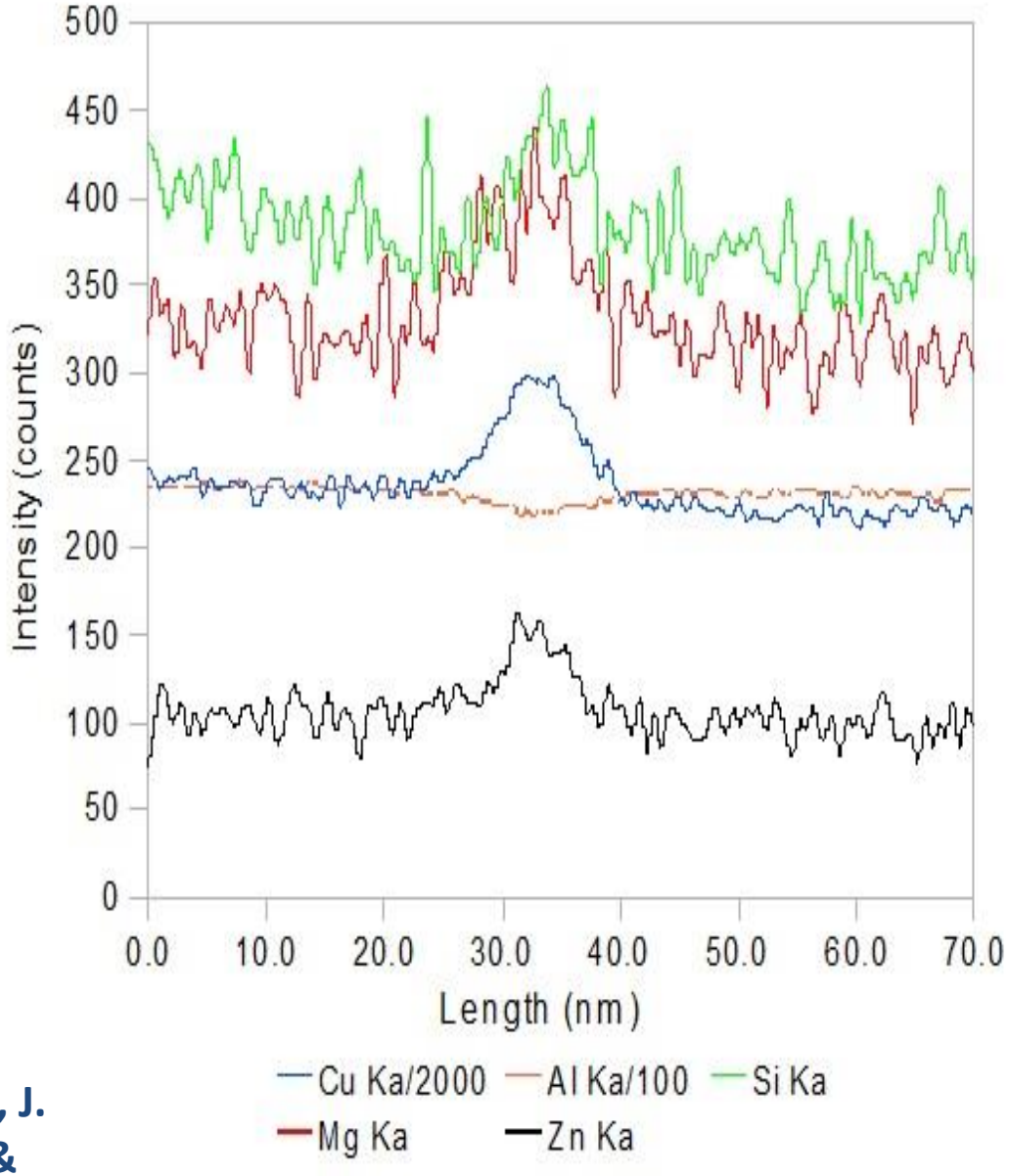

N. Brodush, M. L. Trudeau, P. Michaud, J. Boselli, R. Gauvin (2012), Microscopy & Microanalysis, 18, 6, pp. 1393 - 1409.

Pt particulates on Carbon nanotubes STEM BF – 30 kV

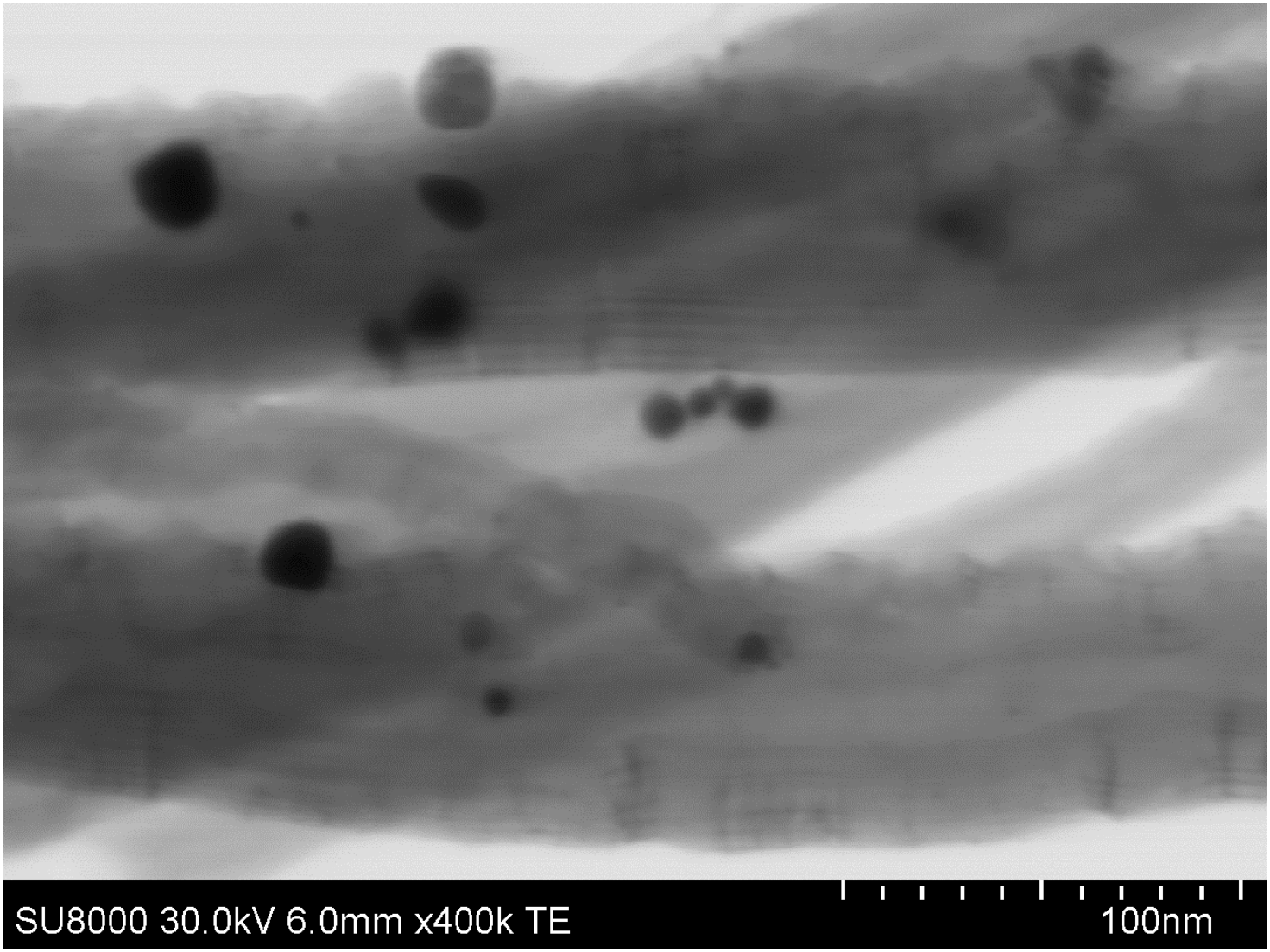

Pt particulates on Carbon nanotubes
BSE – 30 keV – EDS analysis at high resolution

M. J.-F., Guinel, N. Brodusch, Y. Verde-Gomez, B. Escobar-Morales, R. Gauvin (2013), Journal of Microscopy, Vol. 252, No. 1, pp. 49 – 57.

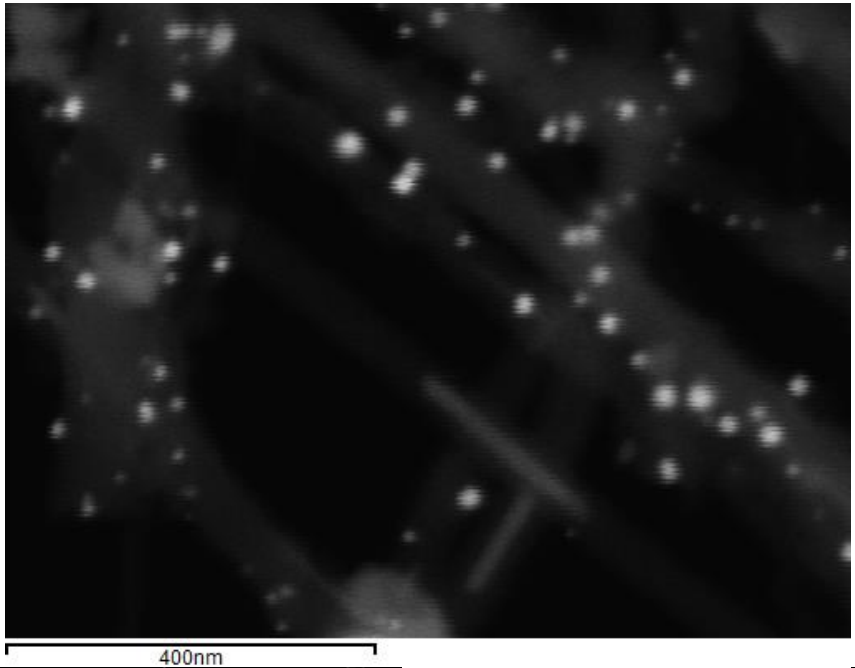

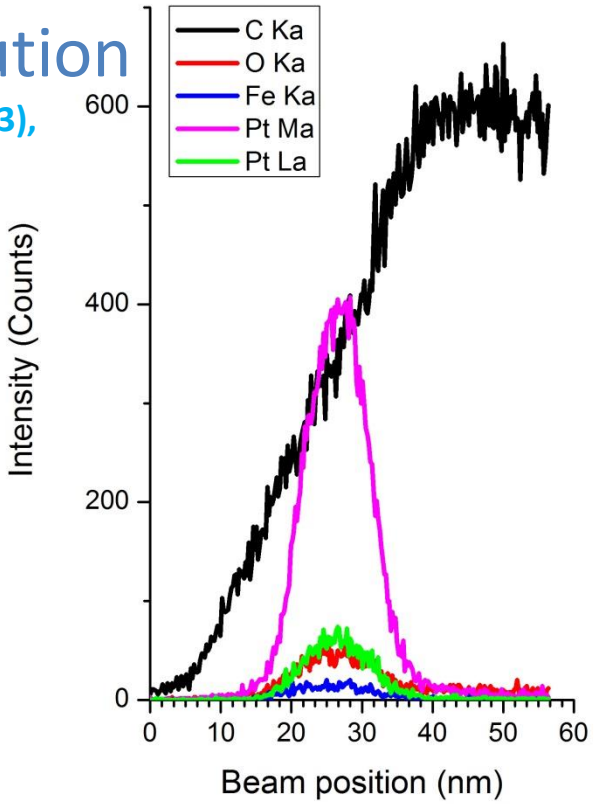

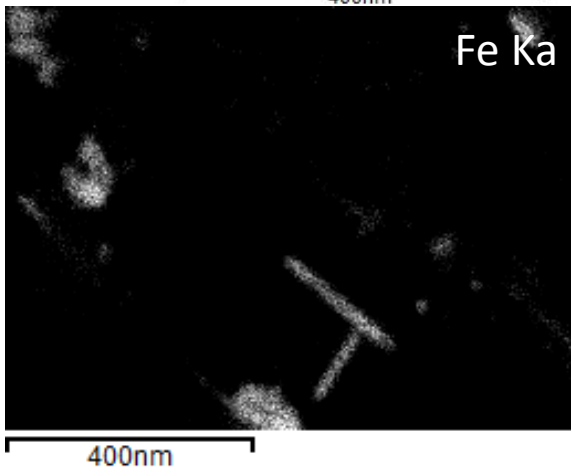

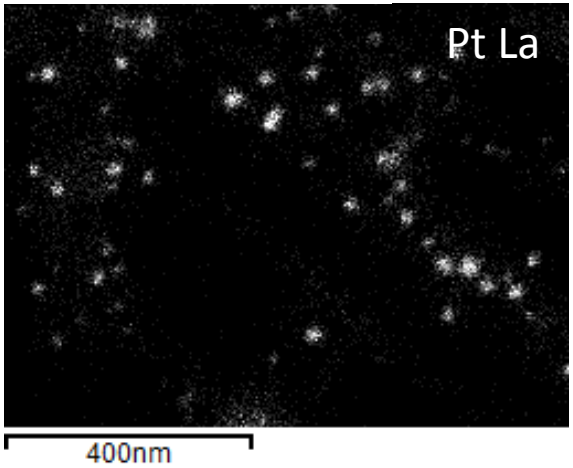

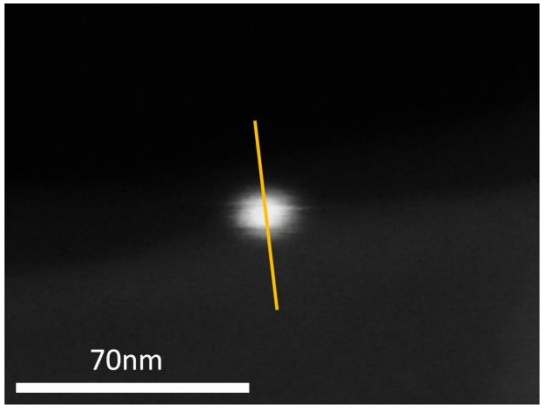

Transmission Electron Forward Scatter Diffraction (t-EFSD)

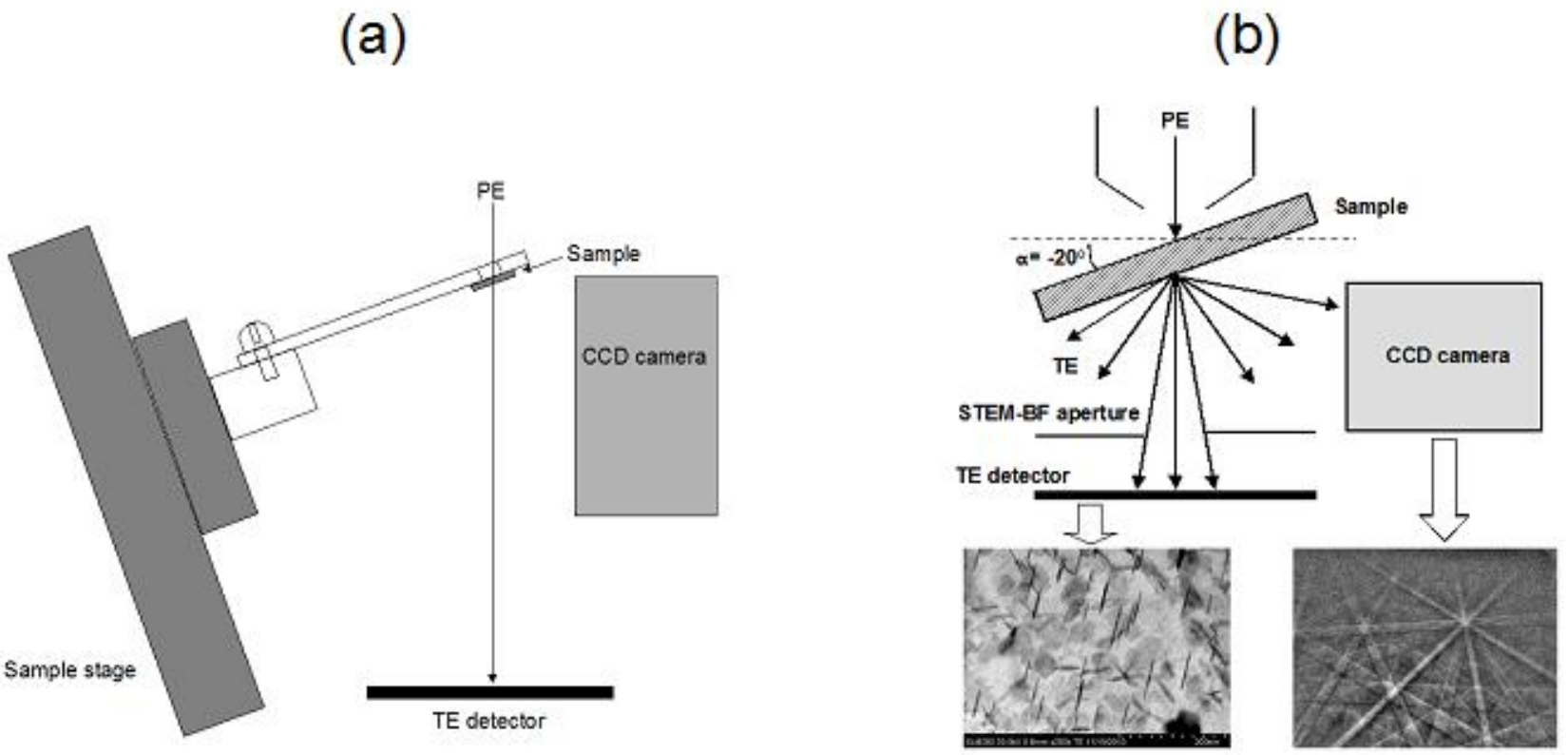

N. Brodusch, H. Demers, R. Gauvin (2013), Journal of Microscopy, 250, 1, pp. 1–14.

t-EFSD: 5.6 nm PdO_2 nanoparticle deposited on a CNT at 30 kV

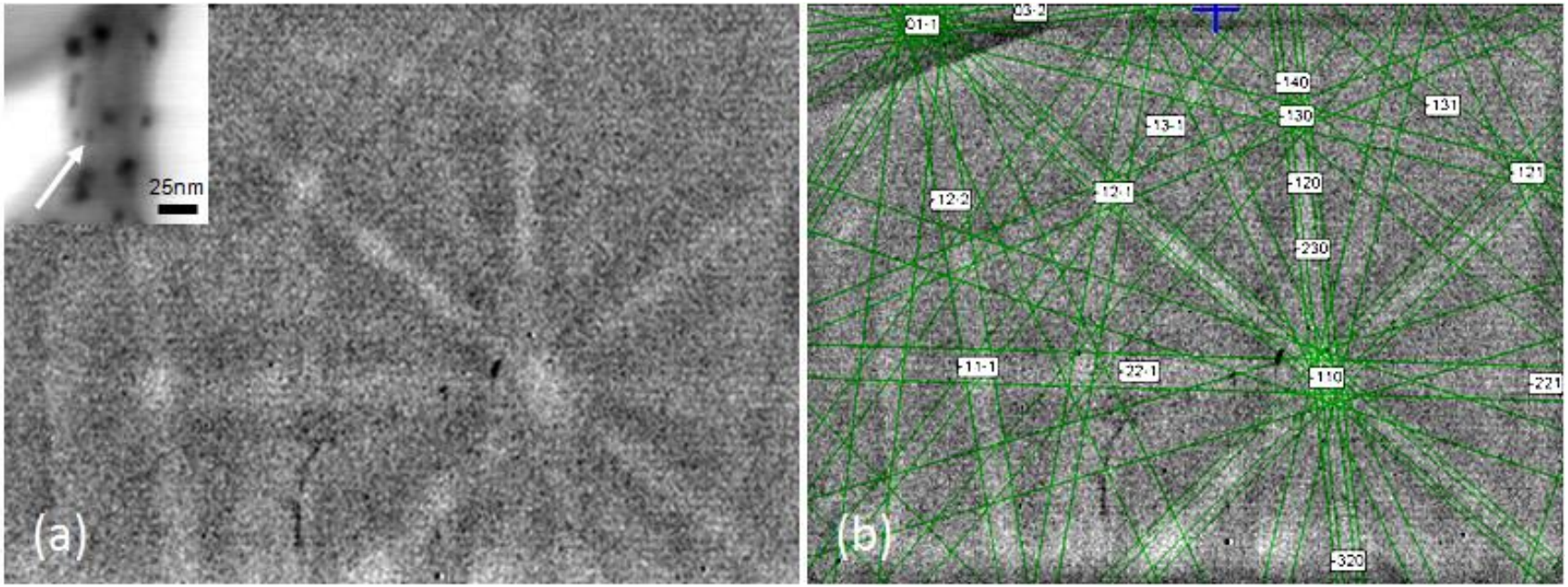

N. Brodusch, H. Demers, R. Gauvin (2013), Journal of Microscopy, 250, 1, pp. 1–14.

TiO_2

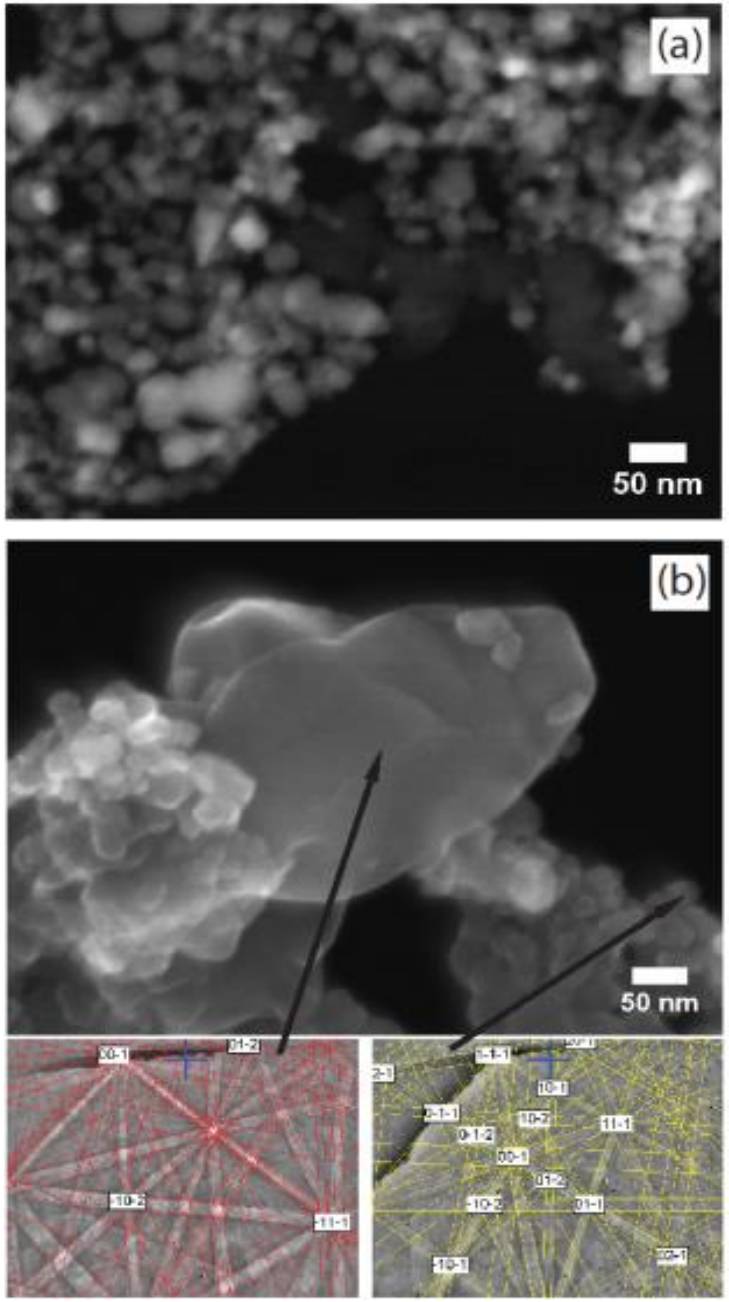

Rutile

Anatase

M. J. Sussman, N. Brodusch, R. Gauvin, G. P. Demopoulos (2013), J. Electrochem. Soc, 160, 5, pp. A3100-A3107.

Dark Field Imaging

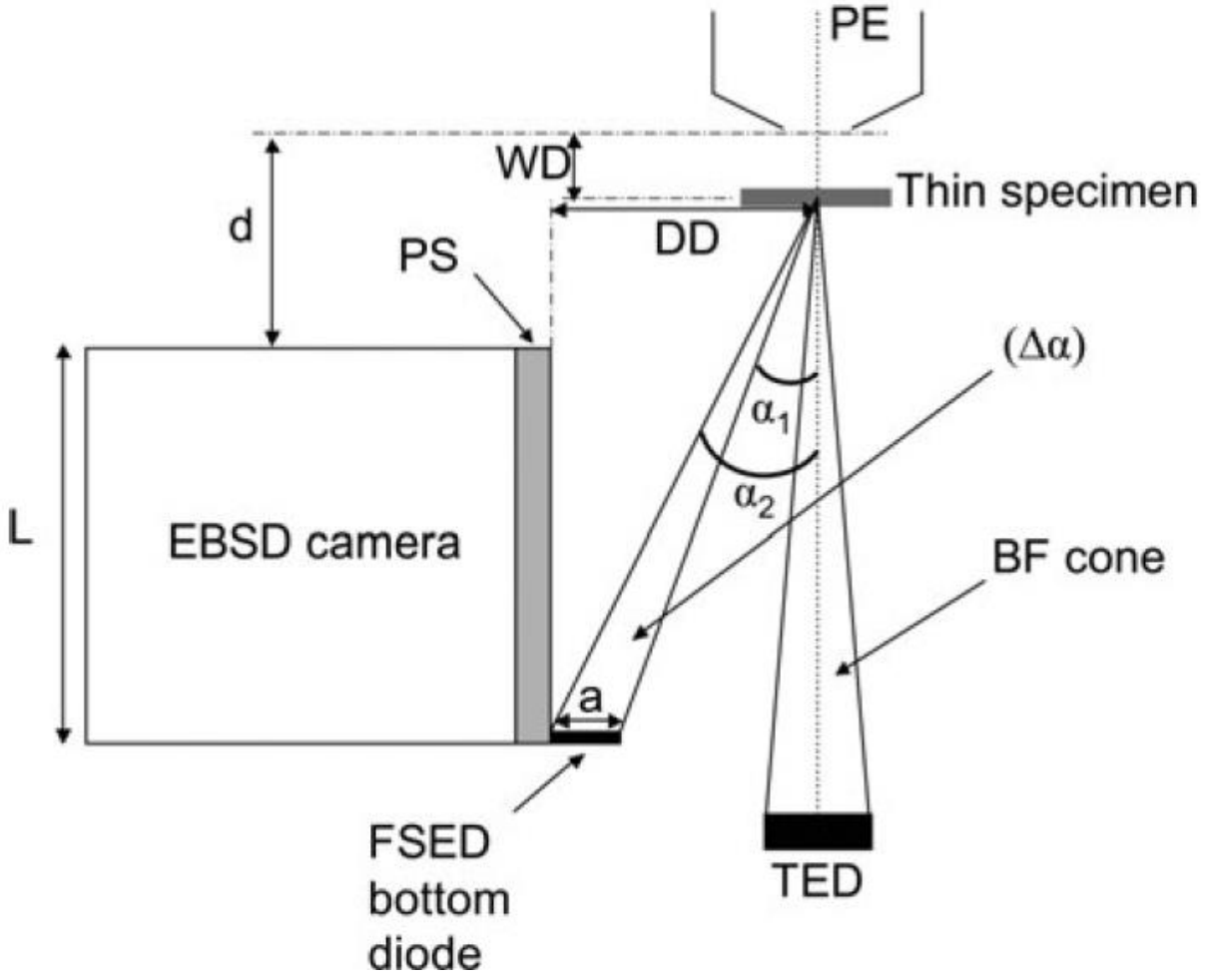

N. Brodusch, H. Demers and R. Gauvin (2013), Microscopy and Microanalysis, Vol. 19, No. 06, pp. 1688 – 1697.

Pt Particulates on WCNT

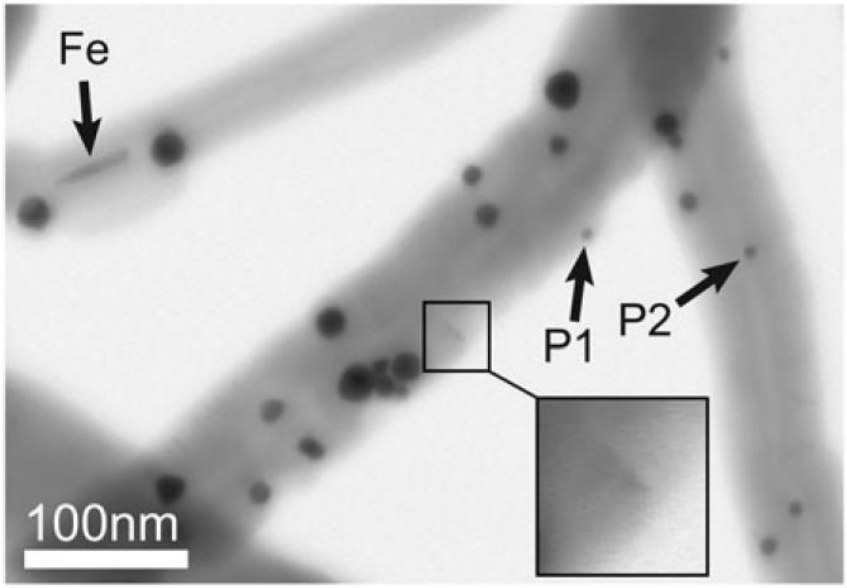

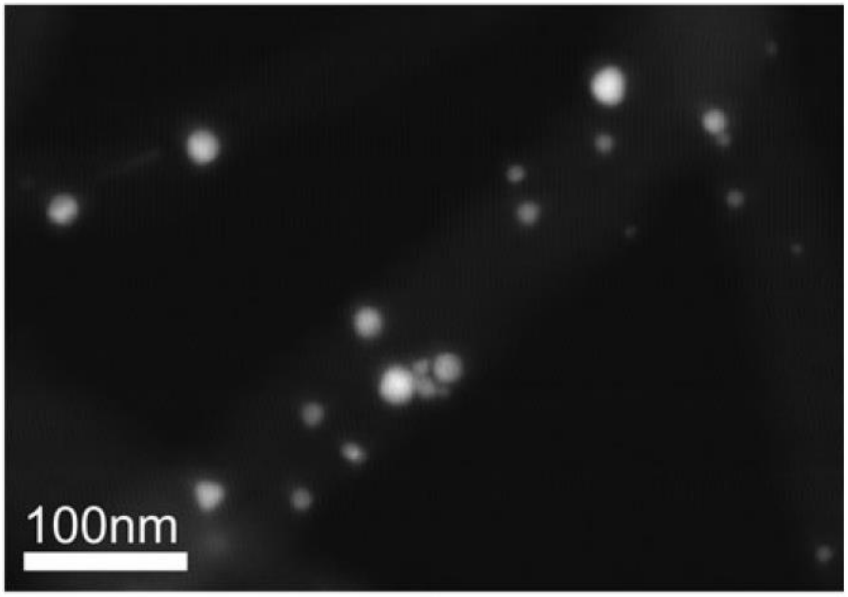

BF-TE
SNR: 22.8
Resolution: 1.5 nm

DF-FSED
SNR: 2.0
Resolution: 9.0 nm

N. Brodusch, H. Demers and R. Gauvin (2013), Microscopy and Microanalysis, Vol. 19, No. 06, pp. 1688 – 1697.

Magnetic contrast with Forcaster Detectors

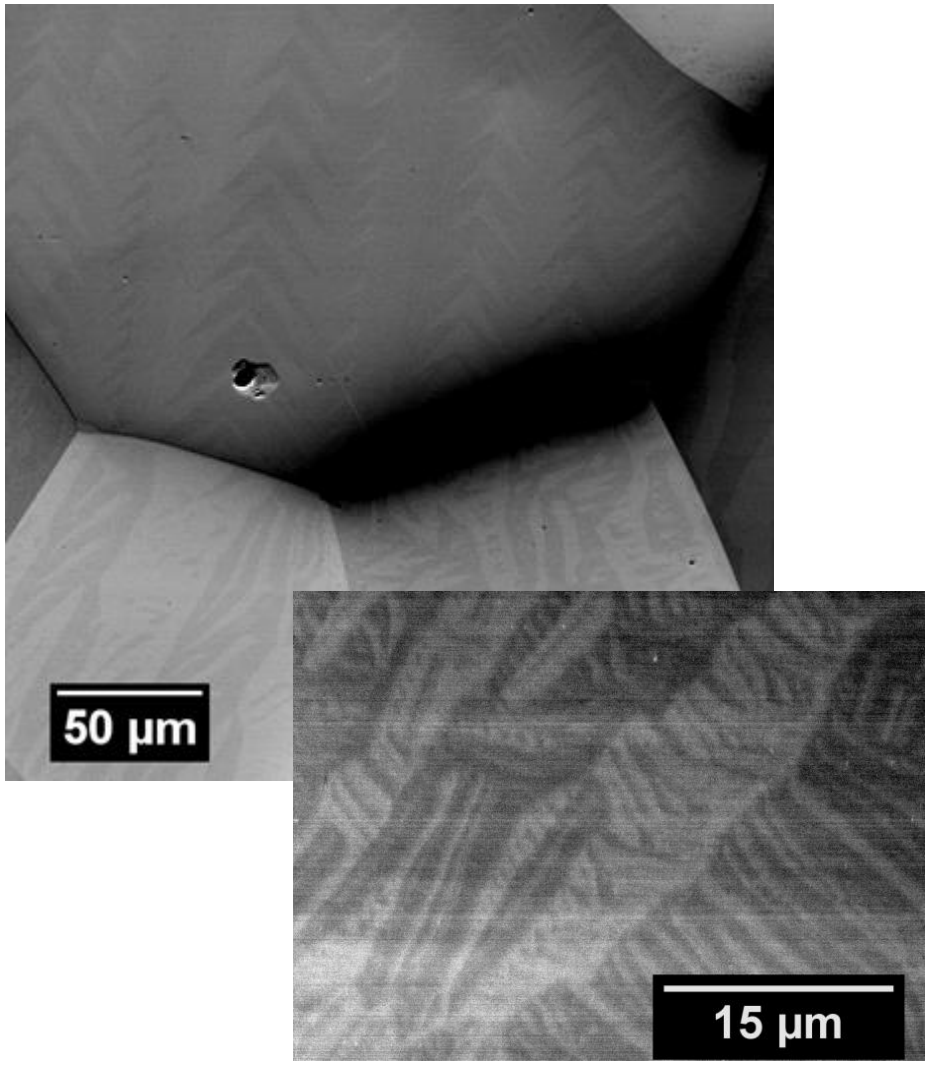

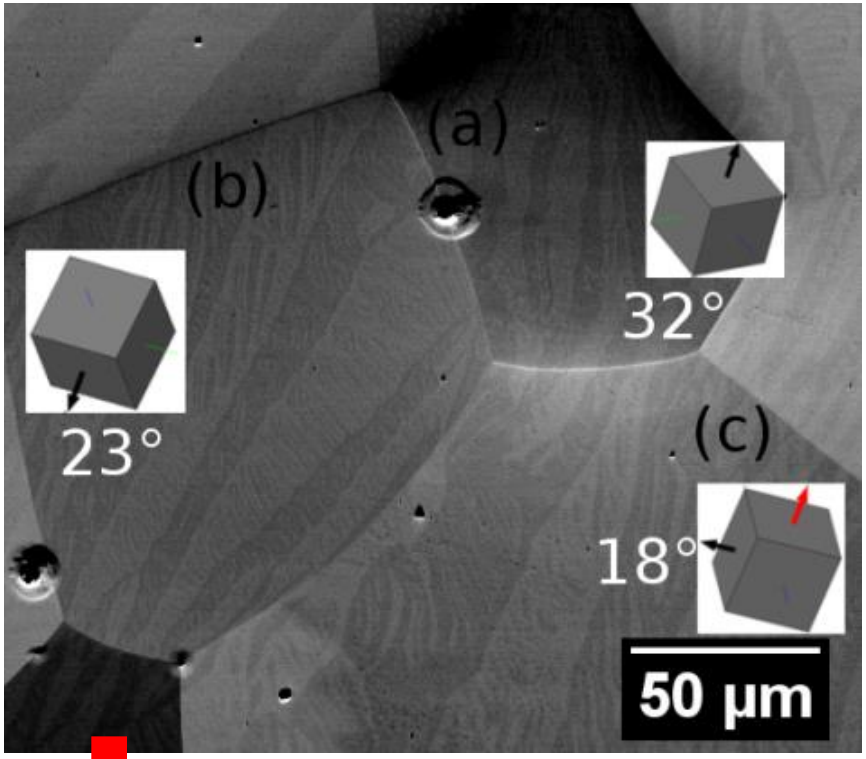

Correlation between EBSD (orientation/easy axis direction) and magnetic domain data

Gallaugher, M.; Brodusch, N.; Gauvin, R. & Chromik, R. R. Magnetic Domain Structure and Crystal Orientation Revealed by a Forescatter Detector and Electron Backscatter Diffraction. *Microscopy and Microanalysis,* **2014**, *20*, 1458-1459

Dark-field imaging based on post-processed EBSD data

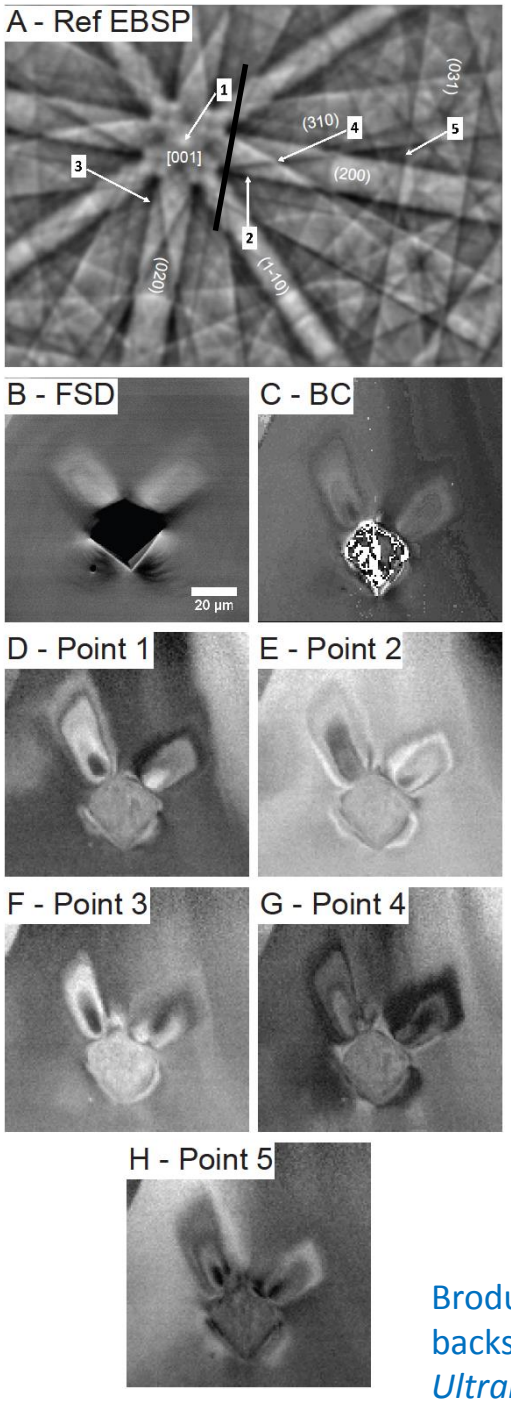

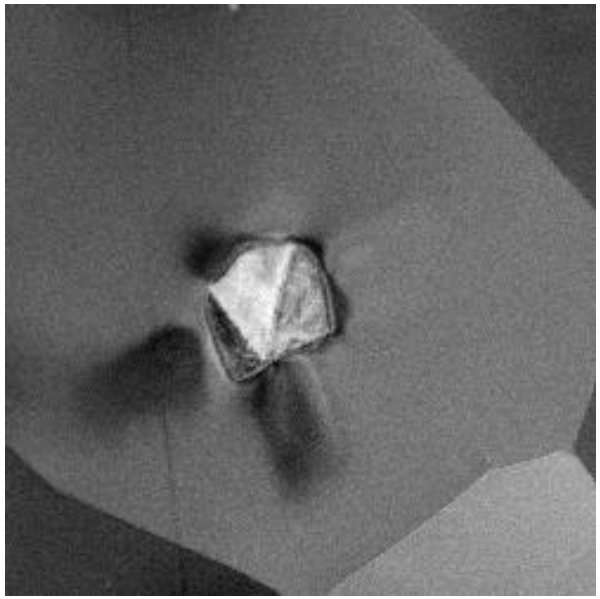

- Need EBSD acquisition with high CCD resolution
- Area intensity on the EBSP reported for each pixel of the map
- Diffraction vector based imaging
- New way to study deformation structures and ECCI contrast

Brodusch, N.; Demers, H. & Gauvin, R. Dark-field imaging based on post-processed electron backscatter diffraction patterns of bulk crystalline Materials in a scanning electron microscope. *Ultramicroscopy,* **2014**

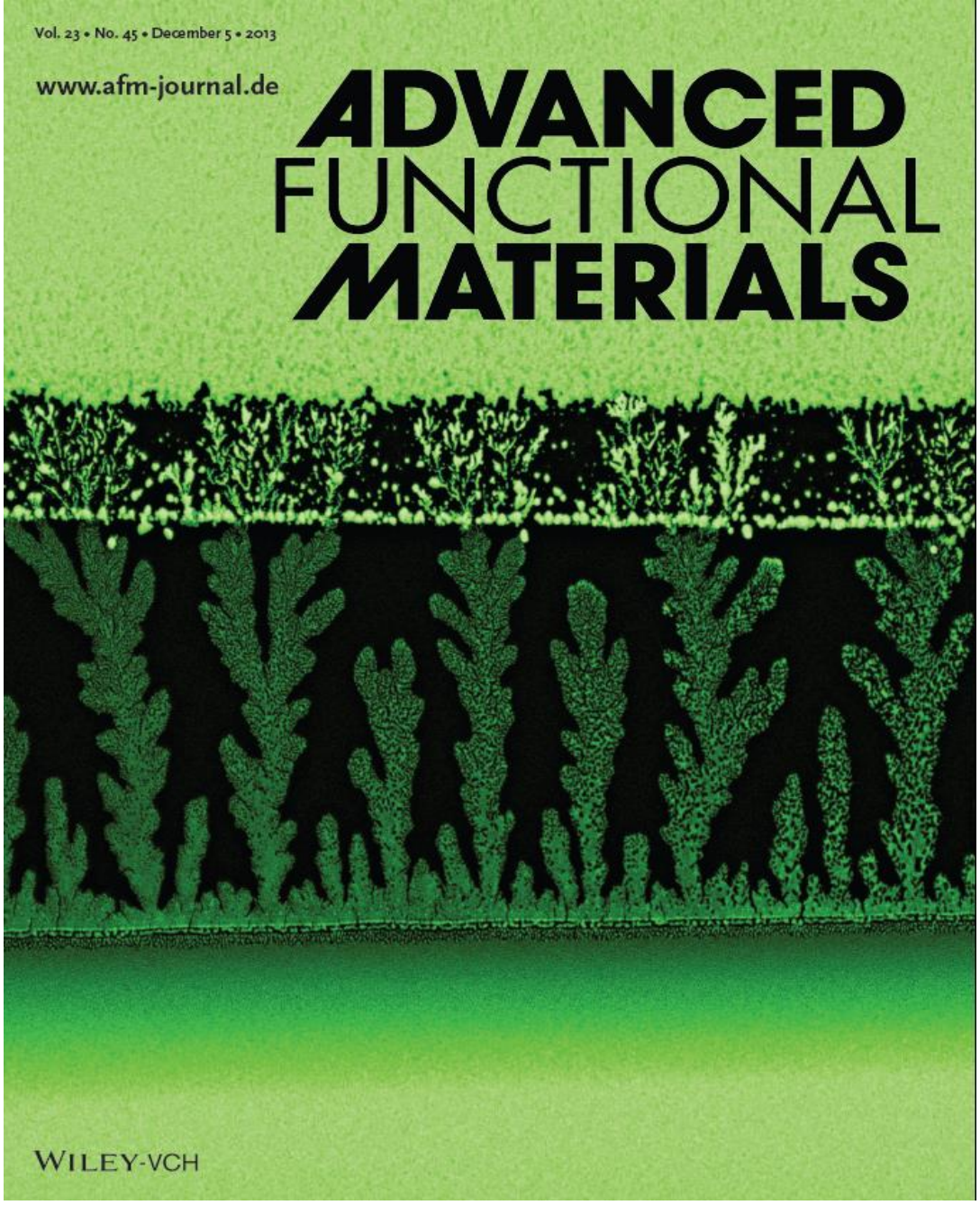

J. Wünsche, L. Cardenas, F. Rosei, F. Cicoira, R. Gauvin, C. F. O. Graeff, S. Poulin, A. Pezzella and C. Santato, (2013), Advanced Functional Materials, Vol. 23, No. 45, pp. 5591–5598.

The Flood… January 28th 2013 McGill University

HITACHI SU-8230 (2014)
Cold FEG Auto Flash

- **0.4 nm at 30 keV, 1.8 nm at 0.2 keV**
- **At least, 2 times more probe current than SU-8000.**

Smart Mild Flashing Technology

Conventional CFE

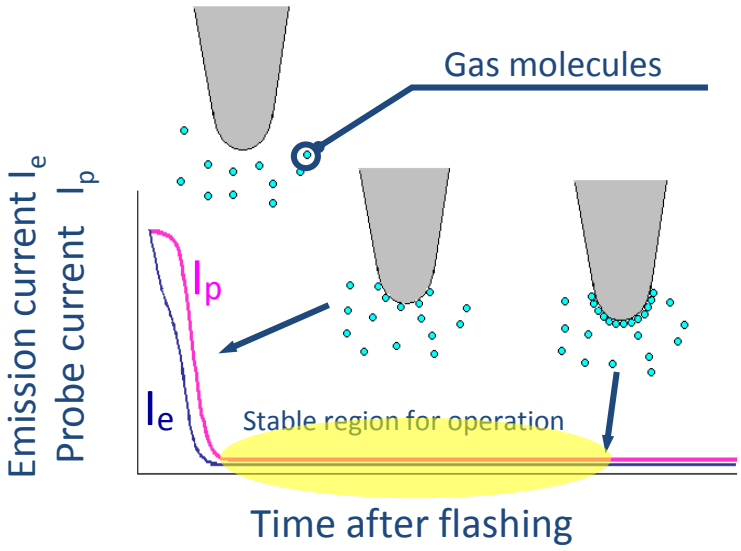

SU8200 series

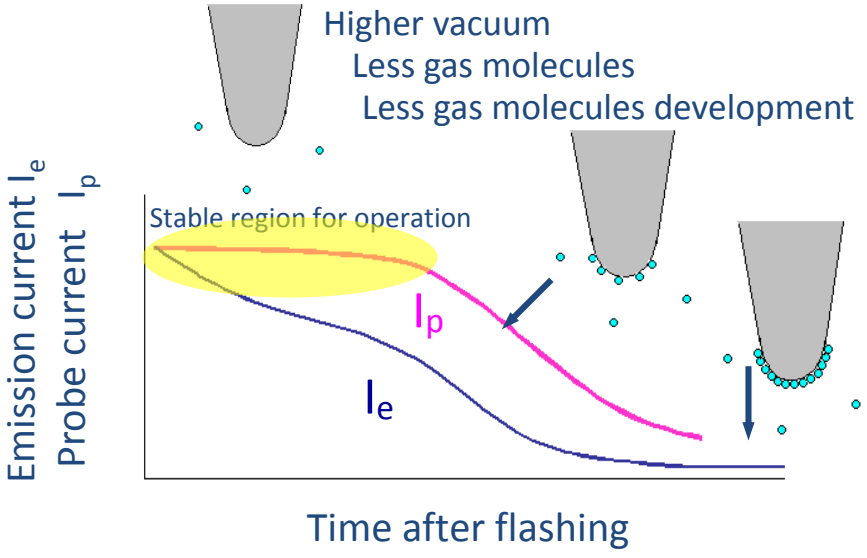

Mild flashing

Automated mild flashing sequence
Probe current deviation: < 10%/12hrs

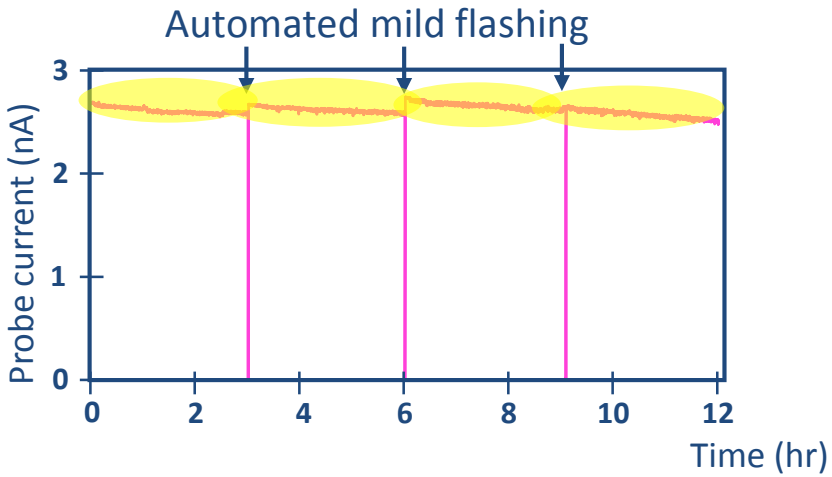

SU-8230 Cold Field Emission SEM

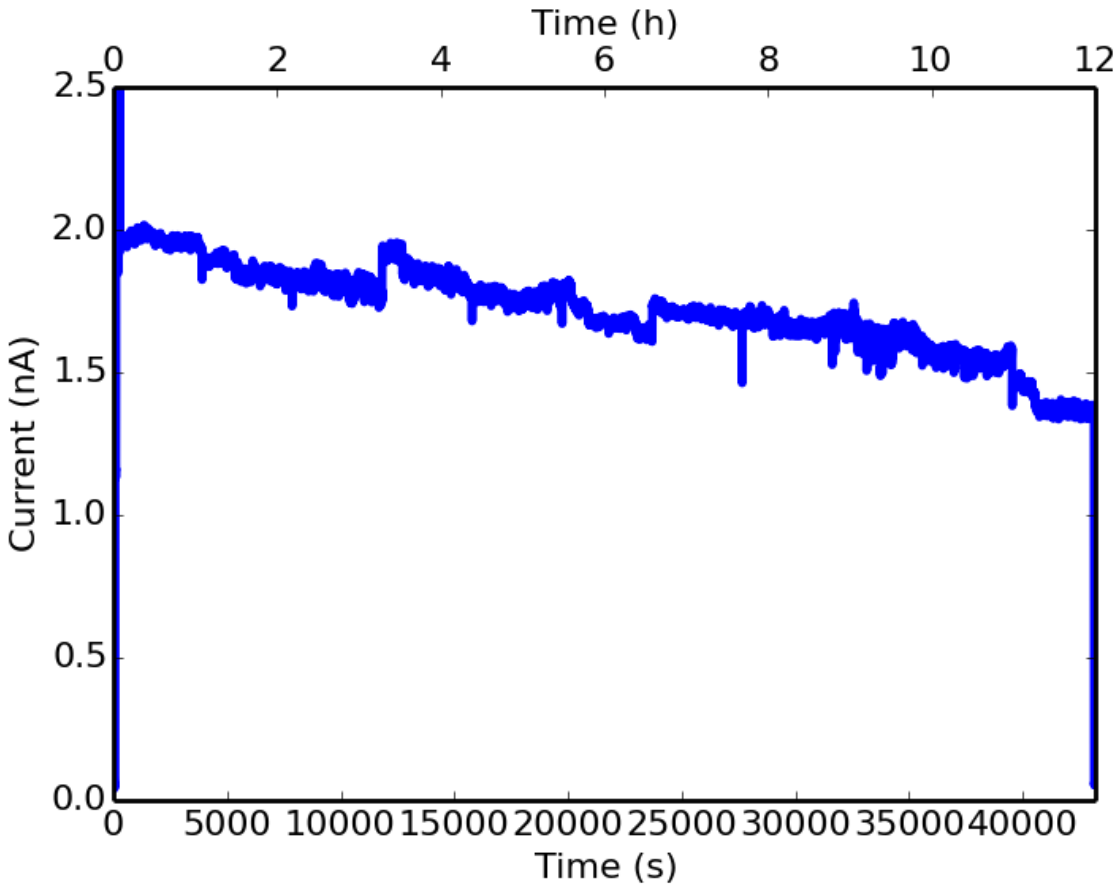

10 kV

Ie of 20 µA

10% Drop after 10 h

Alumina, 0.7 kV

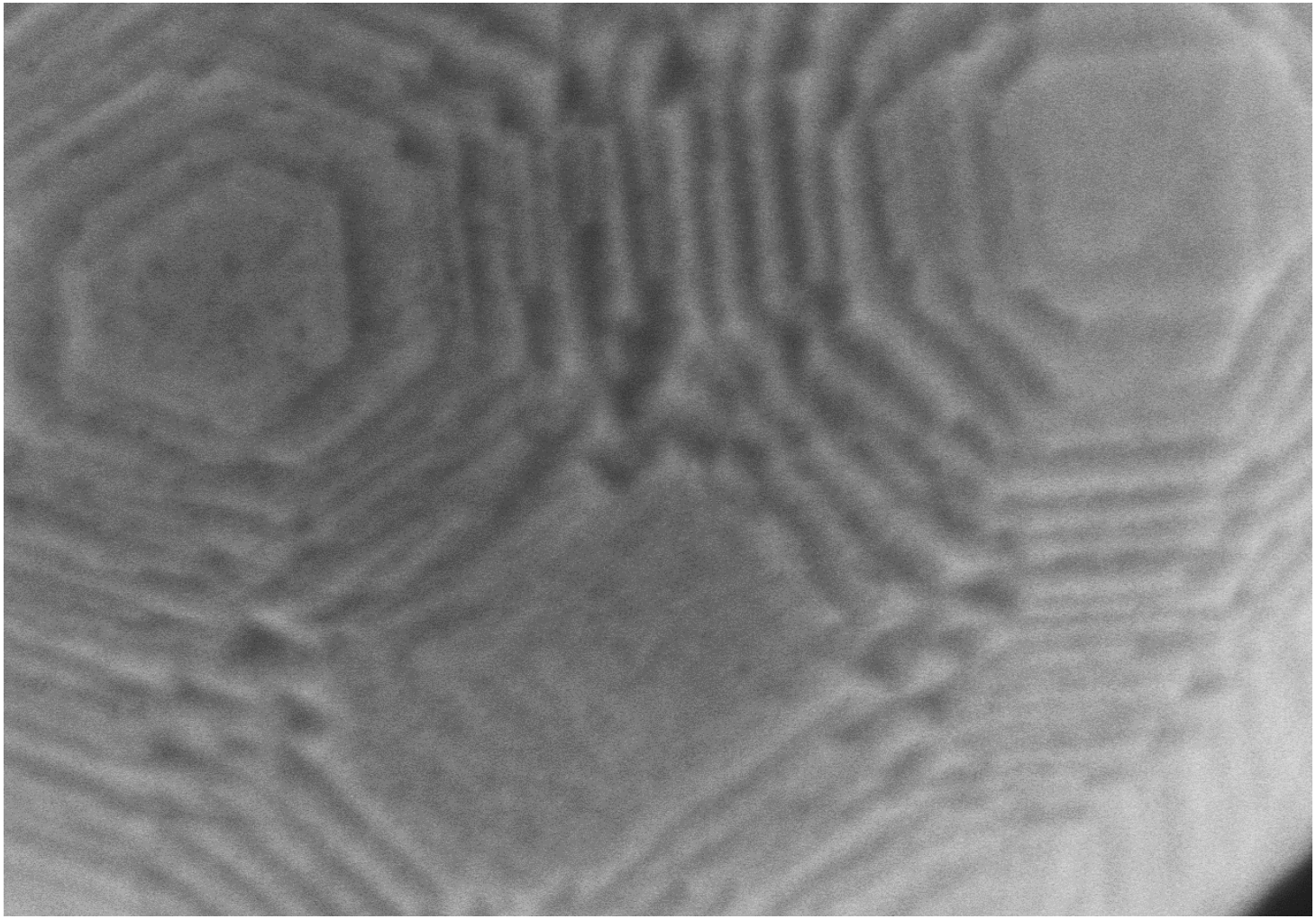

600kX
SE+BSE(U)
FOV: 212 nm
SNR: 1.7
Resolution: 2.0 nm

Alumina, 0.7 kV

SE+BSE(U)

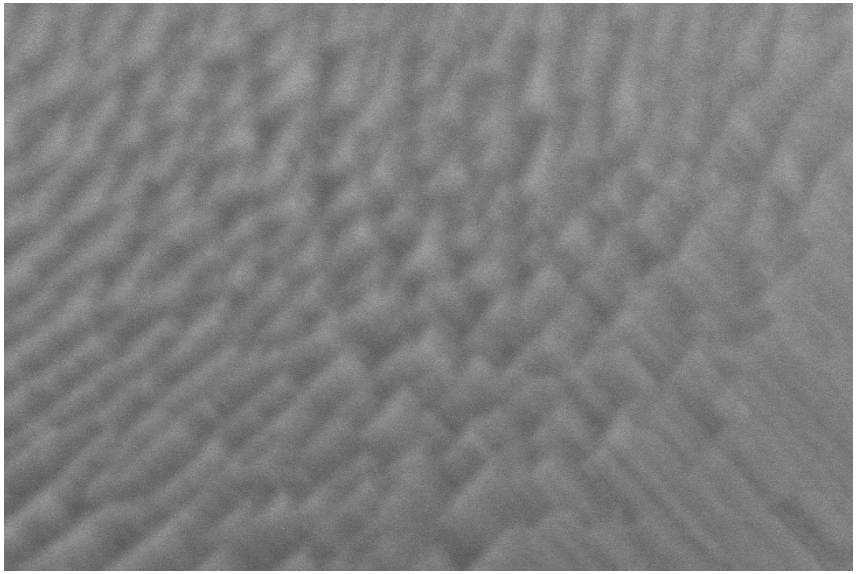

FOV: 212 nm
600kX
SNR: 2.0
Resolution: 2.0 nm

SE(T)

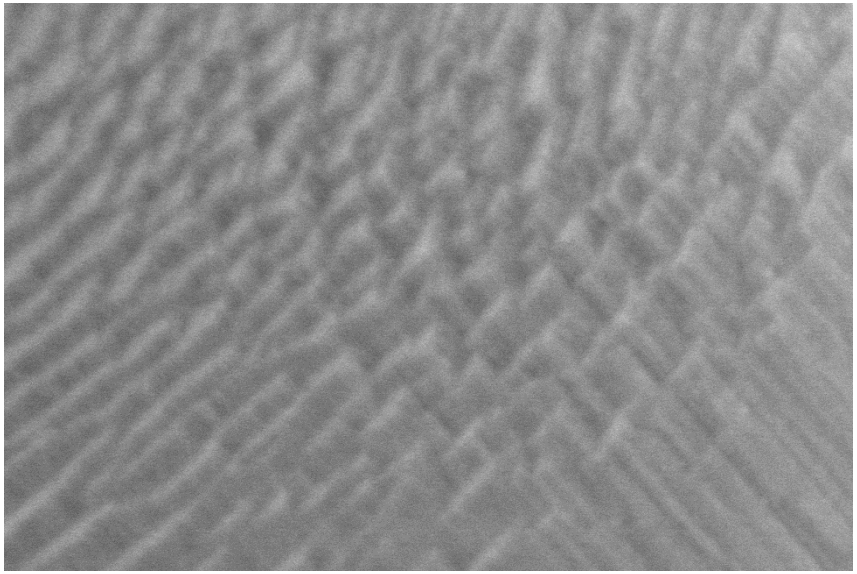

FOV: 212 nm
600 kX
SNR: 2.0
Resolution: 2.0 nm

Al – Li alloy, 2199

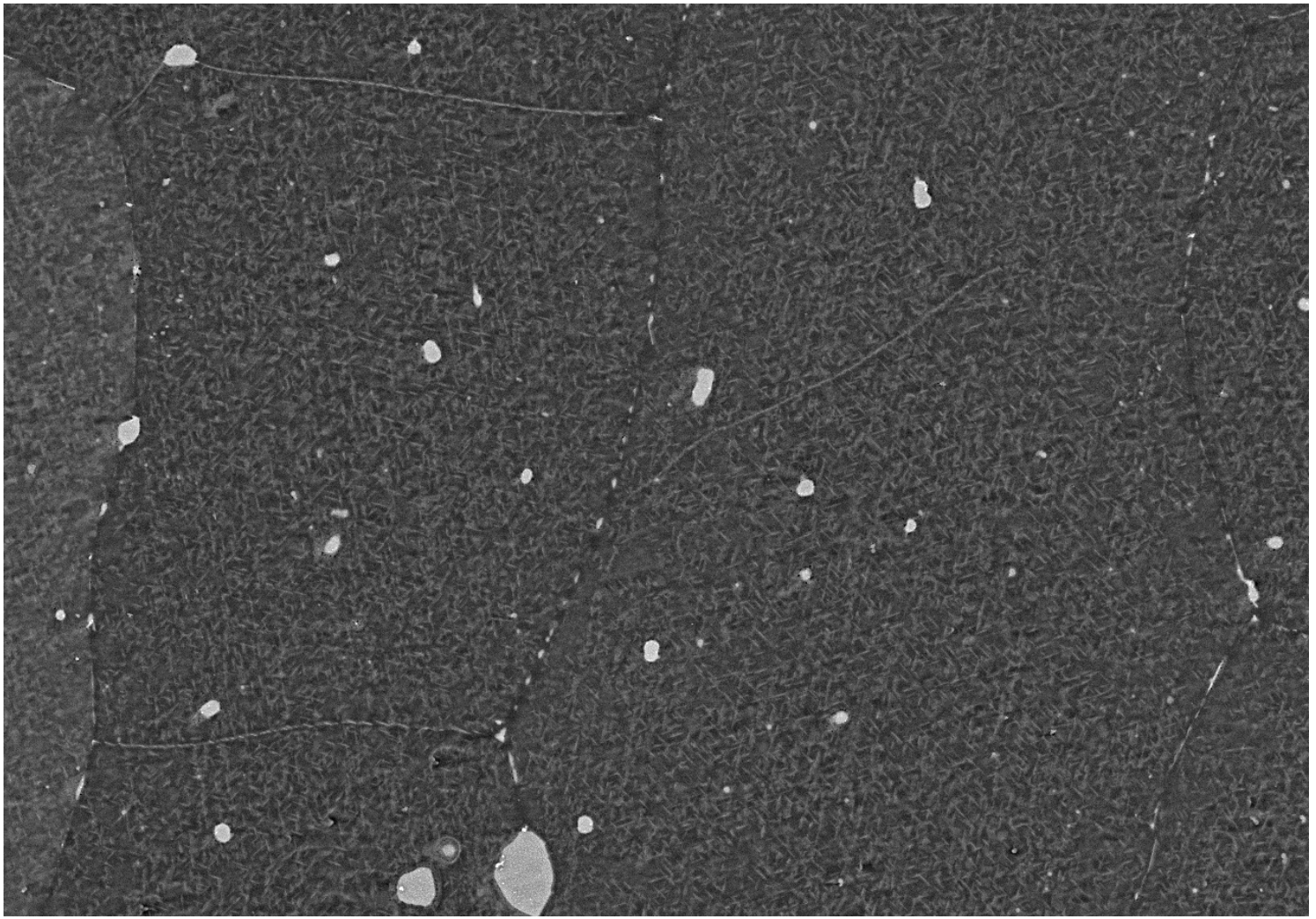

Al - Li Alloy 2099

LA100(U)

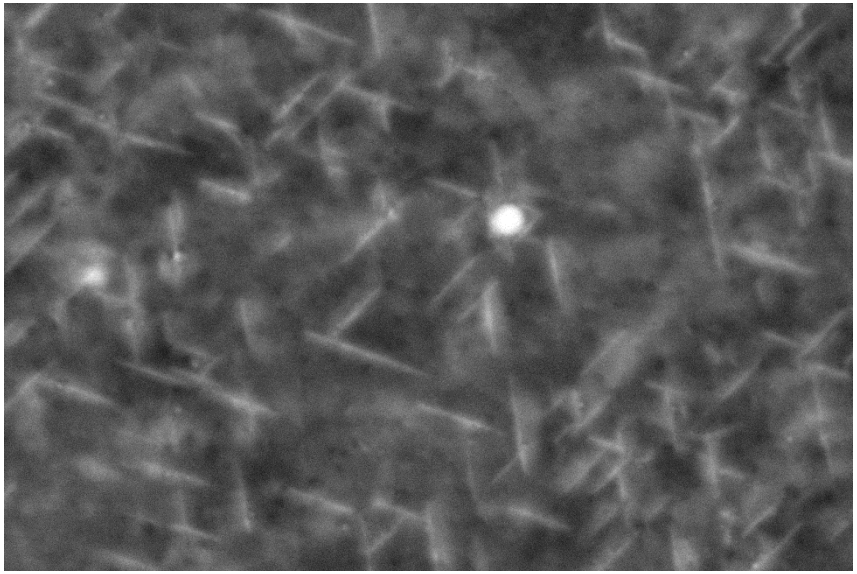

FOV 1270 nm
100 kX
SNR: 1.5
Resolution: 10.0 nm

LA100(U)

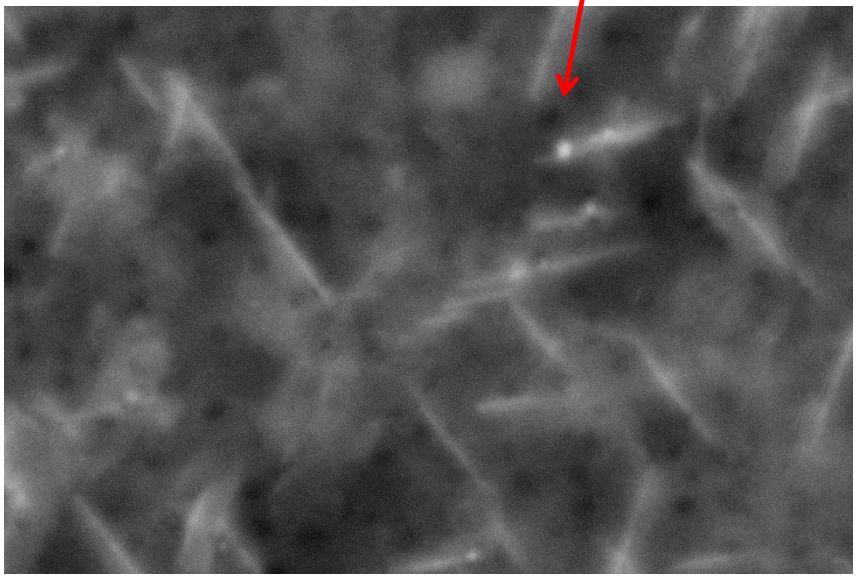

FOV: 635 nm
200 kX
SNR: 1.6
Resolution: 6.6 nm

Li_2CoSiO_4 prepared with an ionic liquid (BMI-BF_4) to reduce charging effects at the particles surface

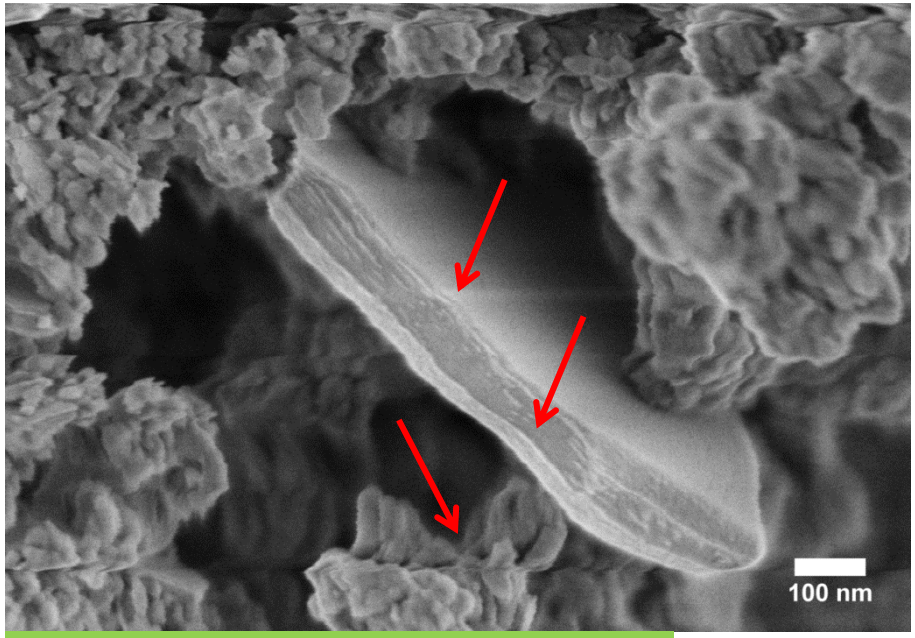

No preparation, no coating

With ionic liquid (BMI-BF_4), no coating

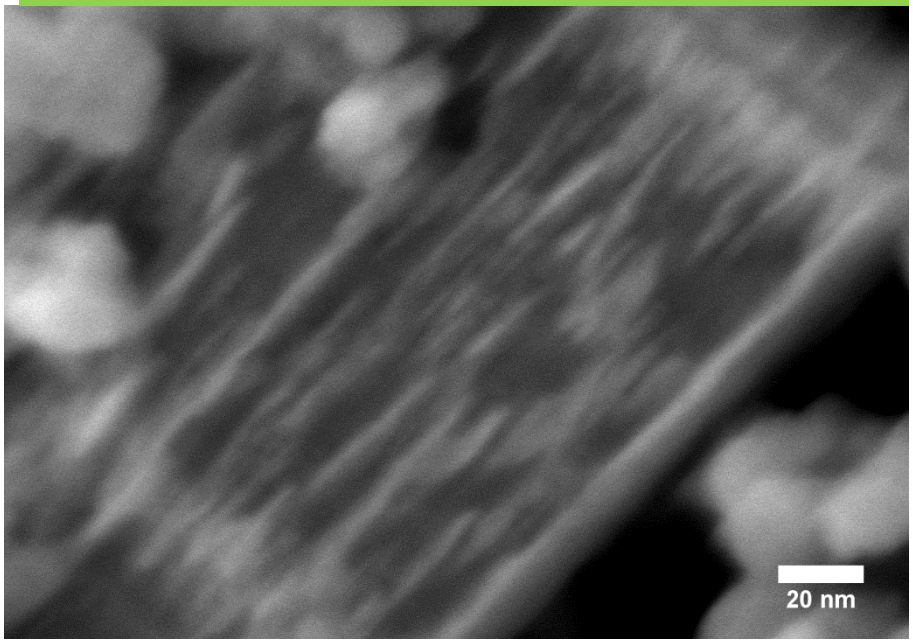

Brodusch, N.; Demers, H. & Gauvin, R. Ionic Liquid Used for Charge Compensation for High-Resolution Imaging and Analysis in the FE-SEM. *Microscopy and Microanalysis,* **2014**, *20*, 38-39

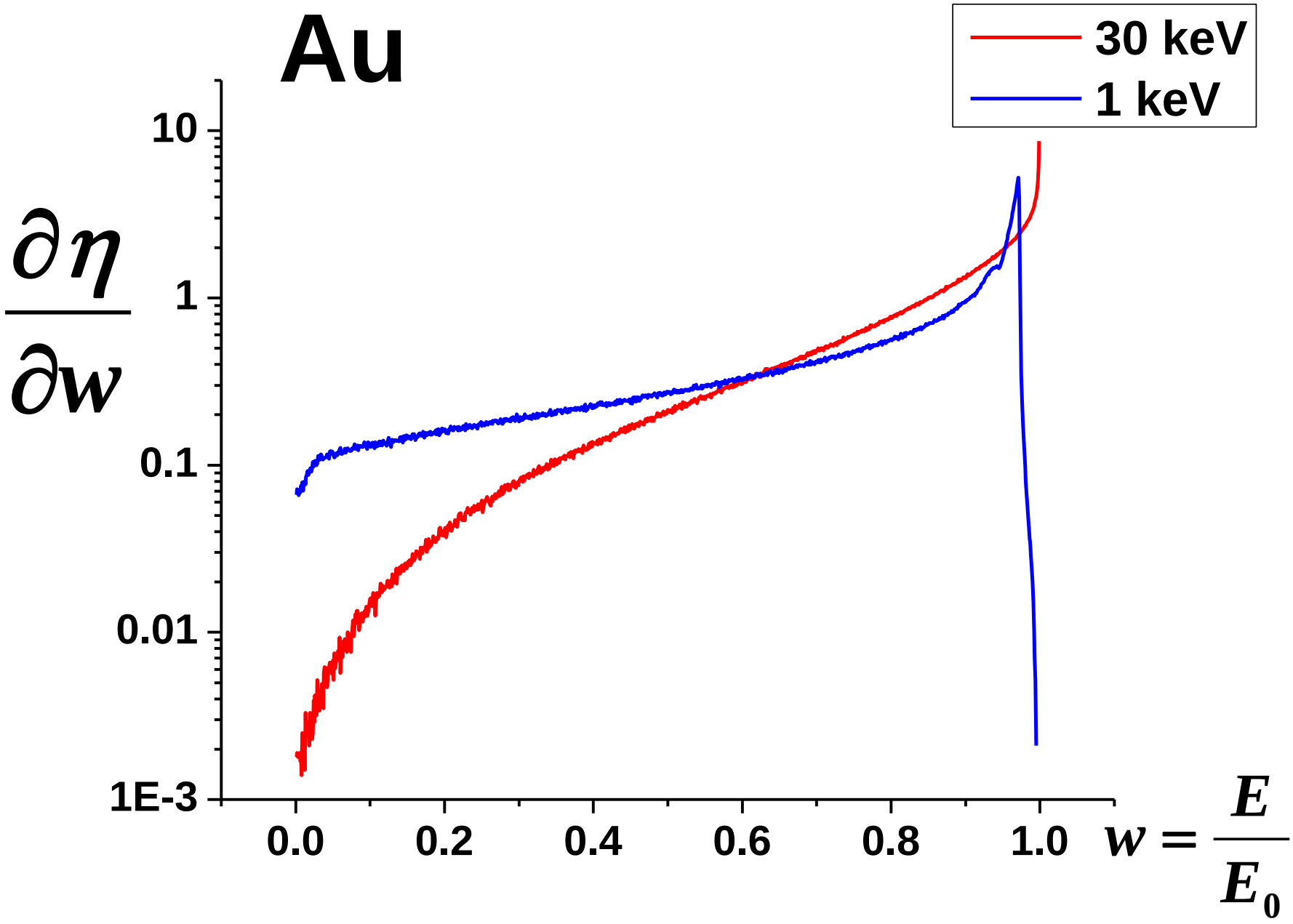
Au
30 keV
1 keV
10
1
0.1
0.01
1E-3
0.0
0.2
0.4
0.6
0.8
1.0
$\frac{\partial \eta}{\partial w}$
$w = \frac{E}{E_0}$

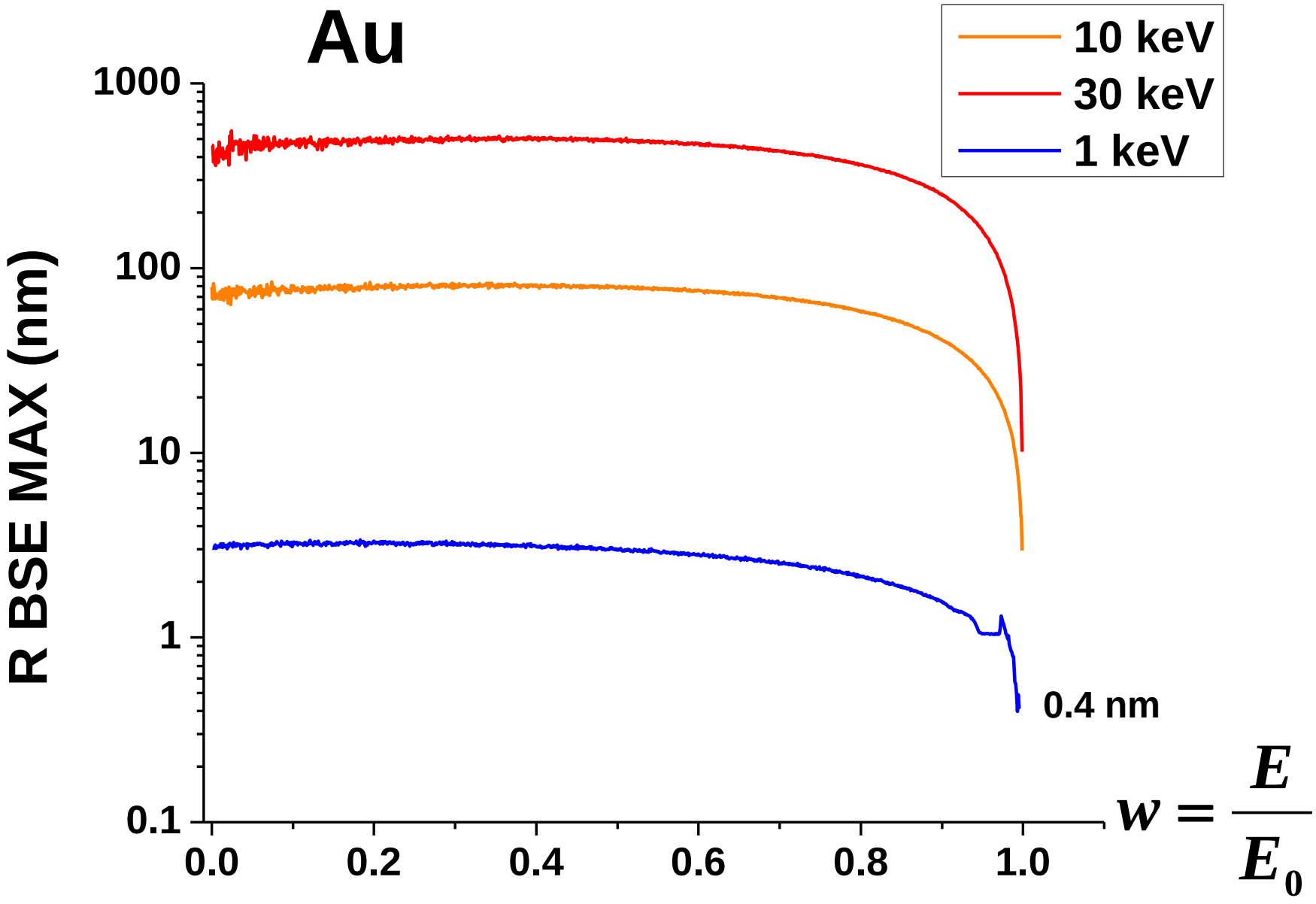
Au
10 keV
30 keV
1 keV
R BSE MAX (nm)
1000
100
10
1
0.1
0.0
0.2
0.4
0.6
0.8
1.0
0.4 nm
$w = \frac{E}{E_0}$

Top filter function (Option)

Top filter function (in Normal optics)

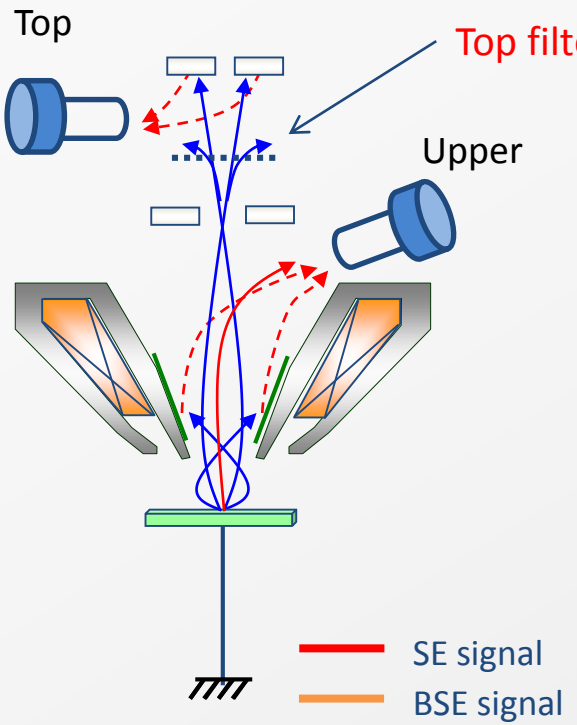

Feature

Low loss BSE will be taken by Top detector

Emphasizing surface composite contrast

【Normal optics】

Top filter is functioned as high pass filter. The inelastic BSE signals are filtered by Top filter. Filtered HA-BSE image represents the elastic scattering BSE information as low loss BSE.
The image will emphasize surface composite contrast.

Gold on Carbon Test Specimen

SE(U)

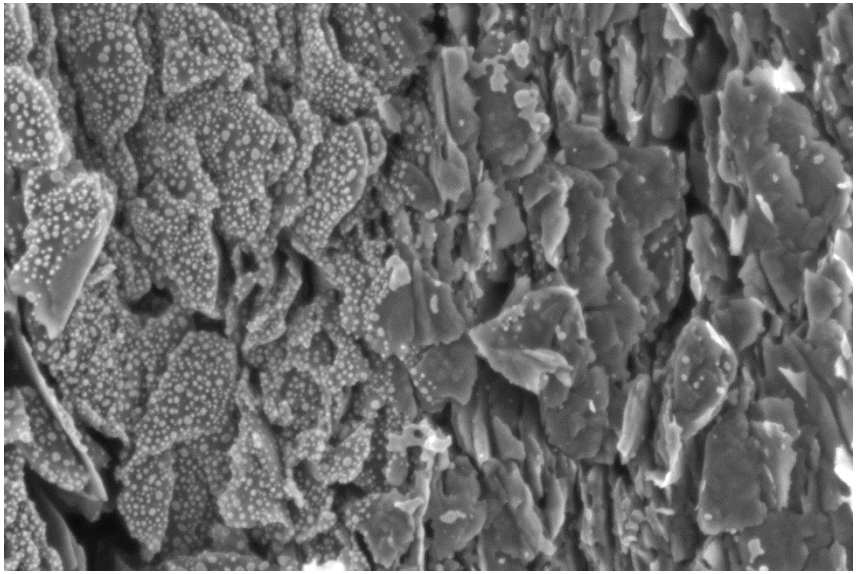

HA(T)F90

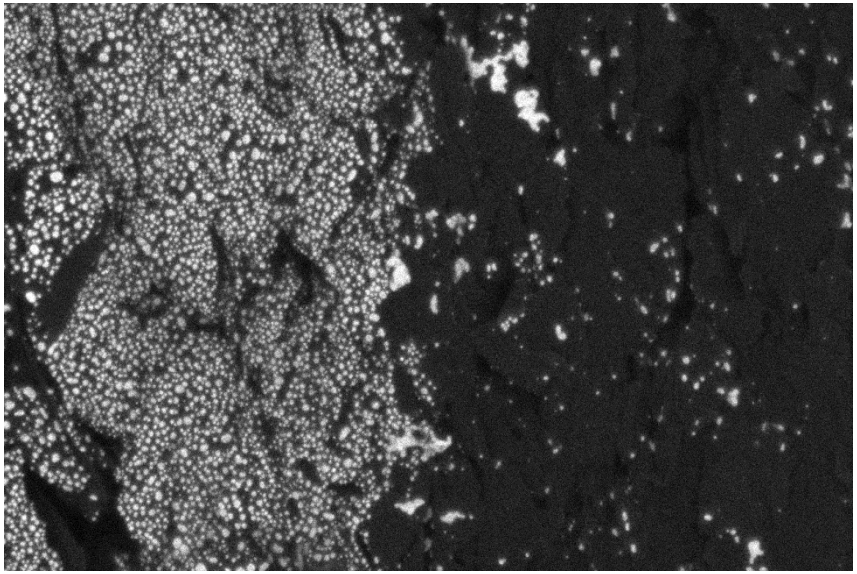

FOV: 2117 nm
60 kX

SNR: 26
Resolution: 5.4 nm

SNR: 3.8
Resolution: 7.1 nm

CNT 1 kV Deceleration

BSE(T)F150

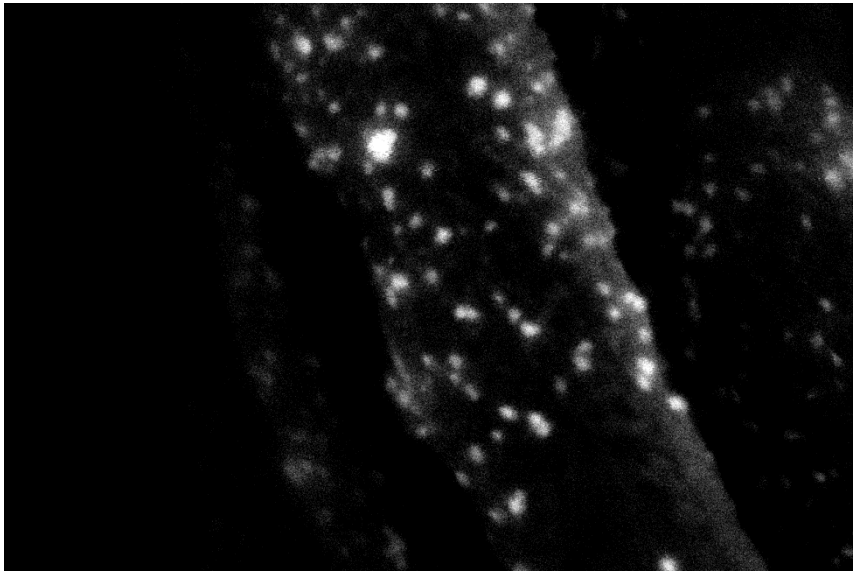

SNR: NaN
Resolution: 1.9 nm

FOV 254 nm
500 kX

SE+BSE(U)

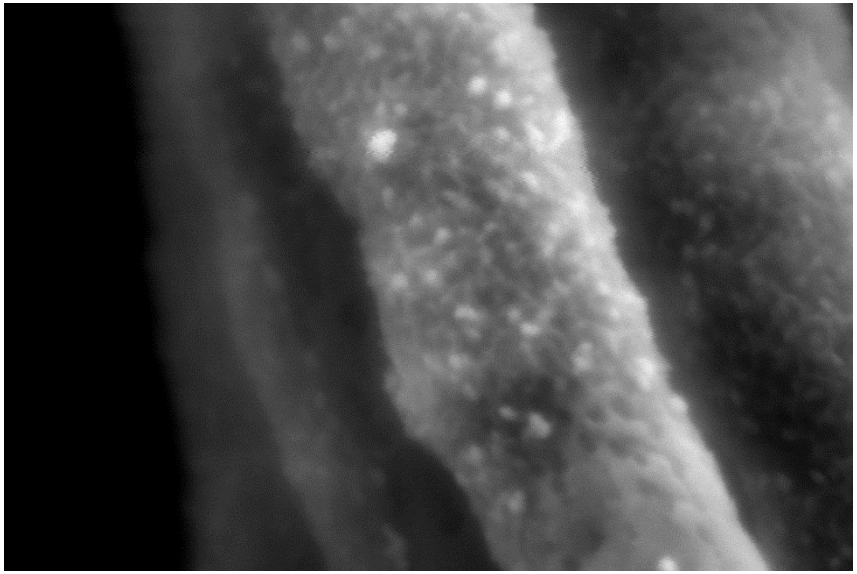

SNR: 6.4
Resolution: 2.5 nm

UltraLow Voltage SEM

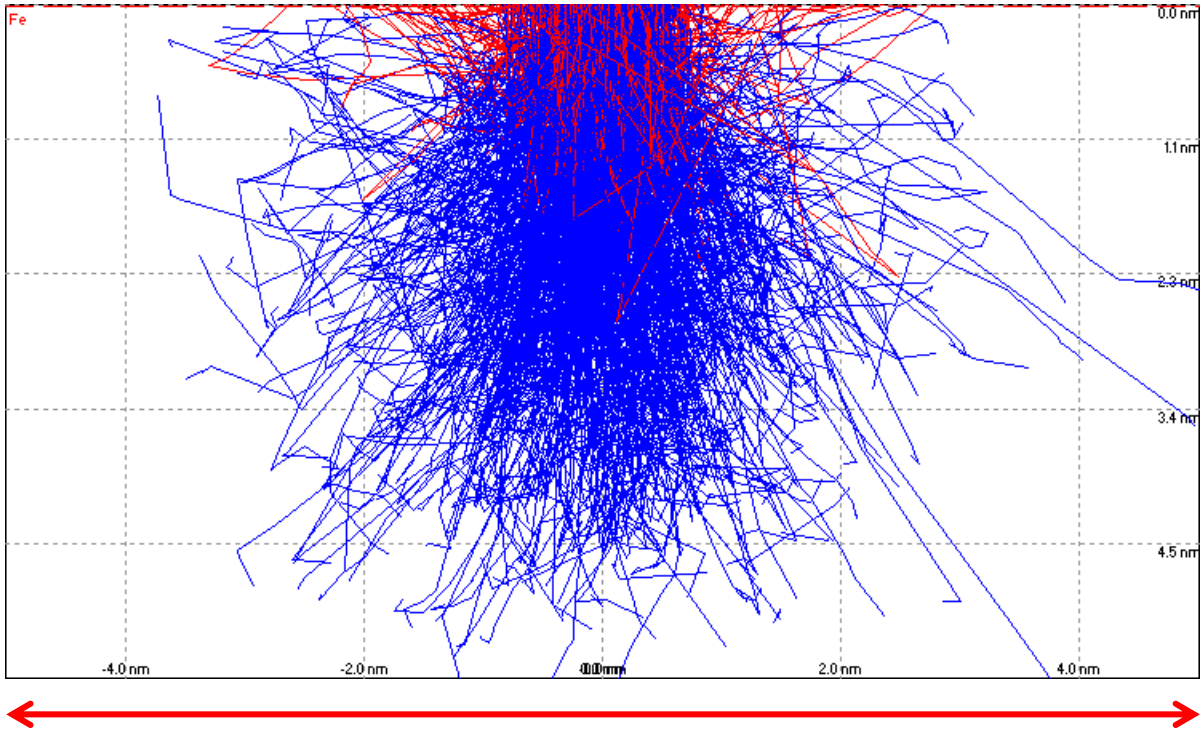

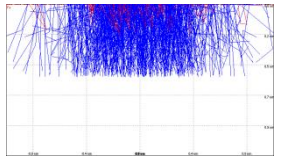

1 nm

0.1 kV

0.5 kV

10 nm

Ultra low voltage imaging:

- Close to atomic scale interaction volume
- SE/BSE signals from the same interaction volume

CNT 500 V Deceleration

SE(T)

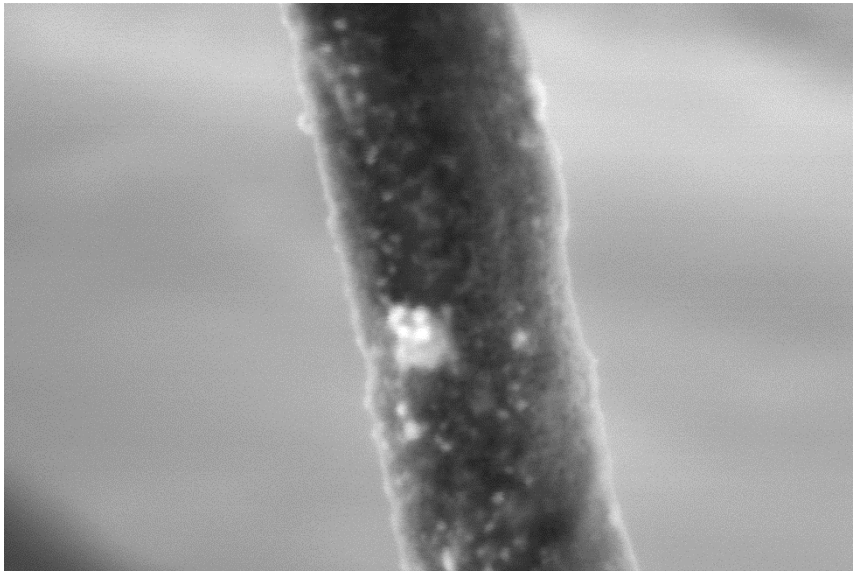

SNR: 3.6
Resolution: 3.0 nm

FOV 318 nm
400 kX

SE+BSE(U)

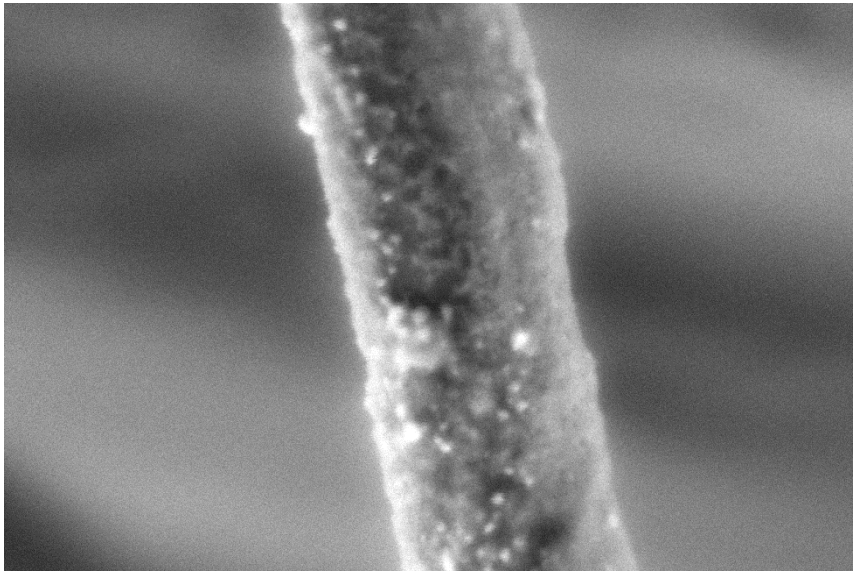

SNR: 16.1
Resolution: 2.7 nm

Top Detector, 100 V

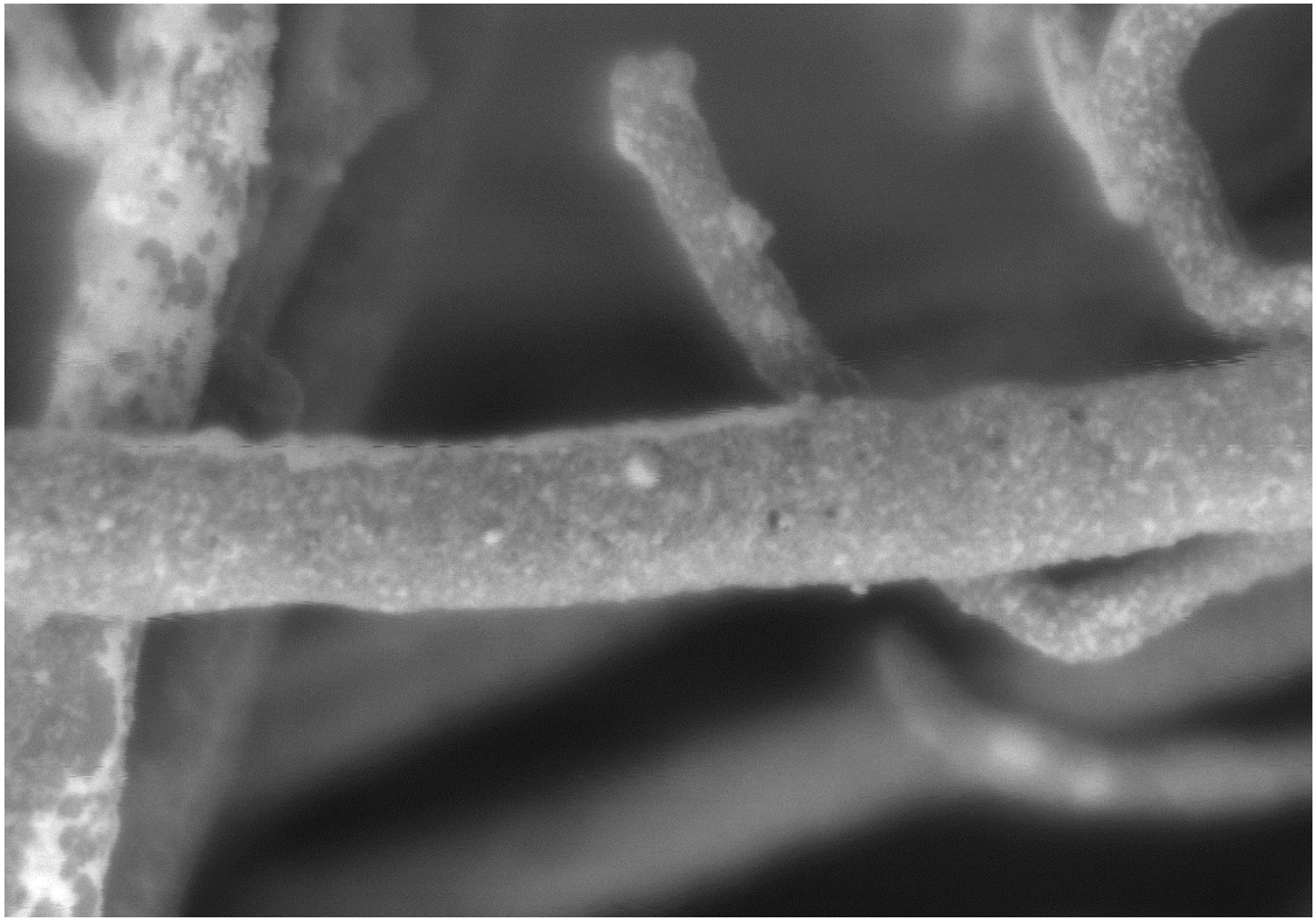

200kX
SE(T)
FOV: 635 nm
SNR: 2.2
Resolution: 5.2 nm

Top Detector, 100 V

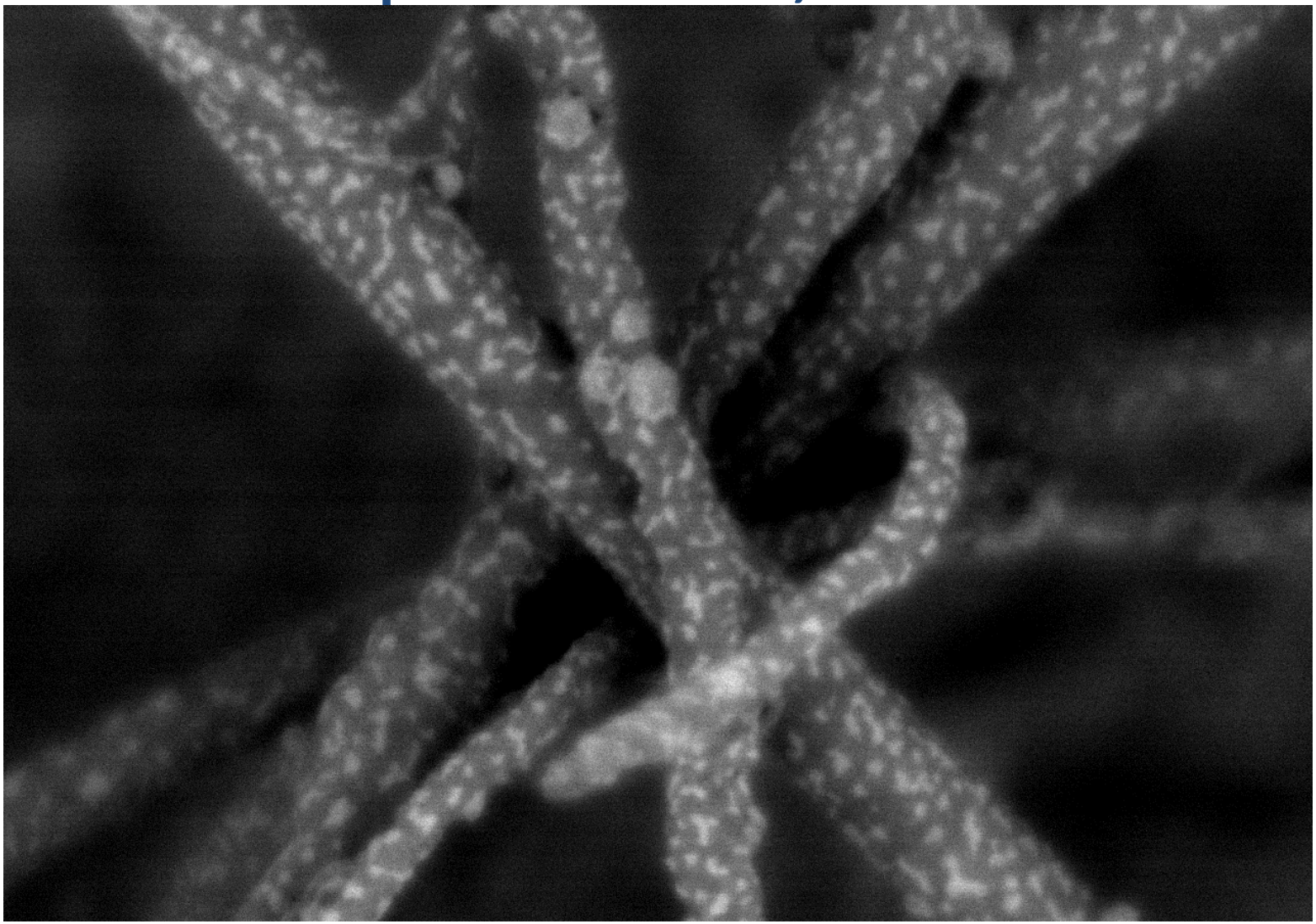

Top Detector, 50 V

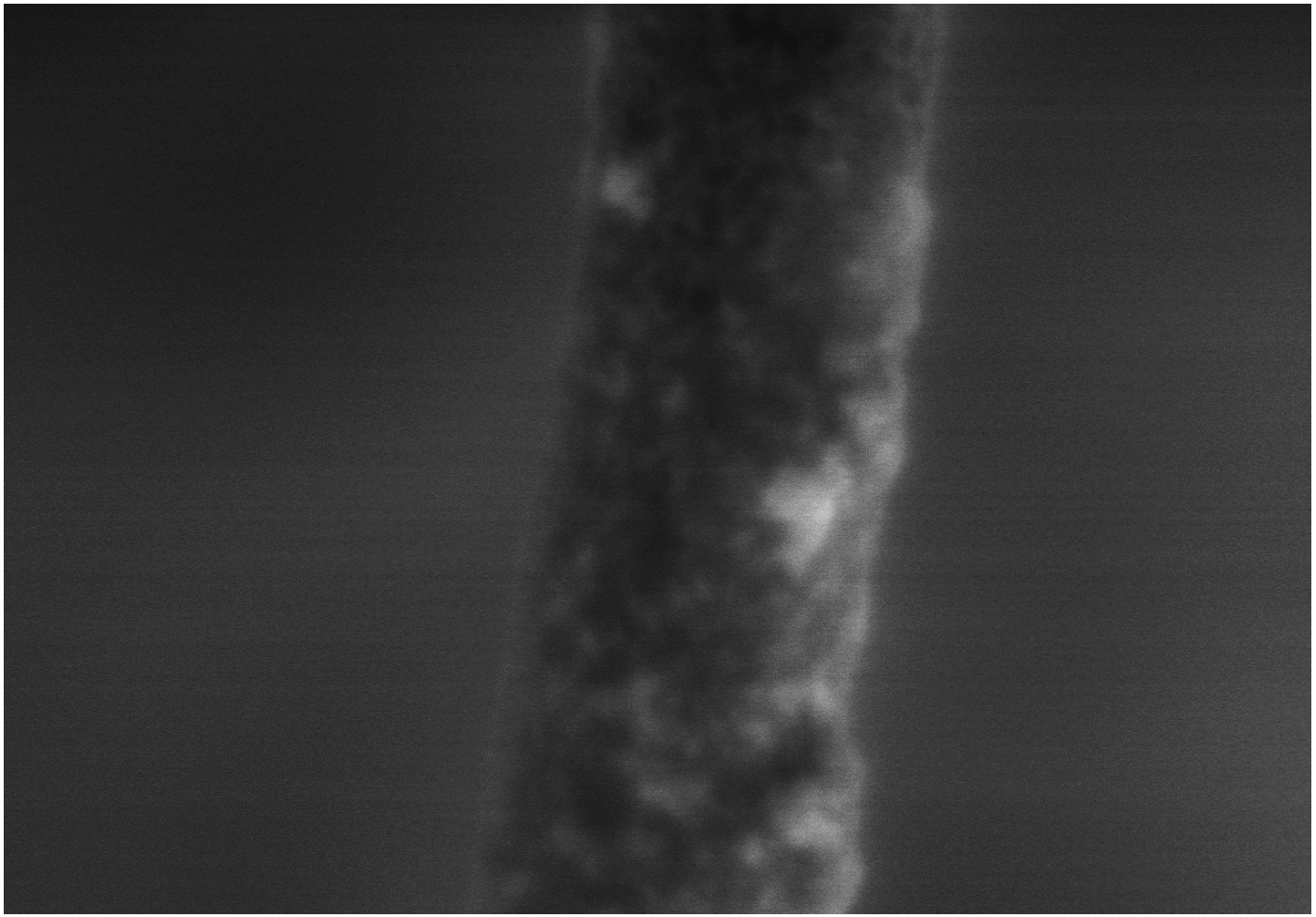

500 kX
SE(T)
FOV: 254 nm
SNR: 1.0
Resolution: 2.8 nm

Pt on CNT, 50 eV

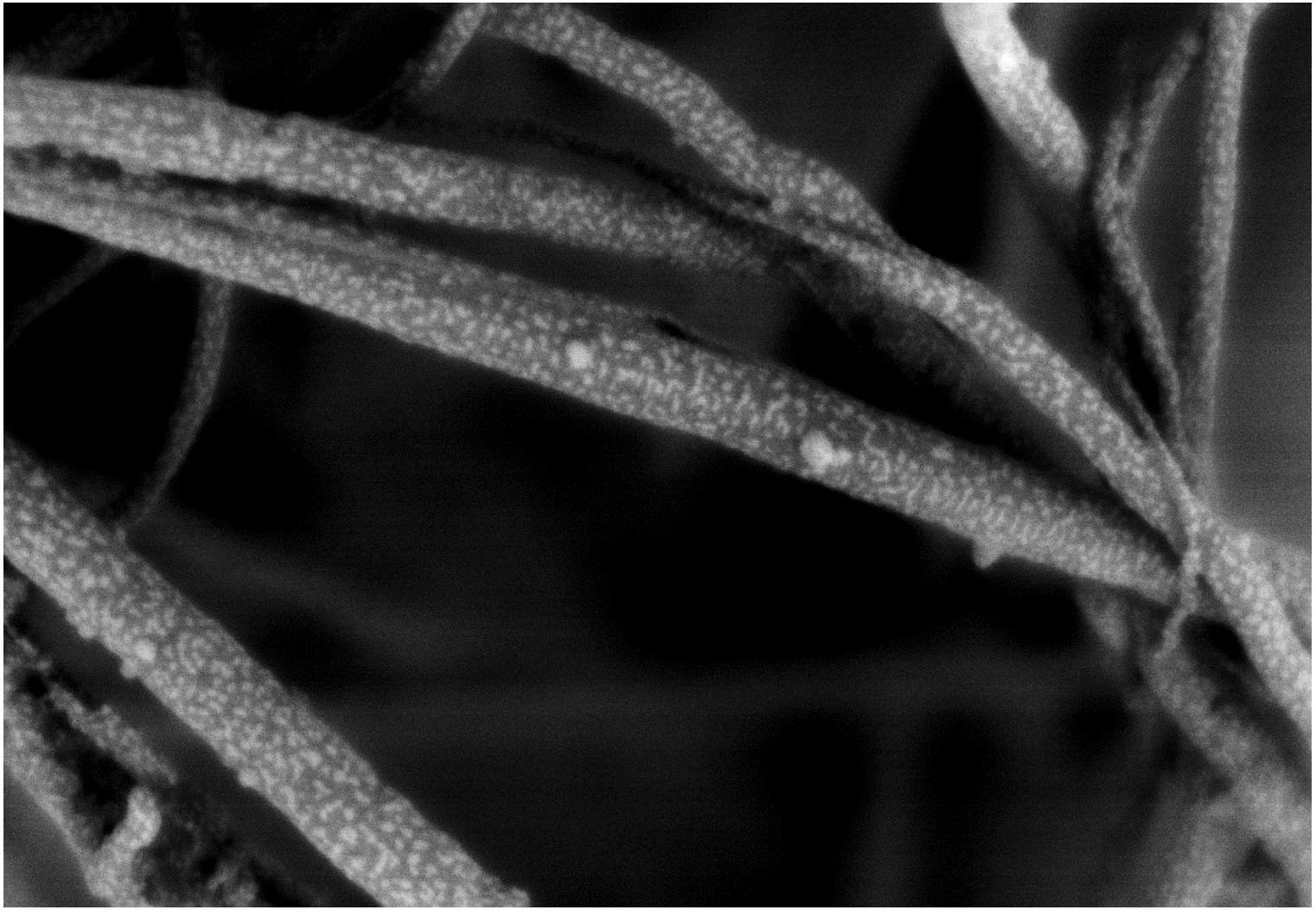

Pt on CNT, 30 eV

Pt on CNT, 10 eV

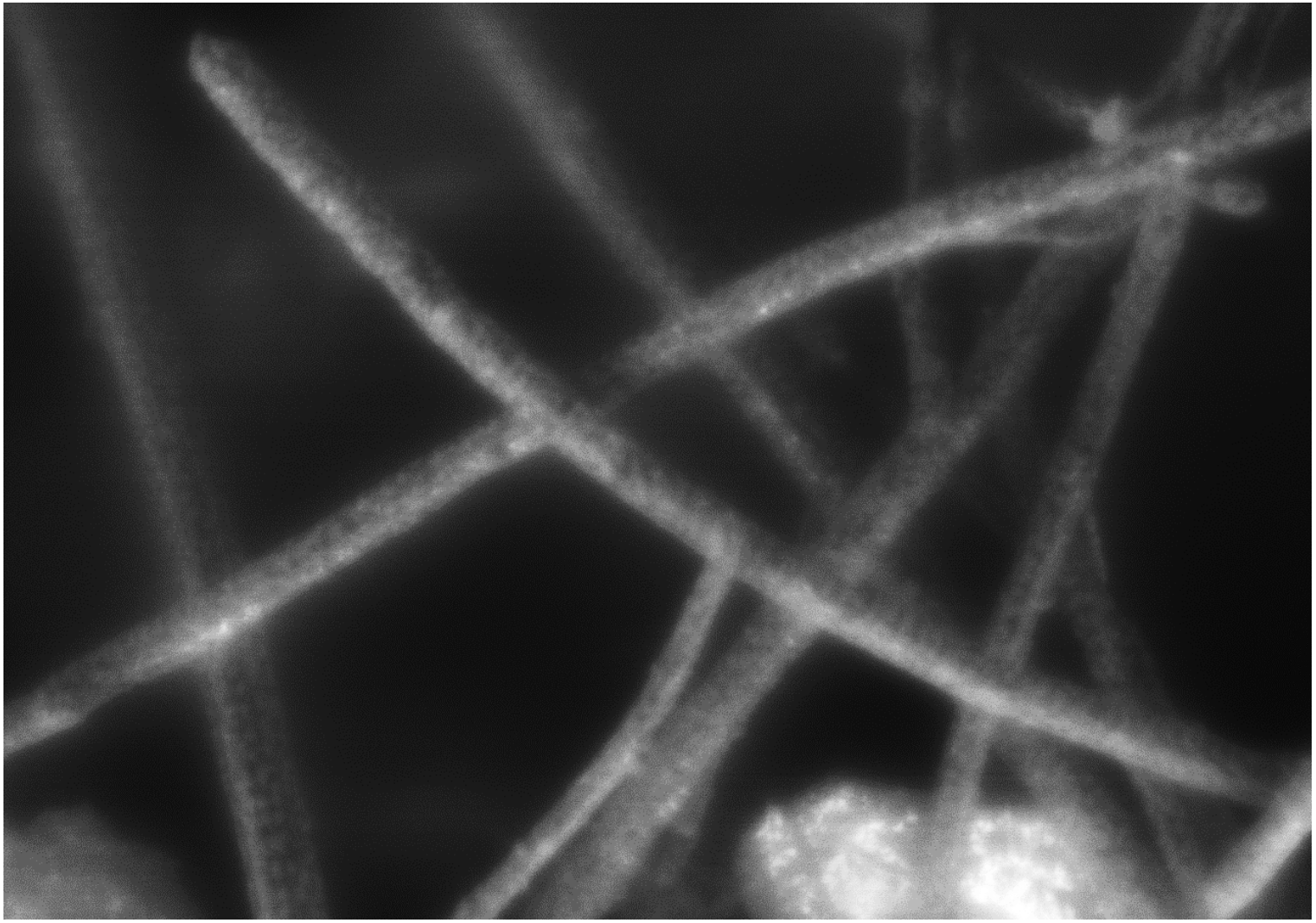

Top Detector, 10 V

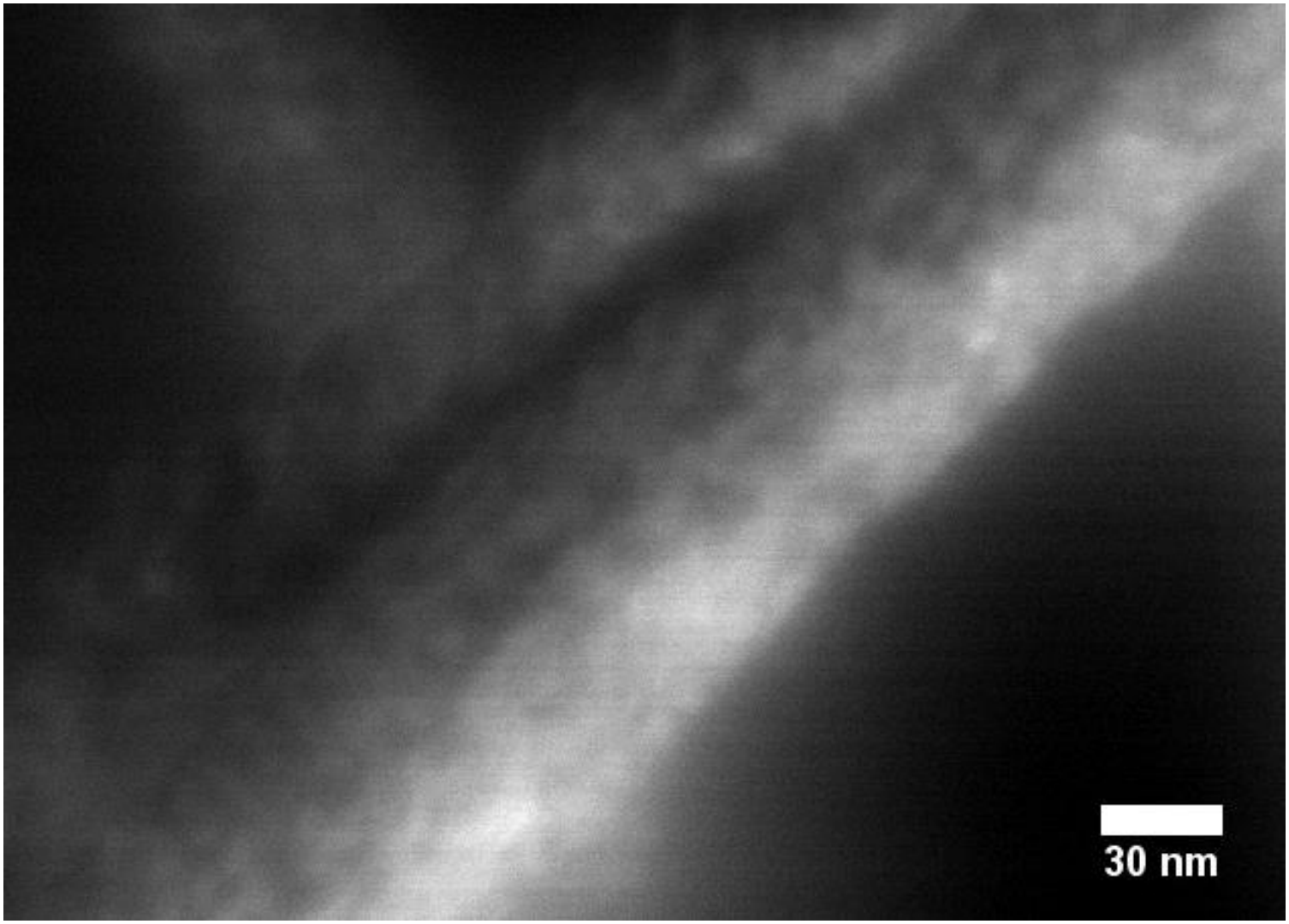

200kX
SE(T)
Resolution: ~4 nm

Bruker Flat Quad XFlash 5060F (BFQ)

- Quad detector
  - 4 x 15 mm^2 = 60 mm^2
- Annular design (below objective lens)
- Equipped with Mylar windows
  - Internal window (1 µm)
  - Additional 2 µm or 6 µm windows (on a special changer)
- High count rate capabilities with high collection efficiency

Image from Bruker Nano GmbH.

Nechalacho Ore

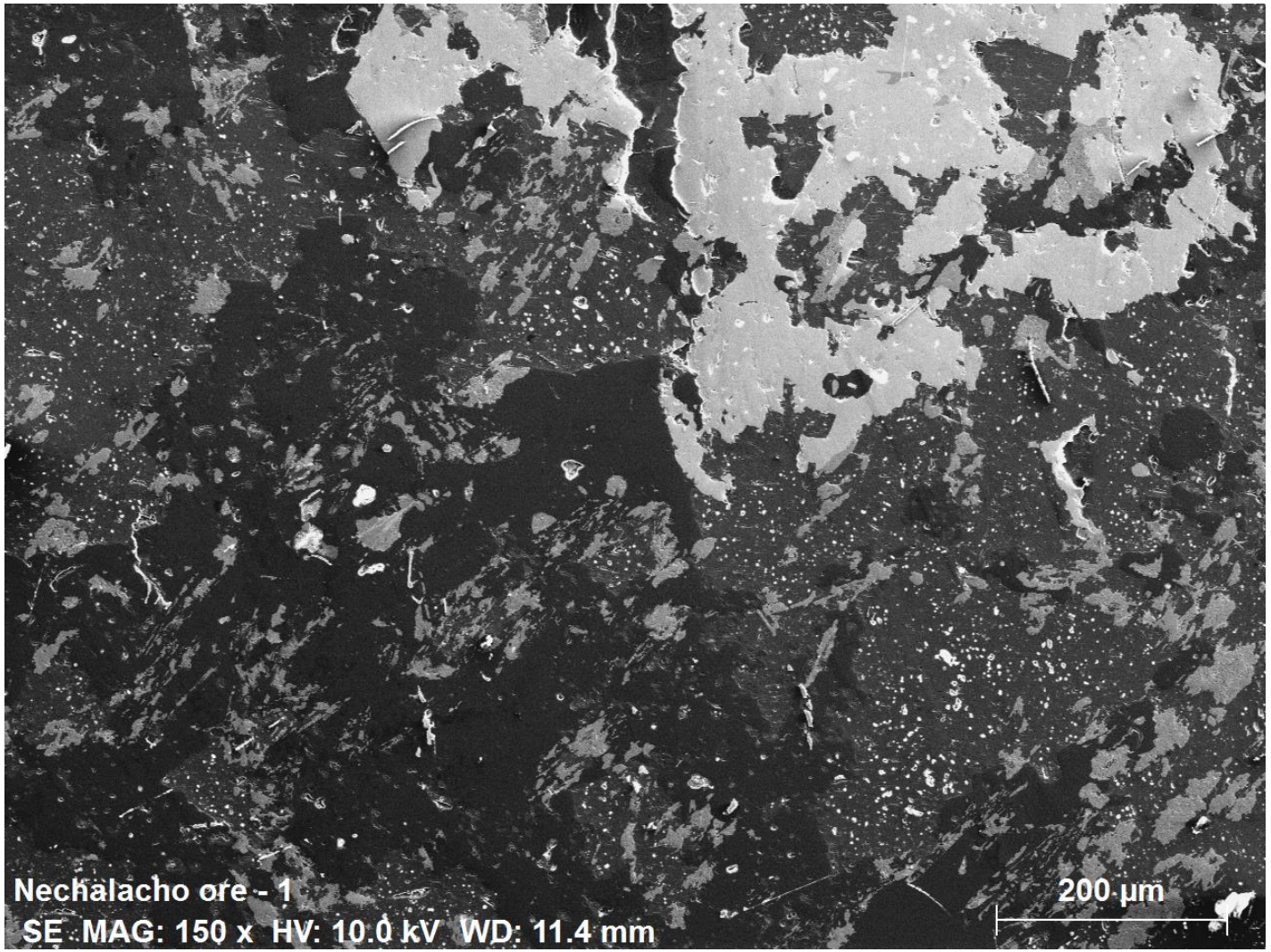

Conventional 60 mm^2 SDD Detector, 20 S, 1280 X 960, 0.016mS/pixel

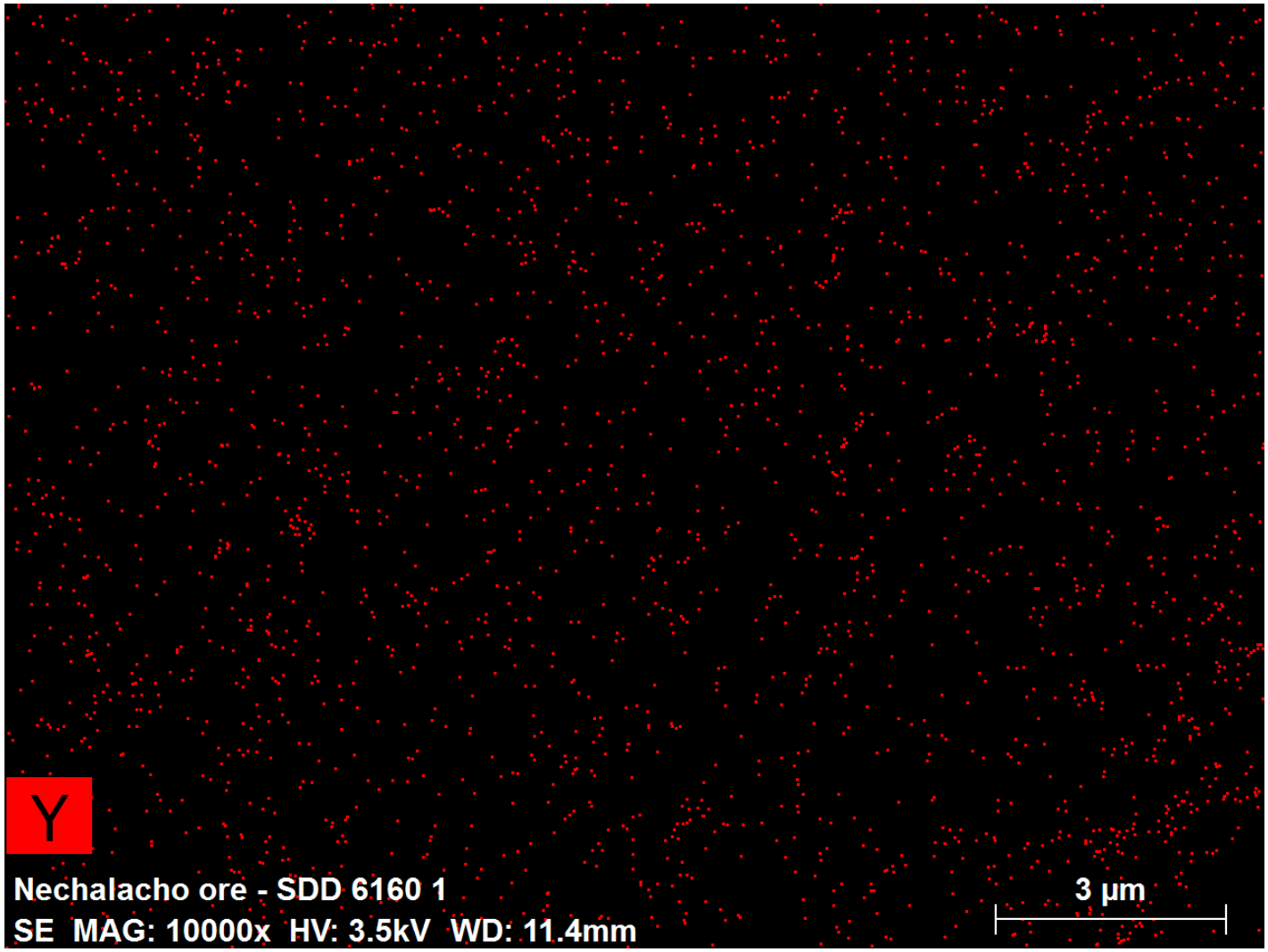

Bruker Flat Quad XFlash 5060F (BFQ) 20 S , 1280 X 960, 0.016mS/pixel

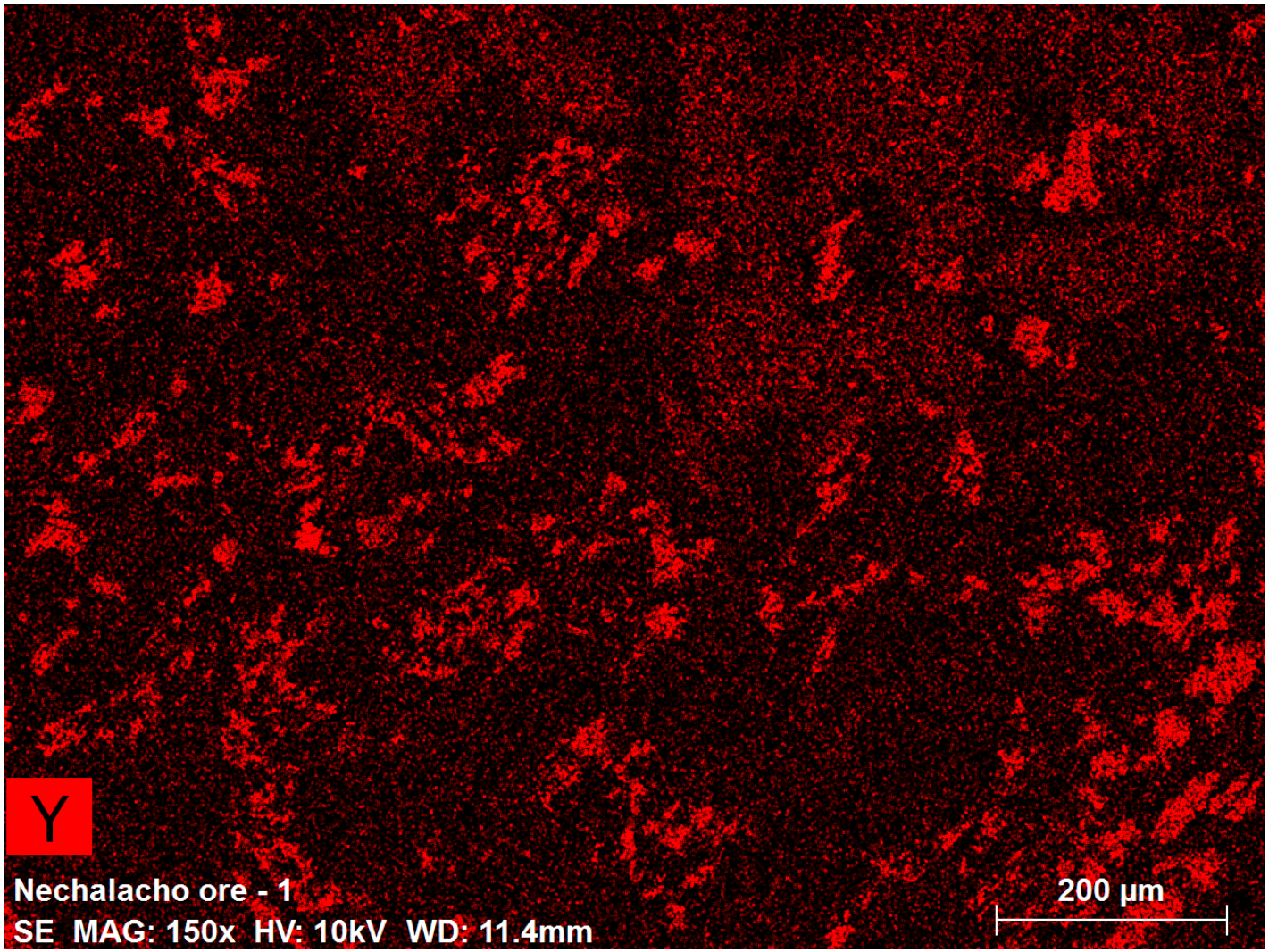

Bruker Flat Quad XFlash 5060F (BFQ) 400 S, 1280 X 960, 0.325 mS/pixel

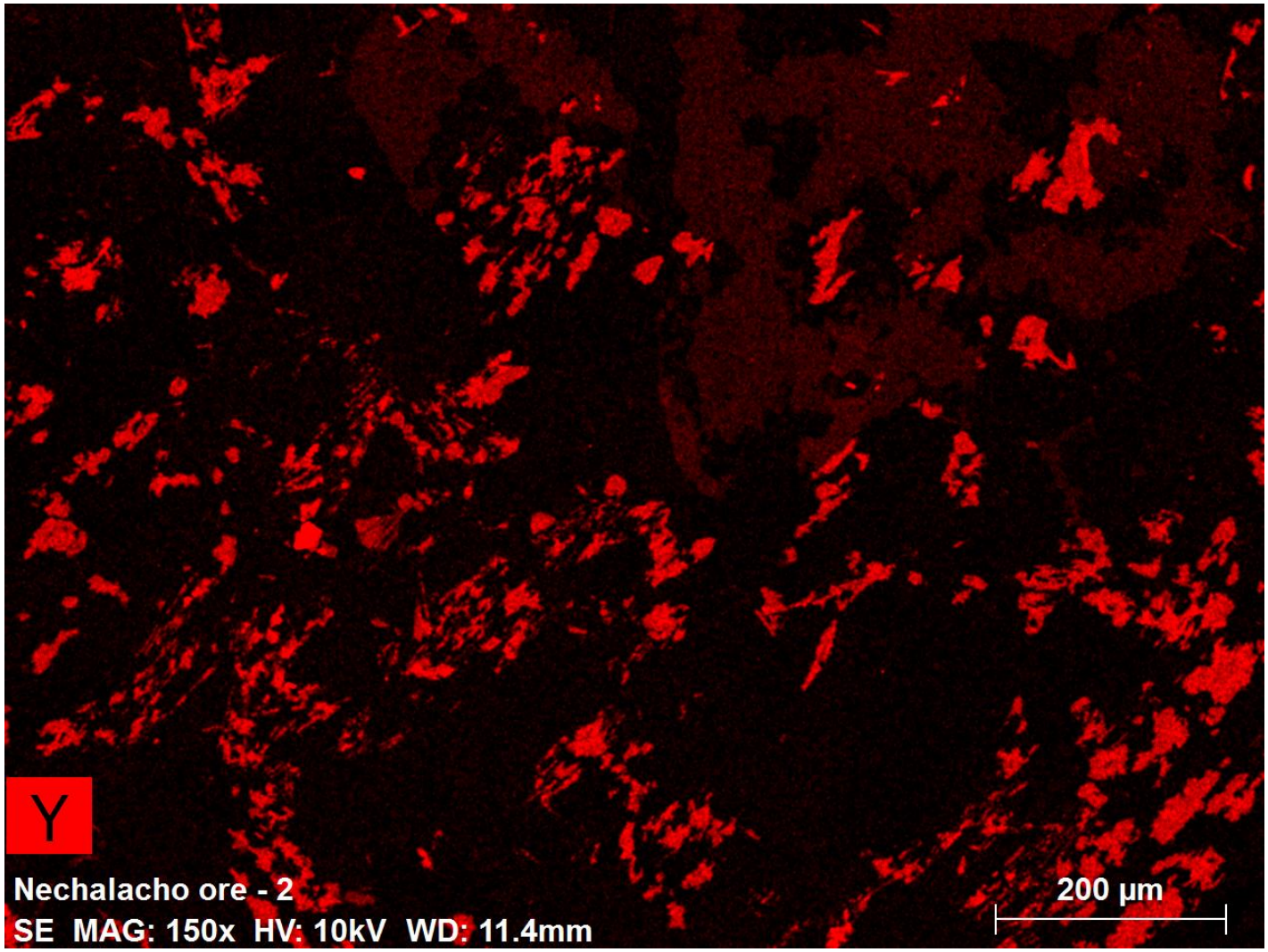

Bruker Flat Quad XFlash 5060F (BFQ) 400 S , 1280 X 960, 0.325 mS/pixel

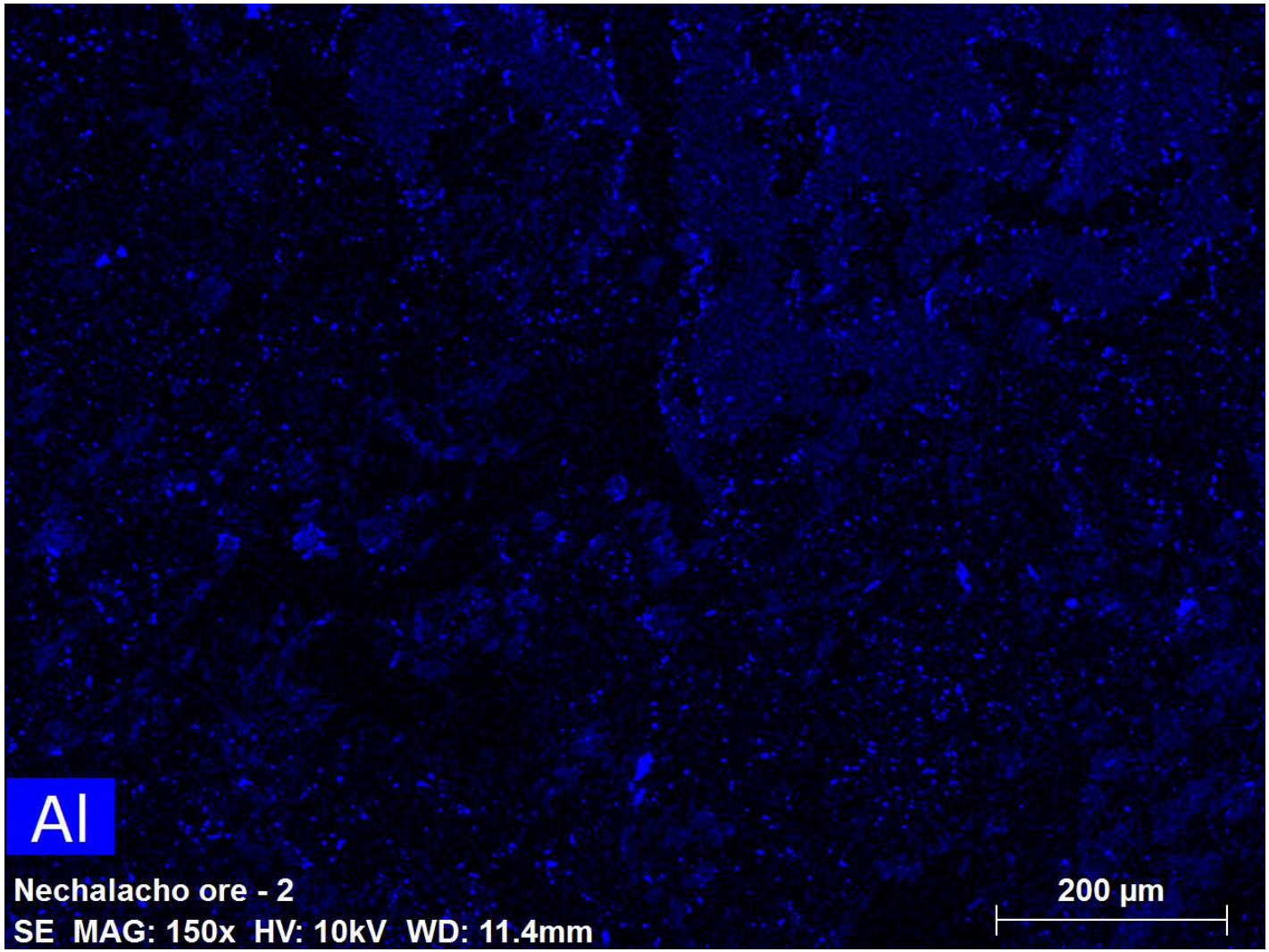

Bruker Flat Quad XFlash 5060F (BFQ) 400 S , 1280 X 960, 0.325 mS/pixel

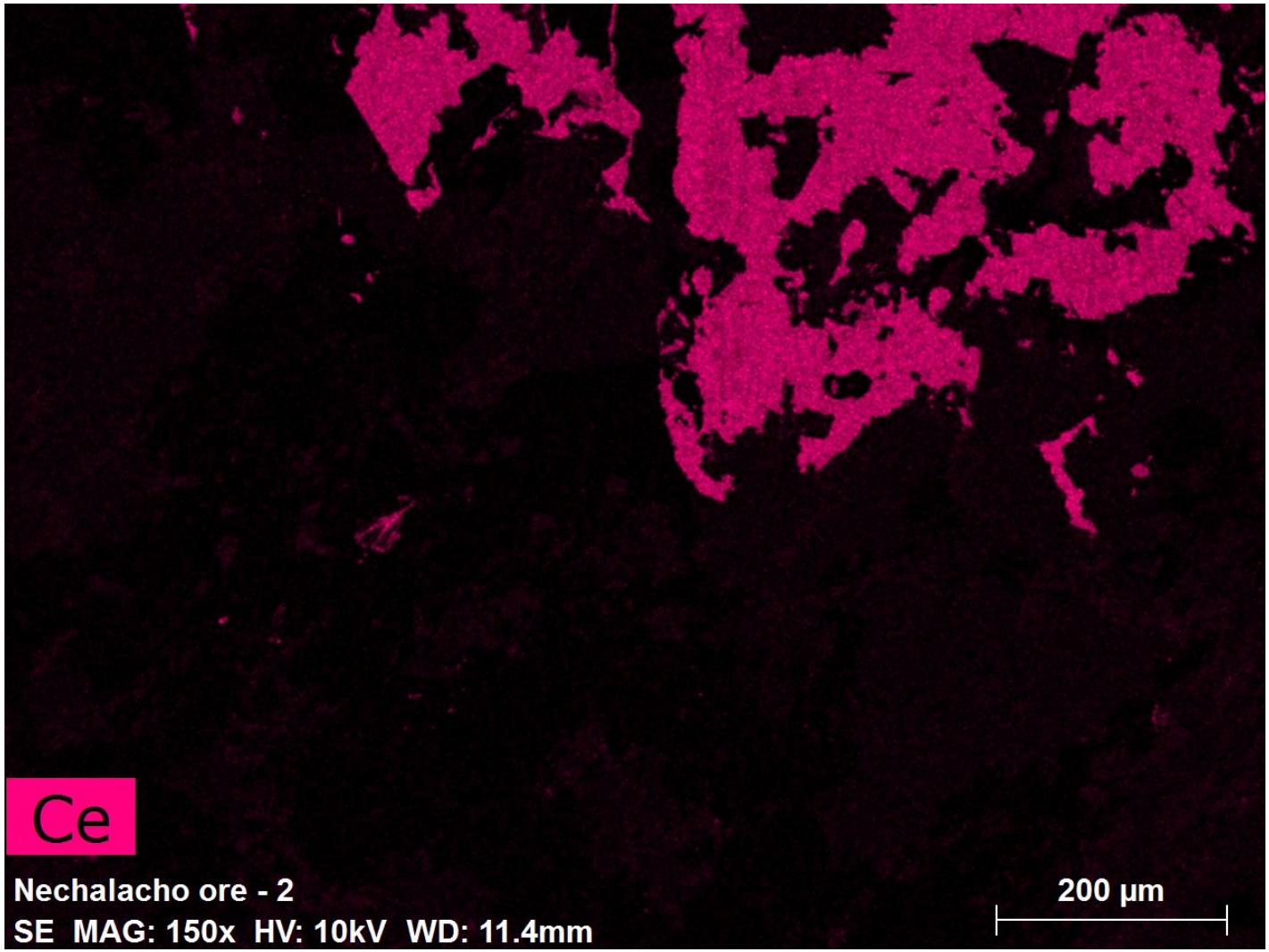

Pt Particulates on WCNT

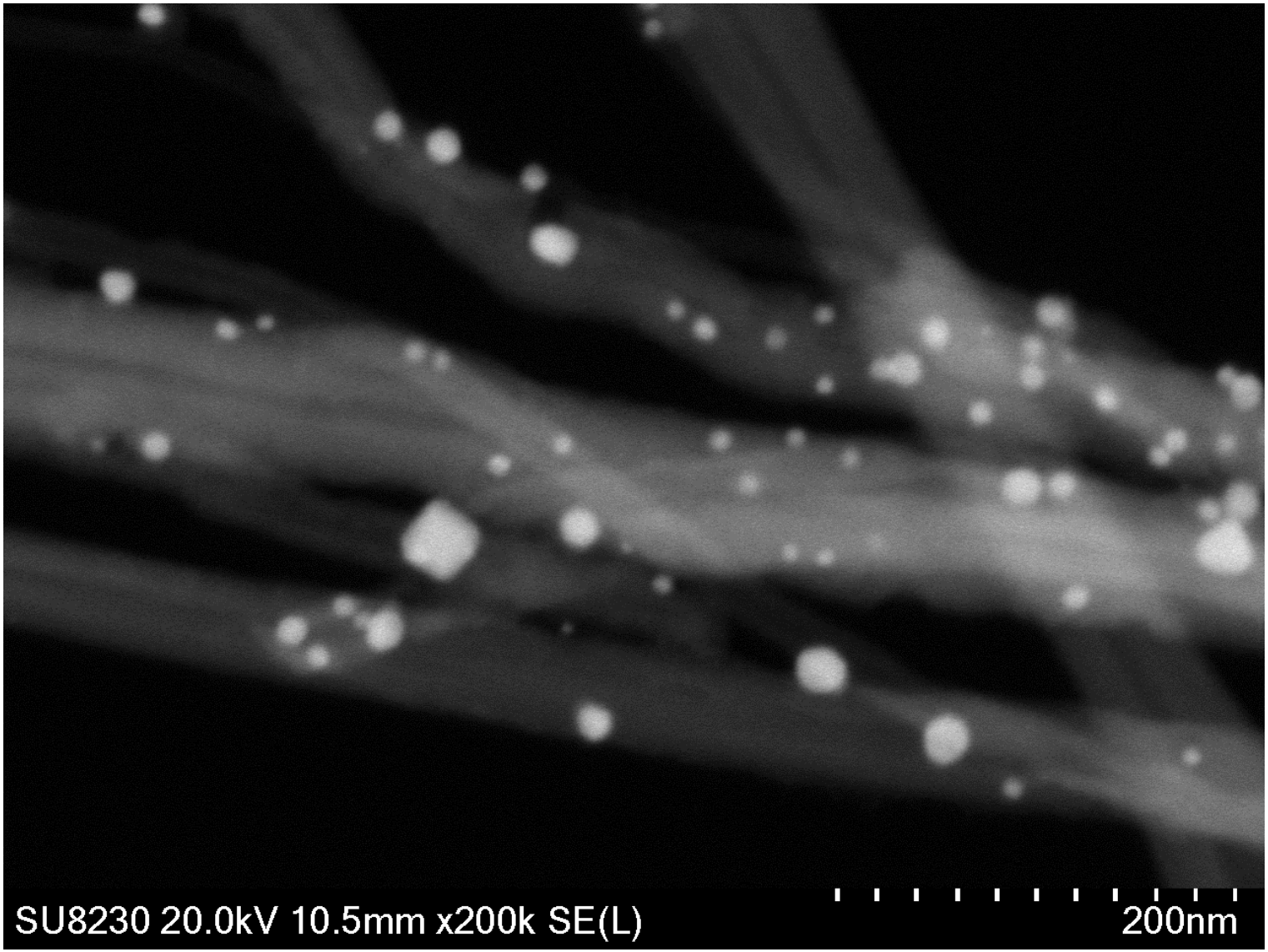

Pt Particulates on WCNT, 7 minutes

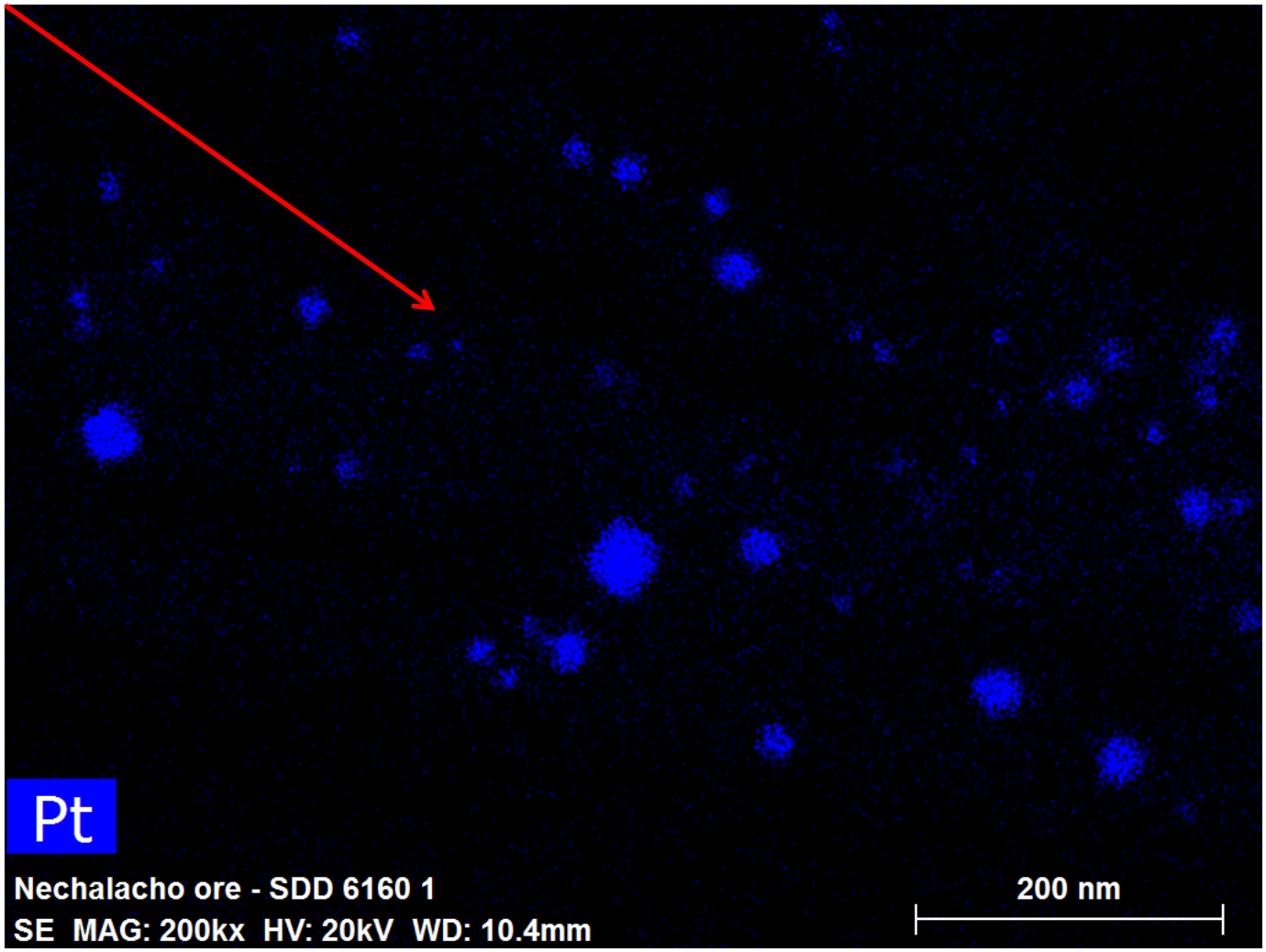


memrg.com